CELL-CELL COMMUNICATION IN THREE DIMENSIONAL MICROENVIRONMENTS

BY

LISA RENEE TRUMP

DISSERTATION
Submitted in partial fulfillment of the requirements
for the degree of Doctor of Philosophy in Animal Sciences
in the Graduate College of the
University of Illinois at Urbana-Champaign, 2011

Urbana, Illinois

Doctoral Committee:

Professor Lawrence B. Schook, Director of Research
Professor John Killefer
Assistant Professor Fei Wang
Assistant Professor Tetsuya Tanaka

ABSTRACT

Cellular behavior is dependent on a variety of extracellular cues required for normal tissue function, wound healing, and activation of the immune system. Removed from their *in vivo* microenvironment and cultured *in vitro,* cells lose many environmental cues and that may result in abberant behavior, making it difficult to study cellular processes. In order to mimic native tissue environments, optical tweezer and microfluidic technologies were used to place cells within defined areas of the culture environment. To provide three dimensional supports found in natural tissues, hydrogel scaffolds of poly (ethylene glycol) diacrylate and the basement membrane matrix Matrigel were used. Optical tweezer technology allowed precision placement and formation of homotypic and heterotypic arrays of human U937, HEK 293, and porcine mesenchymal stem cells. Alternatively, two microfluidic devices were designed to pattern Matrigel scaffolds. The first microfluidic device utilized laminar flow to spatially pattern multiple cell types within the device. Gradients of soluble molecules were then be formed and manipulated across the Matrigel scaffolds. Patterning Matrigel using laminar flow techniques require microfluidic expertise and do not produce consistent patterning conditions, limiting their use difficult in most cell culture laboratories. Thus, a buried Matrigel polydimethylsiloxane (PDMS) device was developed for spatial patterning of biological scaffolds. Matrigel is injected into micron sized channels of PDMS fabricated by soft lithography and allowed to thermally cure. Following curing, a second PDMS device was placed on top of the buried Matrigel channels to support media flow. In order to validate these systems, a cell-cell communication model system was developed utilizing LPS and TNFα signaling with fluorescent reporter systems to monitor communication in real time. We demonstrated the utility of microfluidic devices to support the cell-cell communication model system by co culturing three cell types within Matrigel scaffolds and monitoring signaling activity via fluorescent reporters.

I would like to dedicate this dissertation to my mother, friends, and family for their love and support throughout my studies at the University of Illinois.

ACKNOWLEDGEMENTS

This dissertation would not have been possible without the support, guidance, and assistance of many people. I would like to thank Dr. Lawrence Schook, my Ph.D advisor for his guidance and support throughout my graduate career. I would also like to thank my Ph.D committee, Dr. Tetsuya Tanaka, Dr. John Killefer, and Dr. Fei Wang for their support. Thanks to Dr. Gregory Timp for his expertise and use of laser tweezers. I would also like to thank Dr. Mivandi Shivagru for his patience and expertise while I was learning many microscopy techniques and Janet Sinn-Hanlon for designing images needed for this dissertation. I would like to thank Dr. Paul Kenis and Dr. Amit Desai for their assistance and expertise in designing and troubleshooting the microfluidic devices. Last, but not least, I would like to thank Dr. Laurie Rund for her support and assistance in maintaining my sanity these last few years.

TABLE OF CONTENTS

List of Figures

LIST OF TABLES

CHAPTER ONE

Introduction: Specific Aims and Overview

"Your cells are a country of 10,000 trillion citizens, each devoted in some intensely specific way to your overall well-being. There isn't a thing they don't do for you. They let you feel pleasure and form thoughts. They enable you to stand and stretch and caper. When you eat, they extract the nutrients, distribute the energy, and carry off the wastes…but they also remember to make you hungry in the first place and regard you with a feeling of well-being so that you won't forget to eat again. They keep your hair growing, your ears waxed, and your brain quietly purring. They manage your being. They will jump to your defense the instant you are threatened. They will unhesitatingly die for you- billions of them do so daily. And not once in all your years have you thanked even one of them. So let us take a moment now to regard them with the wonder and appreciation they deserve."

- Excerpt from "A Short History of Nearly Everything"
  By Bill Bryson

1.1 INTRODUCTION

Over the last two decades, significant advances in biomedical sciences and medical technology, such as the sequencing of the human genome and the isolation and derivation of adult, embryonic, and induced pluripotent (iPS) stem cells have unlocked many tools to expand our knowledge of human physiology and the causes, processes, and treatment of disease. Overall, death rates have decreased 12.9% in the last decade (Lloyd-Jones et al., 2010), but there is now an increased burden of disease due to aging populations and a dramatic rise in more expensive, chronic diseases such as diabetes ("Centers for Disease Control and Prevention,"). Furthermore, the demand of donor cells, tissues, and organs available for transplantation far exceeds the amount of available donor tissue, resulting in the deaths of approximately 18 people per day on the organ transplant waiting list ("UNOS"; "Golden State Donor Services - The Basic Facts"). Thus, research in the biomedical sciences has intensified to develop new, novel cell replacement therapies that use patient-derived or donor stem or precursor cells to repair or replace damaged and diseased tissues of the body. Other research

efforts focus on the development of new drug compounds to treat or alleviate disease. Despite these research efforts, few cell replacement therapies have reached clinical usage and new drug approval rates have remained the same over the last two decades (Kola & Landis, 2004). Approximately 4 out of 5 biological molecules and 19 out of 20 small molecule drugs tested by the FDA fail at the clinical trial phase, after years of testing and millions of research dollars are spent (Kola & Landis, 2004). For cell replacement therapies, the limited availability of stem and precursor cells requires the expansion and differentiation of cells outside of the body, yet this expansion and differentiation process is highly inefficient and differentiation outcomes are unpredictable (Passier, van Laake, & Mummery, 2008; Lerou & Daley, 2005). The reason for few therapeutic and drug breakthroughs is twofold; the lack of understanding of the signals and cues that guide cell fate and the absence of appropriate cell culture and model systems that accurately recapitulate normal or diseased tissues, leading to inaccurate predictions of cell function and fate.

Generally, our knowledge of the signals and cues that guide cellular fate are derived from the culture of cells on rigid, two dimensional (2D) plastic surfaces. While these systems have supported basic research of cellular behavior and function, they do not provide environments that mimic *in vivo* cellular environments. *In vivo,* a cell is not an isolated entity; it is part of a three-dimensional (3D) tissue where it is surrounded by other cells, extracellular matrix (ECM), and gradients of signaling molecules and soluble factors. Signals directing cellular fate come from other cells through direct contact through gap or adherens junctions, through diffusible signaling molecules secreted by nearby cells, or from ECM. The ECM provides structural support to cells, soluble factors that are absorbed within the matrix, as well as ligands such as Arginine-Glycine-Aspartic Acid (RGD) that activate intracellular signaling cascades. It is well documented that a cell's environment, i.e. cell-cell contacts; ECM concentration, density, and composition; and the spatial and temporal presentation of soluble molecules all affect cellular fate (Ling et al, 2009; McBeath, et al., 2004; Reilly & Engler, 2010). In terms of drug discovery applications, investigations into cellular behavior and responses to stimuli using these traditional culture systems that lack physiological cues and signal gradients may result in conclusions that do not reflect how the same cell type will respond *in vivo*. Single, bolus

delivery of small molecules characteristic of many cell biology experiments result in uncontrolled concentration gradients of molecules that do not reflect *in vivo* spatial and temporal presentation of molecules. Measurements of response to these molecules are generally population-based, endpoint assays that can mask individual and temporal cell behaviors. On the cell therapy side, a cells ability to self-renew or differentiate in basic culture systems can be affected or limited due to lack or inappropriate presentation of environmental stimuli. The lack of supportive and controllable cell culture environments limits the expansion and differentiation of stem and precursor cells, often resulting in inadequate cell populations required for effective cellular therapies.

A current strategy to provide physiologically relevant cell culture environments is the development of 3D scaffolds and tissue engineering constructs to provide structural support and cell organization found in tissue. 3D scaffolds-either natural or synthetic- give 3D support to cells and allow for diffusion of signaling factors and nutrients. For example, cells can be cultured within or on top of natural scaffolds such as collagen or Matrigel which provide signaling molecules and ligands such as RGD that are not found in 2D polystyrene culture dishes. Engineering approaches, such as dielectropheresis (DEP) and photolithography, have been developed that allow patterning of cells either within or on top of these scaffolds, providing control over cell-cell interactions (Markx et al, 2009). Spatial and temporal delivery of soluble molecules has been achieved through the use of microfluidic devices or controlled degradation and release of stimuli from biomaterials (Krsko & Libera, 2005; Lee et al., 2010; Schudel et al., 2009). While these experimental setups provide tools to recapitulate *in vivo* environments, most have been proof of concept experiments demonstrating technique with little investigation into cellular behavior within the fabricated microevironments. Many cell culture engineering techniques only focus on a single aspect of a cell's microenvironment- they may be limited to a single cell type, which do not account for cell-cell interactions, but provide soluble signal gradients or varying ECM. Cell-cell interactions have been achieved by specifically patterning ECM or 3D scaffolds for co culture of multiple cell types, but the culture environments are static and provide little control over soluble molecule diffusion and signal gradients between cell types (Goubko & Cao, 2009). To achieve an environment for cellular

differentiation or signaling studies, the experimental design should incorporate three aspects: a) patterning of multiple cell types within 3D scaffolds with spatially localized gradients of soluble molecules; b) control the diffusion of these soluble molecules to provide temporal administration of cellular stimuli; and c) systems to monitor cellular activity within these environments throughout the experiment without sacrificing cells. Achievement of these goals will aid in the elucidation of how cells (stem, precursor, or other cell types) behave within spatially defined microenvironments similar to physiological tissue.

1.2 Specific Aims

The objectives of this thesis proposal are to create a defined cell culture model that provided a platform for the spatial patterning of cells, temporal control over soluble molecule diffusion between these cells, and the ability to monitor cellular activity throughout the culture period. To achieve these objectives, three specific aims for this project are as follows:

1.2.1 Create a cell-cell communication model system

In order to validate the objectives of this project, a well-defined cell communication model system must first be created prior to testing unknown cellular communication events. The model system should allow a) rapid genotypic or phenotypic cellular events in response to soluble molecule stimuli released from nearby cells and b) the ability to monitor said genotypic or phenotypic responses throughout the experiment. We hypothesized that signaling events of mouse macrophages in response to lipopolysaccharides released from nearby E. coli bacterium would provide a rapid and sensitive platform for a model cellular communication system, and the development of appropriate fluorescent reporter systems will enable real-time visualization of these signaling events. Chapter three describes the development and validation of this cellular communication model system.

1.2.2 CREATE AND DEFINE APPROPRIATE THREE DIMENSIONAL SCAFFOLDS AND PATTERNING TECHNIQUES TO ALLOW AND MODULATE COMMUNICATION BETWEEN CELLS

We hypothesized that the combination of appropriate biomaterial scaffolds and microscale patterning techniques would permit modeling and manipulation of cellular communications through soluble molecule diffusion in physiologically relevant dimensions while 3D scaffolds provide ECM support and cues. Appropriate scaffolding and patterning systems should permit a) the maintenance of cellular viability without activating the studied signaling cascades; b) spatial patterning of cells within the 3D scaffolds; and c) the ability to control the diffusion of soluble molecules between cell types. We developed optical tweezer technology and two microfluidic devices to specifically pattern cells in physiologically relevant length scales (10-400 μm). First, we hypothesized that the positioning and encapsulation of mammalian cells within 3D poly (ethylene glycol) diacrylate hydrogels by optical tweezer technology would provide a cell culture platform in which cell and signal position could be precisely and repeatedly defined. Secondly, we hypothesized that cells could be spatially patterned and encapsulated in micron sized, thermally curable three dimensional scaffolds (i.e. collagen, Matrigel) in microfluidic devices through laminar flow or within microfluidic trenches fabricated out of polydimethylsiloxane (PDMS). The design of these microfluidic devices would then permit soluble molecule diffusion and medium flow between cells and scaffolds. Chapter four describes the development of optical tweezer technologies, while chapter five describes the development of microfluidic devices for the spatial and temporal patterning of cells and signals.

1.2.3 MONITOR AND CONTROL CELL COMMUNICATION WITHIN THESE ENVIRONMENTS

We hypothesized that appropriate model systems, scaffolds, and patterning techniques will permit the spatial and temporal control over soluble molecule diffusion. This system was

validated through the real-time monitoring of cellular signaling events within the cellular communication model system, and is demonstrated in chapter five.

LIST OF REFERENCES

Bryson, Bill. (2003). *A Short History of Nearly Everything.* New York, NY: Broadway Books.

Centers for Disease Control and Prevention. Retrieved December 21, 2010, from http://www.cdc.gov/.

Golden State Donor Services - The Basic Facts. Retrieved December 21, 2010, from http://www.gsds.org/The Basic Facts.

Goubko, C. a, & Cao, X. (2009). Patterning multiple cell types in co-cultures: A review. *Mat Sci Eng: C*, 29(6), 1855-1868.

Kola, I., & Landis, J. (2004). Can the pharmaceutical industry reduce attrition rates? *Nat Rev. Drug discovery*, 3(8), 711-5.

Krsko, P., & Libera, M. (2005). Biointeractive hydrogels. *Materials Today*, 8(12), 36–44.

Lee, S. T., Yun, J. I., Jo, Y. S., Mochizuki, M., Vlies, A. J. van der, Kontos, S., Ihm, J.E., Lim, J.M., & Hubbel, J.A. (2010). Engineering integrin signaling for promoting embryonic stem cell self-renewal in a precisely defined niche. *Biomaterials*, 31(6), 1219–1226.

Lerou, P. H., & Daley, G. Q. (2005). Therapeutic potential of embryonic stem cells. *Blood Rev*, 19(6), 321-31.

Ling, L., Nurcombe, V., & Cool, S. M. (2009). Wnt signaling controls the fate of mesenchymal stem cells. *Gene*, 433(1-2), 1-7.

Lloyd-Jones, D., Adams, R. J., Brown, T. M., Carnethon, M., Dai, S., De Simone, G., et al. (2010). Heart disease and stroke statistics--2010 update: a report from the American Heart Association. *Circulation*, 121(7), e46-e215.

Markx, G. H., Carney, L., Littlefair, M., Sebastian, A., & Buckle, A. M. (2009). Recreating the hematon: Microfabrication of artificial haematopoietic stem cell microniches in vitro using dielectrophoresis. *Biomed Microdev*, 11(1), 143–150.

McBeath, R., Pirone, D. M., Nelson, C. M., Bhadriraju, K., & Chen, C. S. (2004). Cell shape, cytoskeletal tension, and RhoA regulate stem cell lineage commitment. *Dev Cell*, 6(4), 483–495.

Passier, R., Laake, L. W. van, & Mummery, C. L. (2008). Stem-cell-based therapy and lessons from the heart. *Nature*, 453(7193), 322-9.

Reilly, G. C., & Engler, A. J. (2010). Intrinsic extracellular matrix properties regulate stem cell differentiation. *J Biomech*, 43(1), 55-62..

Schudel, B. R., Choi, C. J., Cunningham, B. T., & Kenis, P. J. A. (2009). Microfluidic chip for combinatorial mixing and screening of assays. *Lab chip*, 9(12), 1676-80.

UNOS. Retrieved December 21, 2010, from http://www.unos.org/.

CHAPTER TWO

LITERATURE REVIEW

2.1 INTRODUCTION

The multipotent nature of stem cells provides enormous potential for clinical applications for treatment of disease, cancers, and for organ replacement. Despite decades of research, robust culture techniques that consistently permit isolation, expansion, and directed differentiation of stem and progenitor cells in adequate numbers remains a major hurdle to ensure full clinical usage of stem cell therapies. *In vivo*, stem cell fate is governed by specialized microenvironments termed 'niches'. The stem cell niche consists of supporting cells, extracellular matrix (ECM), and extrinsic cues such as growth factors and cytokines that are spatially and temporally controlled to direct differentiation and maintain stem cell pools (Watt & Hogan, 2008; Schofield, 1978) (Figure 2.1). When removed from niches and cultured *in vitro*, stem cells rapidly lose self-renewal capabilities and undergo spontaneous differentiation due to the loss of intrinsic and extrinsic cues found in stem cell niches and physiological tissues. This loss of stem cell characteristics in culture *in vitro* severely limits the ability to expand and directly differentiate cells into sufficient numbers for clinical usage.

The ability to recapitulate aspects of physiological tissue environments is key to identifying and understanding the intrinsic and extrinsic cues directing stem cell self-renewal and differentiation. Currently, the understanding of spatial and temporal cues directing stem cell fate is generated from tissue culture systems where the cellular microenvironment is regulated in batch conditions. Typical *in vitro* cell culture techniques rely on the use of two-dimensional (2D), plastic surfaces such as petri dishes and tissue culture flasks to propagate, differentiate, and understand cell behavior in response to various small molecules and chemical stimuli. These conventional cell culture techniques are well established and inexpensive. However, traditional systems poorly recapitulate the complex physiochemical tissue environment and offer little control over cell seeding, cell-cell interactions, the biologically

relevant presentation of soluble molecules and unlike tissue they are not three dimensional. Removed from the niche and cultured in *in vitro*, stem cells display altered phenotypes and gene expression and have limited expansion and differentiation capabilities (Birgersdotter, Sandberg, & Ernberg, 2005; Doane & Birk, 1991; Kale et al., 2000). Furthermore, cell isolation techniques are unable to provide homogeneous populations of stem cells. Contaminating cells may secrete soluble molecules that can affect cellular function, select for a subpopulation of cells, or easily proliferate and overtake populations of stem cells. Since cellular responses are mostly measured on a population basis, responses of a small subset or limited population of cells may be masked.

Though recent efforts have increased our knowledge of stem cell biology, little is known about the combinatorial signals that guide stem cell fate. Thorough understanding of the combinatorial microenvironments that direct the behavior and differentiation properties of stem cells require robust culture systems that permit precise control over cell-cell interactions, ECM properties and extrinsic factor delivery. To circumvent limitations of poorly controlled microenvironments found in traditional batch culture systems, cell biologists are looking towards tissue engineering and microfabrication technologies to design culture systems that more accurately recapitulate *in vivo* cellular microenvironments. These technologies combine biomaterial scaffolds with various engineering strategies that provide the ability to tailor cellular microenvironments and provide signals and cues spatially and temporally (Khademhosseini et al. 2006) (Figure 2.2). This review first briefly discusses how the various components of the stem cell niche guide cell behavior, and then reviews the various microscale technologies currently used to recreate the stem cell niche *in vitro*.

2.2 Three Dimensional Environments and the Stem Cell Niche

Physiologic tissue environments are complex, three dimensional (3D) environments that direct cell function through extracellular matrix (ECM), cell-cell interactions, mechanical stimuli, and soluble factors. The concept of stem cell niches, first proposed by Schofield et al. in 1978, suggests that adult stem cells reside in defined compartments (i.e., 'niches') which balance

stem cell self-renewal and differentiation to maintain tissue homeostasis and the stem cell pool (Schofield, 1978). To date, stem cell niches have been identified in a variety of tissues including the bone marrow (S. Shi & Gronthos, 2003; J. Zhang et al., 2003), skin (Tumbar et al., 2004), hair follicles (Ohyama et al., 2006), intestine (Marshman, Booth, & Potten, 2002), brain (Palmer, Willhoite, & Gage, 2000), and muscle (C. a Collins et al., 2005). The stem cell niche provides signals and cues that balance self-renewal, maintenance, and differentiation as well as protect cells from apoptosis and prevent depletion or overpopulation of stem cells. Cells are physically anchored within niche by ECM proteins and supporting stromal cells, which in combination with soluble signals regulate the maintenance and self-renewal of stem cells. Figure 2.1 details the bone marrow niche and the various cues that maintain stem cell function. Within the niche, stem cells either undergo symmetric division to give rise to identical progeny (self-renewal), asymmetric diffusion to produce one stem cell and a differentiated progeny, division without differentiation, or remain quiescent (Watt & Hogan, 2008). Aberrations within the niche are thought to lead to pathologies such as cancer, ageing, and degeneration of tissue function (I. M. Conboy et al., 2005; Corre et al., 2007).

2.2.1. Extracellular Matrix

The extracellular matrix is composed of a combination of proteoglycans, polysaccharides, and proteins that provide structural support to cells. The ECM varies in composition and stiffness from tissue to tissue and plays an integral role in maintaining cellular phenotypes and cell fate decisions. Cells attach to the matrix through integrin receptors on the cell surface that, when bound to their ECM ligands, activate cellular signaling cascades. Loss of cell-ECM interactions results in a specialized form of detachment-induced cell death termed ‘anoikis’, which is derived from the Greek word for homelessness (Frisch & H. Francis, 1994). For example, when cultured in PEG matrices that do not permit cellular attachment, mesenchymal stem cells (MSCs) undergo anoikis. Restoration of cellular attachment by the cell-adhesive peptide Arg-Gly-Asp (RGD) increases viability of encapsulated cells by engaging cell integrin receptors (Benoit & Anseth, 2005; Nuttelman, Tripodi, & Anseth, 2005). Furthermore,

several studies have reported that the stiffness and elasticity of the ECM affect stem cell processes. When cultured on stiff surfaces mimicking bone tissue, MSCs display hallmarks of osteoproginetor differentiation, while culture on soft surfaces promotes adipose differentiation (Winer, Janmey, McCormick, & Funaki, 2009). ECM interactions also govern cell shape and size, which affect cellular survival, proliferation (C. S. Chen, 1997), and differentiation (McBeath, Pirone, Nelson, Bhadriraju, & C. S. Chen, 2004) McBeath et al. patterned fibronectin ECM in various geometries onto tissue culture substrates and seeded human MSCs onto the ECM. Large islands of fibronectin moieties promoted cell spreading whereas cells had a rounded phenotype on small ECM islands. Cells allowed to spread on large islands displayed osteoprogenitor commitment while rounded cells differentiated into adipocytes. A recent study by Chowdhury et al. explored the effects cyclic strain on embryonic stem cells and embryonic differentiated cells (Chowdhury et al., 2010). Cyclic stress induced cell spreading and down regulation of the stemness marker Oct 3 /4, whereas embryonic differentiated cells demonstrated no genotypic or phenotypic changes from the cyclic stressors. It is hypothesized that the cell softness, defined as the ratio of strain to stress on the cells, affects a cells response to stress. As embryonic stem cells are significantly softer than embryonic differentiated cells, it is concluded that the ES cells showed responses to stressors due to greater cyclic strain.

2.2.2. EXTRINSIC FACTORS

Within the niche, stem cells are exposed to a mixture of extrinsic factors that influence cell fate decisions. Such factors include growth factors, cytokines, small proteins, and ions. The spatial and temporal presentation of extrinsic factors within the niche affect stem cell self-renewal and differentiation fates. Secreted factors arise from adjacent cells, from diffusion throughout the niche, or immobilized to ECM proteins. Soluble proteins that affect stem cells include Wnts, hedgehog proteins, fibroblast growth factors (FGFs) and the BMP/TGFβ superfamily. In the neural stem cell niche, for example, TGFβ secreted by nearby differentiated neurons suppress the division of neural stem cells (NSCs) within the niche. It is important to note, however, that the spatial and temporal presentation of soluble molecules can also affect

stem cell activity. Immobilization of growth factors and small proteins by ECM proteins affect concentrations, stability, and bioavailability to niche cells. FGF-2 tethered to fibrinogen increases endothelial cell (EC) proliferation relative to FGF-2 in solution (Sahni, Sporn, & C. W. Francis, 1999). Similarly, bone marrow MSCs exposed to biomaterial surfaces with tethered EGF promotes cell spreading and survival more strongly than soluble EGF (V. H. Fan et al., 2007) Inorganic ion concentrations and gradients within the niche also affect stem cell behavior. Hematopoietic stem cells (HSCs) situated near the endosteal surface are exposed to high calcium levels from nearby osteoblasts and low oxygen tension. These conditions are thought to help maintain HSCs in the quiescent state. In contrast, HSCs situated closer to microvasculature are exposed to higher oxygen tensions and lower calcium ion levels, which promotes HSC division and differentiation (G. Adams et al., 2005).

2.2.3 Cell-Cell Interactions

Stem cells represent a very small portion of adult tissues and exist as single cells or small clusters of cells and are in contact and respond to a variety of differentiated cell types within the niche. These interactions, mediated by adherens and gap junctions, influence stem cell fate. Chondrogenic differentiation of MSCs is facilitated *in vitro* by increasing cell-cell interactions via pellet culture (Pittenger, 1999). Supporting cells such as stromal cells, vasculature, and basal lamina anchor stem cells within the niche and may direct cellular placement to soluble signals secreted by surrounding cells. Osteoblasts anchor HSCs to the perivascular niche through N-cadherins that are involved in maintaining the quiescent state. The proximity of HSCs to osteoblasts places them in high Ca^{2+} and low oxygen tension microenvironments as discussed above, as well as induces production of cytokines and growth factors. However, exposing HSCs to cocktails of these cytokines is not sufficient to maintain stemness, suggesting that direct HSC-osteoblast contact is required for maintenance of stem cell properties (Shiozawa, Havens, Pienta, & Taichman, 2008). Changes in cell density or loss of adheren junctions initiate cell division or migration out of the niche. Loss of cadherin junctions between HSCs and osteoblasts induces loss of HSC and migration out of the niche.

2.3 Engineering Technologies to Guide Stem Cell Fate

To understand the requirements for cell microenvironments, cell biologists and tissue engineers developed microfabrication techniques that enable precise control over cell seeding onto substrates and biomaterials, as well as control spatial and temporal cues within the culture microenvironment. Borrowed from semiconductor and microelectronics industries, microfabrication technologies are able to pattern ECM proteins onto two dimensional substrates such as glass and three-dimensional (3D) substrates and scaffolds to control cell adhesion and cell-cell interactions. Other microfabrication techniques offer the unique ability to mold 3D biomaterials into desired shapes and precisely place cells within biomaterial scaffolds. Either way, such techniques are reproducible and able to create objects from tens of microns to millimeters in size with high resolution. These microscale technologies promise advances in elucidating the *in vivo* function of stem cells and niche components, generation of tissue engineering constructs and for development of high throughput platforms for drug discovery and cell based biosensors. The following sections will first briefly discuss properties of biomaterial scaffolds and then various 2- and 3-D microfabrication technologies to recapitulate aspects of the stem cell niche microenvironments within cell culture surfaces or biomaterial scaffolds.

2.3.1 Biomaterial Scaffolds

Biomaterial scaffolds serve as the foundation for many tissue engineering and microfabrication technologies. A variety of biomaterial matrices, or scaffolds, have been developed to support the 3D culture of cells and tissues. In comparison to traditional 2D cell culture, 3D scaffolds can provide a variety of environmental signals and cues that can restore *in vivo* phenotypes. Made of natural or synthetic materials such as alginate, collagen, poly (ethylene glycol) diacrylate (PEGDA) and polyesters, these materials form biocompatible networks that provide structural support to the cells, allow rapid diffusion of nutrients,

metabolites, and small molecules to and away from encapsulated cells, and are resistant to protein absorption. Many biomaterial scaffolds can be modified to include extracellular matrix molecules, vary mechanical stiffness, and tune degradation properties. Properties of biomaterial scaffolds vary based on application, and have been shown to enhance osteogenic, neural, and adipose differentiation. When selecting biomaterial scaffolds for cell seeding or microfabrication technologies, cell type, fluid dynamics within the scaffold, material stiffness and surface chemistries, method of polymerization, delivery of bioactive molecules, and matrix degradation properties need to be taken into consideration. Several of the microfabrication technologies discussed below utilizes the tunable properties of biomaterial scaffolds to precisely engineer the cellular microenvironment.

2.3.1.1 NATURAL BIOMATERIALS

Natural biomaterials are an attractive source for biomaterial scaffolds as they are components of natural ECM and therefore have similar properties of native tissue, are biocompatible, and many natural ECM scaffolds are FDA approved for transplantation in tissue defects (Dawson, Mapili, Erickson, & Taqvi, 2008; Lutolf & Hubbell, 2005). Natural scaffolds can be individual purified proteins, such as collagen, hyaluronic acid, or fibronection, or multi component matrices derived from tissue sources such as Matrigel. However, many natural biomaterials may be difficult to purify and sterilize and thus difficult to characterize. Other drawbacks include the limited ability to manipulate and modify the mechanical and material properties of natural ECM, such as the degradation rate and crosslinking density (Badylak, Freytes, & Gilbert, 2009).

2.3.1.2 SYNTHETIC BIOMATERIALS

In addition to naturally derived scaffolds, many synthetic materials are available for the 3D support of cells and tissues. In contrast to natural scaffolds, synthetic materials have reproducible properties and chemistries. Most are easily modified to control matrix stiffness,

crosslinking density, degradation rates, and incorporate ligands or functional groups. Some synthetic materials, such as poly (ethylene glycol) and hydroxyapetite are unable to be remodeled or degraded by cells. A majority of synthetic scaffolds require the addition of specific ligands and functional groups to make functional. For example, poly (ethylene glycol) diacrylate (PEGDA) scaffolds, while biocompatible, require the addition of RGD peptide sequences for optimal cell adherence and viability (Nuttelman, Tripodi, & Anseth, 2005).

2.3.2 MICROFABRICATION TECHNOLOGIES

2.3.2.1. PHOTOLITHOGRAPHY

One of the first techniques used to pattern cells and substrates, photolithography utilizes materials that harden or soften in response to light irradiation. A schematic of the photolithography process is presented in figure 2.3. In most cases, photolithographic micropatterns are created by spin coating glass, silicon, or quartz with a thin layer of liquid prepolymer solution termed photoresist. The photoresist is then hardened by irradiation though an opaque photomask of the desired pattern, and excess unpolymerized photoresist removed. The resulting photoresist 'master' is filled with the material of interest (e.g ECM proteins) and the photoresist is removed from the substrate (T. H. Park & Shuler, 2003). Cells are then patterned by selective adhesion to ECM proteins stamped on the culture substrate. Cell adhesion proteins utilized in photolithographic techniques include fibronectin, collagen, laminins, and Matrigel (Lee, Shah, Zimmer, G.-yu Liu, & Revzin, 2008).

Photolithography is able to accurately pattern substrates with a resolution from 2 to 500 μm (Lee, Shah, Zimmer, G.-yu Liu, & Revzin, 2008). Photomasks of the desired pattern are cheaply and easily fabricated with freely available computer software and printed onto transparencies, microfiche films, or quartz/chromium surfaces, depending on the resolution desired (Whitesides et al., 2001). However, the photolithography process requires expensive clean room facilities and many of the solvents used to process the photoresist can easily

denature biological molecules and toxic to living cells. Once created, the photoresist can be reused for several experiments, but changing patterns or design requires fabrication of new photoresist masters that can be cost limiting.

2.3.2.2. SOFT LITHOGRAPHY

As a cheaper and more biocompatible alternative to photolithography, Whitesides and colleagues developed a patterning process termed soft lithography (Xia & Whitesides, 1998). This method is termed soft lithography since it uses 'soft' elastomeric materials such as poly (dimethylsiloxane) or PDMS. PDMS is a durable, biocompatible elastomer that is permeable to gasses, optically transparent, and permissive for culturing cells. Once a PDMS master is formed, it can be used over an extended period of time with little degradation. In soft lithography techniques, a silicon master of the desired pattern is generated, usually by photolithographic techniques. PDMS is cast onto the silicon master and hardened. The resulting PDMS mold can then be used to directly culture cells or a template to form microchannels filled with material or cells of interest (Kane, Takayama, Ostuni, Ingberb, & Whitesides, 2006). Soft lithography techniques are generally able to pattern structures that are 500 nm or larger. Odom et al. improved the resolution of soft lithography patterns into the 50-100 nm range by using composite PDMS stamps (Odom, Love, Wolfe, Paul, & Whitesides, 2002).

One of the most widely used soft lithography techniques; microcontact printing utilizes PDMS molds created by soft lithography to stamp patterns onto tissue culture substrates. The simplest studies simply absorb ECM molecules onto the PDMS stamp and transferred onto substrates. While this type of microcontact printing has been successful in patterning poly-L lysine (James et al., 1998), laminin (James et al., 1998), immunoglobulins (Bernard et al., 1998), and even lipid bilayers (Groves & Boxer, 2002), it may not be suitable for long term biological studies due to the loose linkage of the stamped material and the substrate. To form stronger bonds of the protein and substrate, self-assembled monolayers (SAMs) of alkalinethiols are deposited onto gold surfaces. While non-patterned areas are rendered protein resistant, ECM that is added only absorbs to the SAMs. In most cases, the resolution of this technique is ~100

μm**.** However, using stamps made of polyolefin plastomers Csus et al. were able to stamp fibrinogen proteins using microcontact printing with nanometer scale resolution (Csucs, Kunzler, Feldman, Robin, & Spencer, 2003). Microcontact printing is cost effective and flexible, allowing various substrates and printing material. However, ligand density can vary from experiment to experiment since transfer efficiency of the stamp can vary. Furthermore, physioabsorbed ECM proteins can degrade from the substrate when in contact with the culture medium.

The elastomeric properties of PDMS stamps provides a unique ability to quickly and reversibly seal surfaces to form microfluidic devices. Microchannels formed by the bonding of PDMS to glass substrates can be used to selectively deliver ECM or cells onto the tissue culture substrate through capillary action. In addition, etching of culture surfaces can be created by flowing etching solutions through the microfluidic channels which form grooves to guide cell placement. For patterning in 3D, an etching solution can be carried through the microchannels to create grooves to guide cell placement. In recent studies, biomaterial scaffolds have been patterned by flowing prepolymer solution into the microchannels, then polymerized to form three dimensional structures. Once patterned, the microfluidic device can be used as a culture vessel or is easily removed from the substrate. Drawbacks of microfluidic technology include limited spacing between microchannels- too little spacing between channels can compromise the structural integrity of the PDMS stamp. Due to the requirement of fluid flow, patterns with continuous features can only be implemented. To overcome this problem, Khademhosseni et al. used microfluidics in combination with patterned substrates to trap cells in specific location within the microchannel. They successfully used this technique to pattern embryonic stem cells and MEF feeder cells (Khademhosseini, L. Ferreira, et al., 2006).

2.3.2.3. OPTICAL FABRICATION

Developed by Ashkin et al in 1987, optical trapping techniques utilize tightly focused laser beams to manipulate dielectric particles (Ashkin, J.M. Dziedzic, & Yamane, 1987). Optical tweezers allow precise manipulation and placement of objects in both 2D and 3D. They have

found many uses in biological applications, such as measuring molecular forces (Visscher et al. 1999, 184), manipulating DNA (Wang et al., 1997), cellular organelles (Shelby et al. 2005), viruses (Ashkin, J.M. Dziedzic, & Yamane, 1987) bacterium (Ashkin, J.M. Dziedzic, & Yamane, 1987), and more recently, mammalian cells with minimal damage to cell viability (Uchida et al. 1995).

A typical set up of optical tweezers consists of Nd:YAG or Ti:Sapphire lasers, beam steering optics, and an inverted microscope with high numerical aperture (NA) objectives. To form optical traps, a tightly focused laser beam is directed through a high NA lens onto a dielectric particle. Photon from the point of focus from the laser beam creates an electrical field that attracts dielectrical particles and traps the object near the focal point of the laser. Trapping forces depend on the size and shape of the particle in question as well as properties of the surrounding medium (Berns, 2007; Mazolli, Maia Neto, & Nussenzveig, 2003; Sun, Roichman, & Grier, 2008). Average trapping forces are ~<1 nN, which are sufficient for manipulating most bacterium and mammalian cells. Often, the manipulation of biological molecules requires the use of one or more optical traps. Acoustic optical deflectors (AODs) allows for time sharing of the laser beam between different positions in a planar field. The laser beam dwells at a position for a predetermined period of time before moving to the next position. As long as the 'dark time' is faster than the Brownian motion and diffusion of the cell, the beam is able to fix the position of the object and is as effective as a continuous beam (Brouhard, Schek, & Hunt, 2003).

In addition to directly manipulating cells, optical tweezers have been used to study the effects of mechanical forces on cells. Microbeads are attached to the cell surface through ligands and act as handles for the optical tweezers. Displacement of the microbeads on the cell membrane by optical tweezers generates stretching or bending forces. These techniques can recreate physiological forces from stretching, compression, and ECM stiffness. Wang et al. used this technique in combination with fluorescent resonance energy transfer (FRET) to study the mechano-activation of Src, an important signal transduction molecule playing an important

role in self-renewal and differentiation of stem cells, as well as in many cancers (Wang et al., 2005).

Minimizing damage to cells during manipulation is a major factor in optical trapping design and optimization. Cellular viability is dependent on laser wavelength, laser power, and duration of exposure to the traps. Biological specimens typically absorb light in the near infrared range, and thus most lasers are often tuned in the 800-1000 nm range (Vorobjev, Liang, W. Wright, & M. Berns, 1993). Vorobjev et al. reported faulty mitosis and abnormal chromosome bridges in PtK2 cells exposed to continuous wave optical traps in the 760-765 nm range and minimal damage to 700 and 800-820 nm light (Vorobjev, Liang, Wright, & Berns, 1993). Similarly, Liang et al. demonstrated wavelength dependence on the growth of Chinese hamster ovary (CHO) cells. When exposed to 740-760 and 900 nm light, CHO cells had poor growth and cell division characteristics compared to non-irradiated controls. Light in the 950-990 nm wavelengths resulted in the highest clonablilty of all wavelengths tested. In all cases, shorter exposure and lower power of traps result in increased cellular function (Liang et al., 1996). Time shared optical traps, as described above; reduce the exposure of biological samples to laser light as compared to continuous wave (CW) technology. Mirisaidov et al. discovered that, under the same wavelength and duration of trapping, *E. coli* bacterium displayed higher viability with time shared optical traps than with CW traps (Mirsaidov et al., 2008).

Optical trapping provides stringent control of the cell and its placement within an environment with a resolution of ~19 nm. To permanently fix cells in position for long term studies, Jordan et al and Akselrod et al. entrapped cells into 3D scaffolds with minimal effect on cellular viability (Akselrod et al., 2005; Jordan et al., 2005). Optical tweezers, however, require some knowledge of optical technologies for set up and use. As of yet, most cellular studies utilizing optical trapping are relatively low throughput and monitoring only 10-1000 cells in a single experiment.

In recent years, a new field of optical trapping termed plasmonic trapping has emerged. When light is applied to metal nanoparticles, photons excite the electrons in the nanoparticles

that form energy waves and strong electromagnetic fields. Plasmonic trapping was first coupled with optical tweezers for nanotechnology applications as a method to enhance optical gradient forces from optical tweezers, and therefore reducing the Brownian motion of nanoparticles in traps. Combining optical tweezers and plasmonic traps, the power required to manipulate and trap biological objects can be greatly reduced (Righini, Zelenina, Girard, & Quidant, 2007). More recently, Huang et al. designed a plasmonic trapping device in a microfluidic system for lab on chip applications. Whereas cell viability was not explored, the team was able to successfully trap single nanoparticles and *S. cerevisae* cells in plasmonic traps without the complex optical setup required for optical tweezers (L. Huang, Maerkl, & O. J. F. Martin, 2009). Still in its infancy, plasmonic trapping holds great potential as a new cell patterning technique or to augment biological optical trapping setups.

Another form optical trapping technologies to pattern cells is laser guided direct writing (LGDW). Utilizing the same principles as optical trapping, a weakly focused laser beam is used to trap and direct cells down hollow fibers onto cell culture surfaces. This method provides single cell manipulation with ~1 μm scale resolution (Odde & Renn, 2000). Nahimas et al. have used LGDW to create vascular and sinusoid-like structures onto collagen scaffolds (Nahmias, Schwartz, Verfaillie, & D.J. Odde, 2005). It is unknown what effects laser power has on cell viability. Unless the substrate is patterned with adhesion molecules, the cells will randomly spread on the substrate after patterning.

2.3.2.4. DIELECTROPHORESIS (DEP)

Dielectrophoresis has emerged as a promising technique to identify and place cells and microparticles through their electrical properties, size, and shape of the entrapped specimen. When presented to a non-uniform electric field, all objects exert some dielectrical forces that can change the motion of the particle. The strength of the force and movement depends on the size, shape, and electrical properties of the object and the surrounding medium (Chiou, Ohta, & Wu, 2005)(H Morgan, Hughes, & Green, 1999). DEP technology has mainly been utilized in cell sorting applications, as no modification or manipulation is required prior to

sorting. Recently, DEP has undergone resurgence in for micromanipulation and patterning of DNA, viruses, proteins, and cell applications (Chou et al., 2002; Pethig & Gerard H Markx, 1997).

To pattern cells using DEP, electrodes are microfabricated into a microfluidic chip or other culture devices. Thousands of individual electrodes can be placed on a centimeter of surface area using common microfabrication techniques. Cells are introduced into the system and pulled toward the electrode surface through DEP forces. Fluid flow across the surface removes unpatterned cells. After trapping, cells can then either be encapsulated in 3D scaffolds or adherent cell lines can be cultured on the surface. As with optical trapping technology, the duration and intensity of electrical stimulation can affect biological activity of living cells. Grey et al. demonstrated DEP patterning of mammalian cells using bovine aortic endothelial cells (Gray, 2004). The group patterned a 1 x 1 cm^2 array within 5 minutes with minimal effect on cell viability. Suzuki et al. further modified the procedures by exposing C2C12 cells to DEP forces for 5 minutes to allow cell adherence, flushed the device, and electropatterned again with a second cell type (Suzuki, Yasukawa, Shiku, & Matsue, 2008). Albrect et al. successfully patterned cell laden alginate beads with DEP technologies (Albrecht, Underhill, Mendelson, & Bhatia, 2007).

With DEP technology, the precise location of cells and microparticles can be patterned onto various substrates. The technology is rapid and easily scaled for larger experiments. However, there is little control over the exact cells that are patterned, and co-culture experiments so far have only been established by engaging one set of electrodes, removing the cells, then flowing in the next cell type. Exposure to high power traps must be limited as they may result in cell death or local heating of the medium. In DEP applications, the cells must be suspended in low conductivity medium, as physiological medium has high electrical conductivity and will not allow DEP to occur. This medium may be toxic to living cells, so exposure to the medium must be limited. Alternatively, negative DEP occurs when the object is less polarizable than the surrounding medium, allowing patterning in physiological medium (Thomas, Hywel Morgan, & Green, 2009).

2.3.2.5. INKJET PRINTING

Another microfabrication technique that adapted technologies from an electronics industry is inkjet printing of biomaterials, scaffolds, and cells. Commercially available inkjet printers reproduce electronic images by depositing nanoliter sized drops of ink onto the paper substrate. Inkjet patterning technologies utilize these same commercial inkjet printers and ink cartridges to deposit small drops of 'ink' (i.e proteins, alkanethios, scaffold materials, and more recently, cells) onto 'paper' (i.e., tissue culture substrate) into desired configurations. More recently, this technology has been used to pattern cells in the same manner. The resolution of inkjet printing is approximately 350 μm. While the resolution of inkjet printing is significantly lower than other microfabrication techniques, the configuration of deposited patterns is easily changed without the costs and time constraints of fabricating new masters (Phillippi et al., 2008).

2.4 CULTURE HANDLING SYSTEMS

2.4.1. BIOREACTORS

Expansion of progenitor cells in traditional static cultures leads to a loss of proliferation and differentiation potential of stem and progenitor cells, therefore severely limiting the number of cells available for tissue engineering and stem cell therapies. Once seeded into culture, cells require a proper balance of nutrients, oxygen, soluble molecules, and waste removal that is typically provided *in vivo* by the vasculature system. The static culture of cells in either 2D or 3D results in gradients of nutrients and small molecules. Further limiting the application of 3D scaffolds is that nutrients and oxygen can only penetrate the scaffold for a few hundred microns, leaving large constructs with a hypoxic and necrotic center surrounded by viable cells (Martin, Wendt, & Heberer, 2004). Static culture conditions so do not recapitulate the laminar flow and shear stress features found in physiological tissue environments. These limitations severely inhibit the continued expansion of cells, the size of scaffolds available for use and differentiation capabilities of seeded stem cells. Another

limitation to the clinical usage 3D scaffolds and stem cells is the isolation, expansion, and differentiation of stem cells in sufficient quantities to seed into scaffolds or for cell based therapies. Bulk cultures of cells and scaffolds also result in local microenvironmental changes which form concentration gradients that can affect cell behavior.

Bioreactors are cell culture vessels designed to provide strict control over culture conditions such as temperature, pH, oxygen levels, and for the perfusion of medium in large cultures of cells and 3D constructs. Many different types of bioreactors have been used for the culture and expansion of stem cells and 3D scaffolds such as stirred flask bioreactors, rotating wall vessels, perfusion chambers, and microfluidic bioreactors. These bioreactors offer a distinct advantage over traditional cell culture as they provide automation, the ability to control and change culture parameters, and offer a more homogeneous environment for cell culture. Parameters can easily be changed from one experiment to another and are highly dependent on the objective of the experiment (i.e. expansion or differentiation). Continuous mixing of oxygen in nutrients in bioreactors reduces concentration gradients and increase nutrient diffusion throughout cellular colonies and constructs (Zhao, Grayson, Ma, & Irsigler, 2009).

Initial studies of stem cells in bioreactors reported the increased expansion and long term maintenance of HSC over static culture systems. In particular, recent studies have revealed that HSC expansion is improved in bioreactors as compared to static culture conditions. Murine hematopoetic stem cells cultured in stirred flask bioreactors showed a 5 fold increase of the stemness marker Sca1+ and a 4 fold increase in long term culture initiating cells (LTC-IC) over 21 days of culture. Expansion of murine ESCs increased without the need of feeder layers or loss of differentiation potential (Zandstra, Eaves, & Piret, 1994). Bioreactors have also enabled the scaling the expansion of embryoid body culture. Cameron et al. reported increased expansion, more uniform morphology and maintenance of differentiation potential of embryoid bodies in stirred vessel bioreactors (Cameron, Hu, & Kaufman, 2006).

Bioreactors have also been extensively used to seed progenitor cells onto 3D scaffolds. Important for the development of functional tissue engineering constructs, cell seeding of scaffolds remains a highly variable process. Bioreactor based seeding methodologies have

resulted in increased seeding densities and efficiencies and more uniform distribution of cells within the scaffold (Wendt, Riboldi, Cioffi, & Ivan Martin, 2009). Seeding efficiency depends on cell type and density, scaffold type, and flow rates of culture medium. Both murine and human MSC have been efficiently seeded onto a variety of scaffolds using stirred flask and perfusion bioreactors. In general, most studies have reported increased seeding efficiency, density, cell penetration, and overall more uniform distribution of cells throughout the scaffold using spinner and perfusion bioreactors. MSCs seeded and cultured onto 3D scaffolds increased expansion while maintaining differentiation capacity as compared to cells cultured in traditional culture vessels (Braccini et al., 2005).

High flow rates needed for efficient seeding and nutrient diffusion however, can greatly affect cellular processes. Structural integrity of seeded scaffolds can be compromised by fluid channel formation at high flow rates. Even at low velocities, shear stresses imparted onto cells can be significant (Tada et al., 2000). Often, the fluid flow required for efficient cell seeding and nutrient mixing is significantly higher than what is found in physiological tissues (100 µl/sec and 0.1-10 µl/sec, respectively) (Zhao, Grayson, Ma, & Irsigler, 2009). Shear tolerance of cells and scaffolds depends on the cell type, scaffold used, and experimental parameters. Mechanical loading imparted by shear can affect cellular differentiation. Higher fluid rates are conductive to osteogenic differentiation of MSCs where lower rates facilitated expansion. Fluid rates also affect ECM distribution, for example. Zhao et al. reported decreased collagen and laminin I deposition in cell seeded scaffolds (Zhao, Grayson, Ma, & Irsigler, 2009) Differentiation into osteoblasts was promoted at high flow rates. Similarly, bovine chondrocytes seeded on PGA scaffolds had increased GAG formation and synthesis, while net GAG accumulation throughout the scaffolds was reduced, most likely by release of GAG into culture medium in stirred flask bioreactors (Martin et al., 1999). To protect cells from shear stressors in bulk culture systems, cells have been encapsulated in alginate microbeads and cultured in bioreactors.

2.4.2. MICROFLUIDICS

In vivo cellular microenvironments are highly dynamic environments in which soluble factor concentration can vary drastically on a scale of microns. In traditional cultures, soluble factors and medium exchange require the physical removal of culture medium and bolus delivery of soluble factors, resulting in a homogeneous mixture that is difficult to control in real-time on a microscale level. Microfluidic bioreactors, on the other hand, allow soluble factor delivery and replacement in a matter of seconds, allowing real-time control over the cellular microenvironment. Fluid flow rates, pressures, and soluble factor concentration and delivery are easily manipulated using these devices (Yarmush & King, 2009). Microfluidic bioreactors are formed by creating a master of desired pattern with soft lithography techniques and stamps are most commonly made of PDMS. The PDMS stamps contain one or more channel systems to direct nutrient, oxygen, and soluble factor flow on a micro-scale level. Fluid flow is typically controlled by syringe pumps that allow for rapid and pulsatile delivery of stimuli and can also maintain cultures for weeks at a time. Microfluidic devices designed with two or more channels permit the controlled mixing of soluble factors. Laminar flow in microchannels allows one or more streams of fluid to combine with limited mixing of streams. Thus, a single cell can be exposed to multiple microenvironments by placement at an intersection of streams carrying different soluble molecules (Eriksson et al., 2010).

2.5 READOUT SYSTEMS

Once cells are exposed to various microenvironments, the activity of the cells in response to its stimuli can be assessed. There are several well established techniques to monitor cellular activity. On a large scale, dynamic responses of the culture in whole can be measured by degree of expansion and apoptosis, morphological changes, migration, and differentiation. Stem cell differentiation has been readily identified through histochemistries such as alkaline phosphatase/von Kossa staining, oil red O, and safranin staining to elucidate bone, fat, and cartilage differentiation of mesencyhmal stem cells (Pittenger, 1999). Molecular characteristics can be measured by western blotting, RT-PCR, ELISA and other well established

techniques. However, such measurements are end-point assays that require fixation or cell lysis. Since these methods measure the population as a whole, the signature of stem cells may be lost due to contaminating cell types. The discovery of green fluorescent protein (GFP) and its variants has enabled single and live cell imaging to visualize cellular processes. GFP can be expressed as a fusion tag to proteins of interest to explore protein-protein interactions and gene activation and expression (Chalfie, Tu, Euskirchen, Ward, & Prasher, 1994; van Roessel & Brand, 2002). Specific organelles can be targeted, such as the staining of the actin cytoskeleton. Other assays have been developed using variants of GFP, such as fluorescent resonance energy transfer (FRET) and fluorescent resonance after photobleaching (FRAP), which uses fluorescent protein pairs to monitor cellular interactions in real-time (Ha et al., 1996). Recently, to improve dynamic sensing of cellular activity, a mutated form of GFP has been developed. This GFP mutant shifts color spectrum as the protein matures. When the protein is first synthesized, the cell is green in color, but shifts to red fluorescence in a time dependent manner. Thus, readouts of gene expression dynamics and protein synthesis can be monitored in real time by the ratio of green to red fluorescence (Terskikh et al., 2000).

2.6 Conclusions and Future Directions

Tissue engineering and microfabrication technologies have arisen as an invaluable tool to probe the spatial and temporal cues that govern stem cell fate. The ability to precisely pattern cells and external signals in 2- and 3-D enables investigations into the roles of niche components on stem cell plasticity and differentiation. These approaches require 1) biocompatible scaffolds with defined mechanical properties; 2) microfabrication of scaffolds and signals into specific geometries; 3) controlled seeding and placement of cells and signals; 4) effective culture systems for nutrient delivery; and 5) readout systems to monitor cellular activity during culture. While extensive research has been conducted in establishing these technologies, the generation of functional stem cell niches and culture systems will require a multi-disciplinary approach that combines and applies these technologies into functional stem cell environments. Combination of engineering approaches with traditional cell biology

approaches will facilitate recapitulation of functional stem cell microenvironments and advance our knowledge of functional stem cell niches.

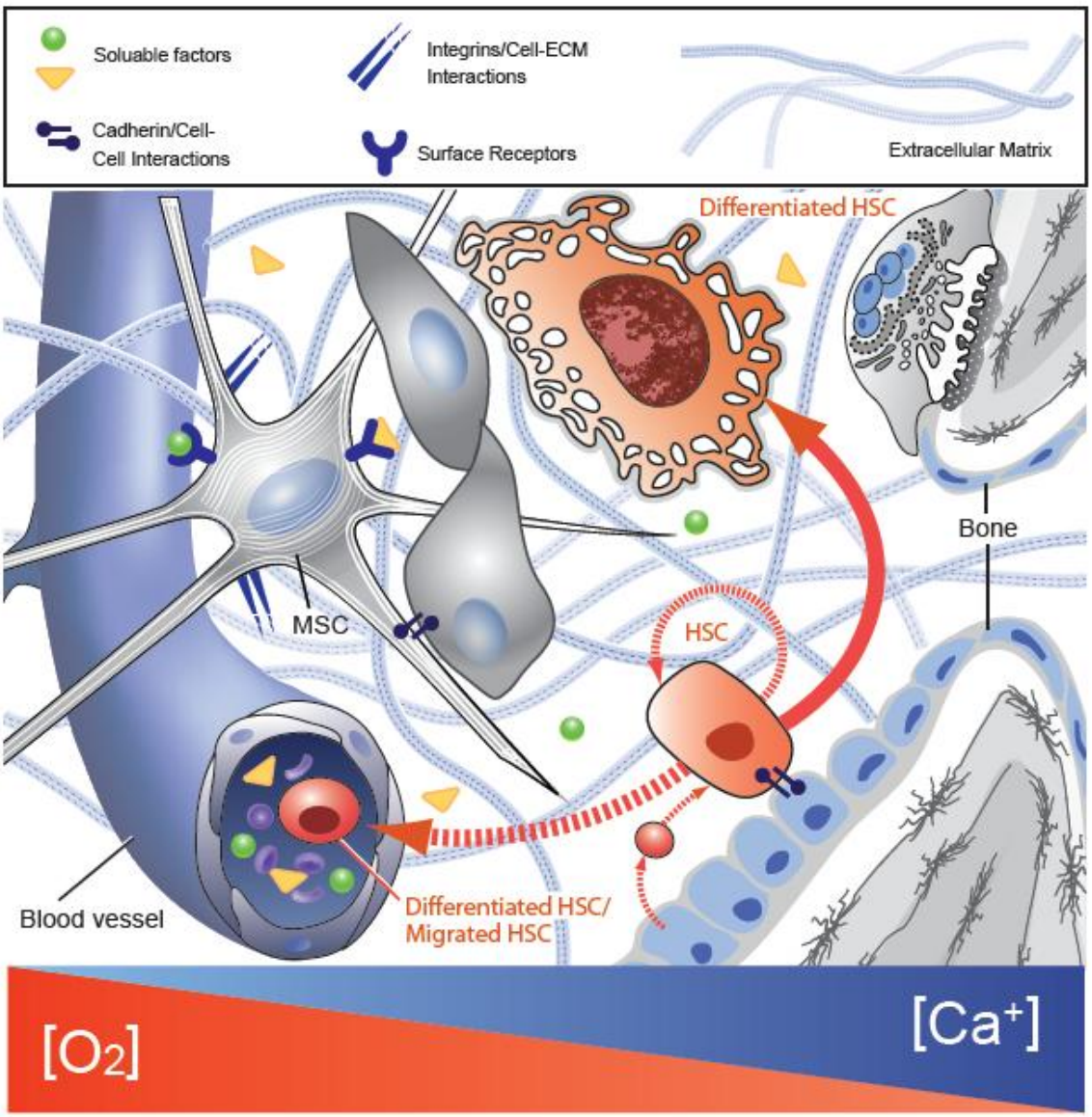

Figure 2.1. **The Perivascular and Endosteal Bone Marrow Niche: Example of Signals and Cues Regulating Stem Cell Function**. The stem cell niche is a complex microenvironment that guides stem cell fate through a combination of extracellular matrix (ECM), cell-cell interactions, and extrinsic factors such as growth factors and cytokines. In the bone marrow, hematopoetic stem cells (HSCs) situated in the endosteal niche are physically anchored to the niche by cadherens junctions with osteoblasts (cell-cell interactions). In this location, cells are exposed to high Ca^{2+} concentrations, low oxygen tension, and a variety of autocrine, paracrine, and endocrine signals (extrinsic factors), and are attached to the ECM through integrin receptors. These signals and cues maintain the quiescence and self-renewal of HSCs. In the perivascular niche, however, HSCs are exposed to low Ca^{2+}, high oxygen tension, different cell-cell interactions and ECM composition that promote migration and differentiation of stem cells. While a majority of these signals are found in a variety of stem cell niches, their utilization and effect of niche components vary from niche to niche.

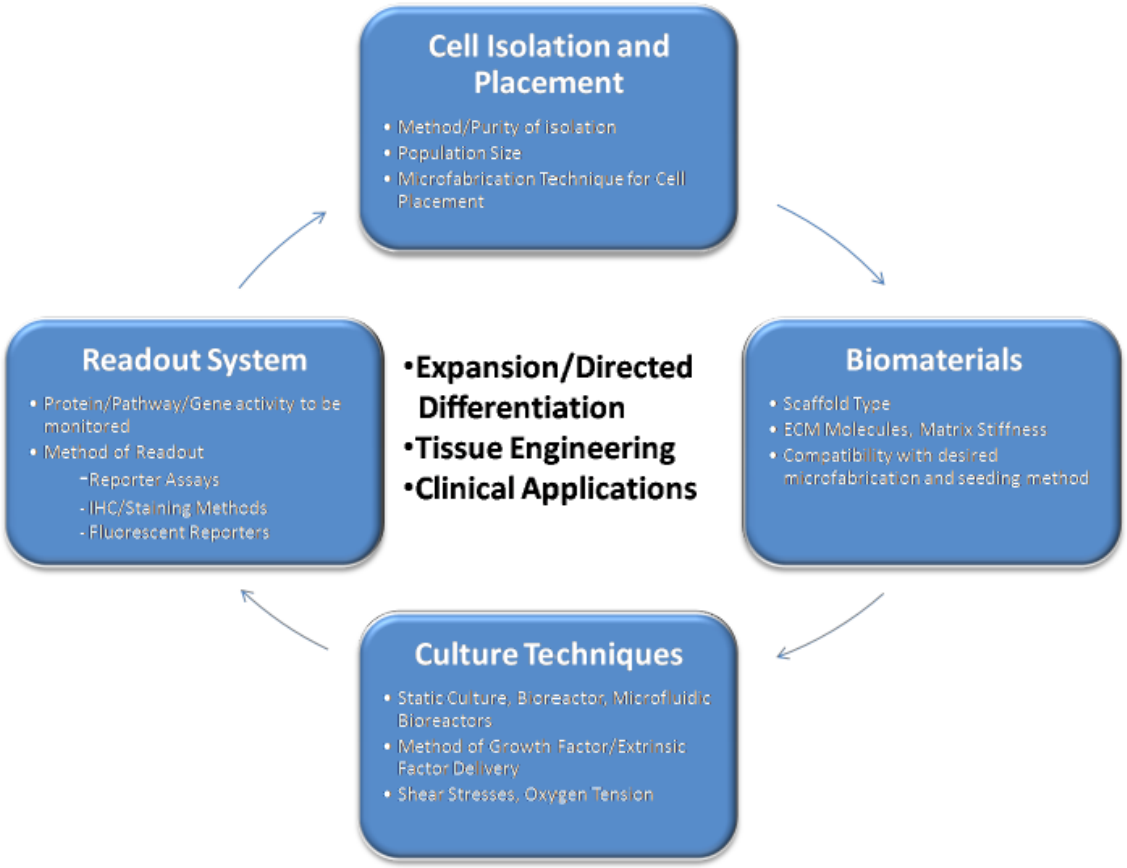

Figure 2.2. Overview of Processes to Design Environments that Guide Cell Fate. First, the cell source or line, isolation, and optimal microfabrication technique for the study or application must be identified. Biomaterials selected for microfabrication techniques must be compatible with the cell and microfabrication technique of interest. Modifications of biomaterials such as the incorporation of ECM molecules or material stiffness can affect cellular processes. Culture techniques provide nutrient delivery and waste removal to microfabricated cells. Spatial delivery of growth factors, cytokines, and other extrinsic factors can be controlled by bioreactors and microfluidics bioreactors. The culture technique or bioreactor type can affect nutrient delivery throughout scaffolds, provide shear stresses, affect cell seeding into scaffolds, or modulate ECM deposition by cells. Lastly, systems to monitor cellular activity in your microfabrication system must be identified. Assays can be end-point such as cellular staining, or measured in real time by reporter assays. Each of these factors must be taken into consideration when designing microfabrication experiments.

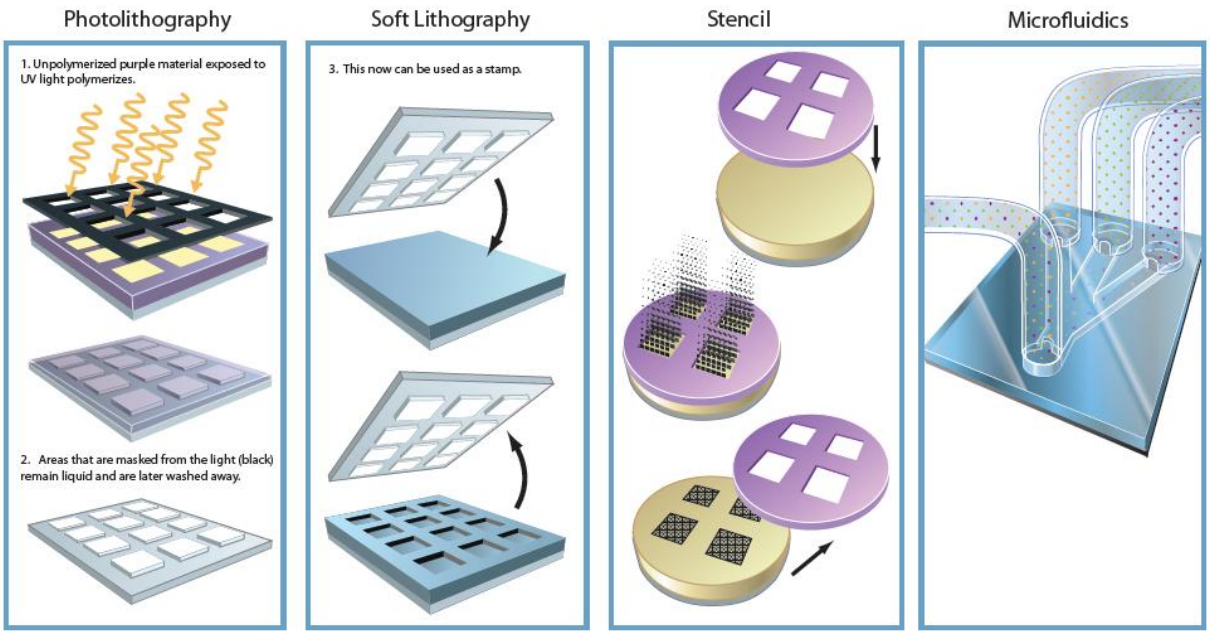

Figure 2. 3. Micropatterning Techniques. (A) Photolthithography. To create patterns using photolithography, a thin film of photopolymerizable material such as photoresist or poly (ethylene glycol) diacrylate hydrogel (PEGDA) is spun onto a glass substrate. The material is photopolymerized through a mask of the desired pattern. The material only hardens where exposed to light, and unexposed material is washed away. The resulting material can be used to directly culture cells, as a master to mold and shape 3D scaffolds, as a stamp in for soft lithography (b) as a stencil (c), or as a microfluidic device (d). (B) Soft Lithography. A master is formed in the desired pattern using photolithographic techniques and then filled with material such as PDMS, a soft elastomateric material that is commonly used for soft lithographic techniques. This stamp can be dipped directly into extracellular matrix molecules such as fibronectin, or functionalized with alkanethiols, and stamped onto substrates. (C) Stencil. The master created by photolithographic techniques can be used as a stencil to limit exposure of the substrate to molecules. (D) Microfluidic devices. Generally, microfluidics devices are formed in the same manner as stamps for soft lithography, but have continuous channels to allow for fluid flow. These microfluidic devices can be used as guides to deposit ECM or cells, and then are peeled off the substrate. Additionally, they are used as bioreactors to control fluid flow, soluble molecule presentation, and cell deposition.

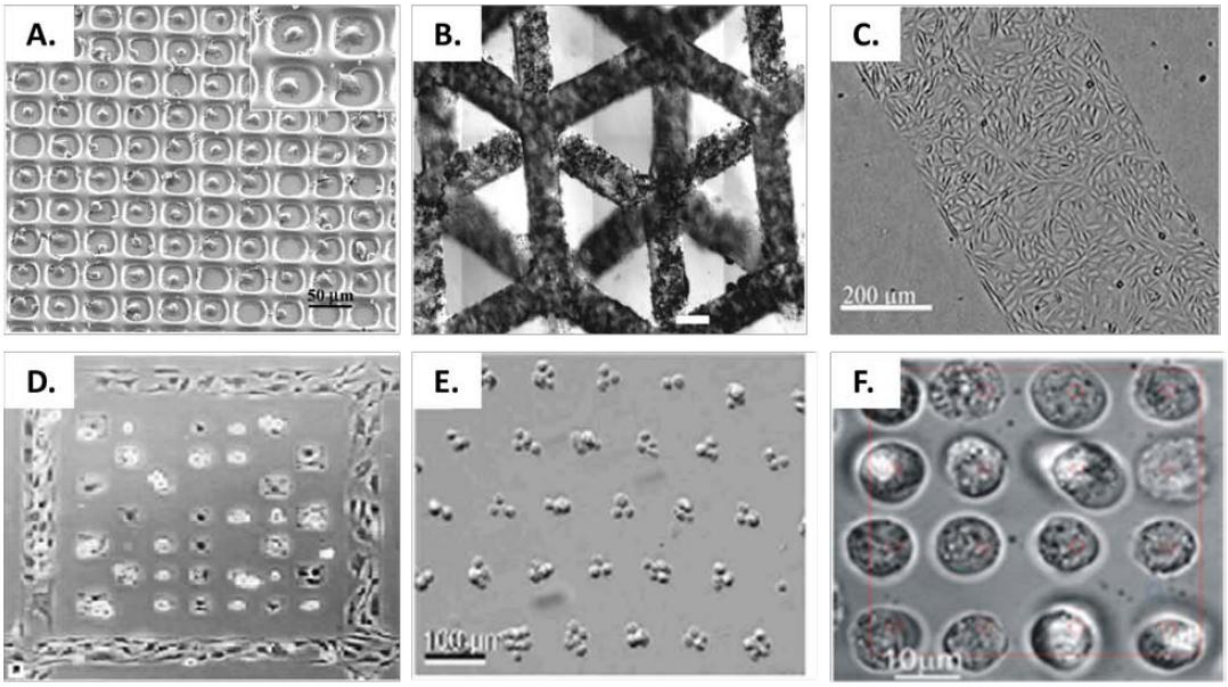

Figure 2. 4. Micropatterning Techniques. (A) and (B) 2 and 3 dimensional photolithography. (A) Mouse 3T3 fibroblast cells seeded into poly (ethylene glycol) (PEG) wells created by photolithography. The PEG wells guided and patterned cellular adhesion to the glass surface. Reprinted with permission from Revzin et al. Copyright 2003 American Chemical Society. (B) Hepatocytes were patterned into three dimensions by additive photolithography of photopolymerizable poly (ethylene glycol) diacrylate (PEGDA) hydrogels. Reprinted with permission from Tsang et al. Copyright 2007 FASEB. (C) Inkjet Printing. Defined patterns of collagen were deposited onto cell-repellant agarose surfaces by inkjet printing. Smooth muscle cells (SMCs) were seeded onto the surface and adhered only to patterned collagen surfaces. Reprinted from Roth et al. Copyright 2004 with permission from Elsiver. (D) Soft lithography/microcontact printing. Hexadecanetholate and tri (ethylene glycol) were printed onto gold surfaces by microcontact printing. The ECM molecule fibronectin absorbs to the hexadecanethilate but not onto tri (ethylene glycol). Bovine capillary endothelial cells (BCE) were patterned by selective adhesion to the fibronectin coated areas. Reprinted from Kane et al. Copyright 1999 with permission from Elsiver. (E) Dielectropheresis. Arrays of fibroblasts patterned through dielectropheresis methodology and encapsulated in PEGDA hydrogels. Albrecht et al. Reproduced by permission of The Royal Society of Chemistry. http://dx.doi.org/10.1039/b406953f (F) Optical Tweezers. Human monocytic U937 cells manipulated into a 4x4 array by optical tweezers and encapsulated in PEGDA hydrogels. (Trump, unpublished data).

Niche Component	Engineering Strategies	Examples	References
Extracellular Matrix			
Substrate Stiffness	Scaffold/Substrate Type and Design	Human ESCs cultured on PDMS surfaces of varying stiffness affected cellular spreading, growth rate, and osteogenic differentiation. Culture of cells on stiff surfaces increases the degree cell spreading, attachment, and osteogenic differentiation as compared to softer substrates.	(Evans et al., 2009)
Ligand Presentation and Gradients	Inkjet Printing	Patterns of collagen printed onto agarose films directed smooth muscle cell and primary neruon attachment in pre-defined patterns	(Roth et al., 2004)
	Microcontact Printing	Microcontact Printing techniques have been used to specifically place ECM ligands onto cell repellant surfaces to determine effects of ECM on cellular activity	(McBeath, Pirone, Nelson, Bhadriraju, & Chen, 2004) (Offenhausser et al., 2007)
	Microfluidic Patterning	Microfluidic chips create gradients of Fc-tagged fusion proteins through laminar flow deposition	(Cosson, Kobel, & Lutolf, 2009)
	Photolithography	Two photon laser scanning photolithography micropatterned RGDs onto 3D hydrogel scaffolds to direct cell migration	(Lee, Shah, Zimmer, G.-yu Liu, & Revzin, 2008)(S.-hong Lee, Moon, & West, 2008)
Topography	Laser Guided Direct Writing	Direct writing techniques fabricate biomaterial scaffolds with precise 3D architecture and composition to guide cell patterning and behavior	(Lewis, 2004)
	Photolithography	Photolithorgraphic masks precisely pattern poly (ethylene glycol) diacrylate (PEGDA) scaffolds into desired architectures. Sequential patterning allows for development of 3D architectures	(Hahn et al., 2006)
Cell-Cell Interactions			
Direct Cell Placement in 3D	Optical Tweezers	Time-shared optical tweezers used in conjunction with microfluidic devices allow precice 2- and 3D placement of *E. coli* bacterium within hydrogel scaffolds	(Mirsaidov et al. 2008)
	Dielectropheresis	Dielectophereisis techniques enable trapping of single cells and cell laden hydrogels within 3D scaffolds	(Albrecht, Underhill, Mendelson, & Bhatia, 2007)
	Plasmonic Trapping	*S. Cerivisae* were arranged into arrays of defined architecture using plasmonic traps and microfluidic devices	(Huang, Maerkl, & Martin, 2009)

Table 2.1 (cont. on next page)

	Bioreactors	Rotating Wall Vessel (RWV) bioreactors improve cell seeding density and uniformity within 3D scaffolds	(Martin, Wendt, & Heberer, 2004)
Direct Cell Placement in 2D	Microcontact Printing	Microcontact printing of ECM modulates placement and cell-cell interactions by selective adhesion of cells to defined substrates	(Ruiz et al., 2008)
	Laser Guided Direct Writing	Optical forces directly placed chick neuronal cells onto glass surfaces in various 2D patterns with minimal loss in cellular viability	(Odde and Renn 2000)
	Inkjet Printing	Chinese Hamster Ovary (CHO) Cells were specifically placed onto biomaterial substrates in predefined patterns via inkjet printing technologies	(Xu et al. 2005)
Extrinsic Factors			
Growth Factor, Culture Medium, and Inorganic Ion Delivery	Inkjet Printing	Muscle derived stem cells (MDSCs) cultured on patterns of BMP-2 printed onto fibrin substrates. Cells cultured on BMP-2 patterned substrates in myogenic conditions differentiate into osteoblasts while unpatterned cells differentiate into myoblasts	(Phillippi et al., 2008)
	Microfluidic Bioreactors	Oxygen gradients of differing size and shape were created in specially designed microfluidics where fluid flow was controlled by a computer controlled gas mixer. Pressure driven laminar flow quickly switches solution streams presented to cell, enabling rapid microenvironmental changes and growth factor delivery.	(Allen, Milne, Doepker, & Chiu, 2010) (Adler, Polinkovsky, Gutierrez, & Groisman, 2010)
	Bioreactors	Mass transport of growth factors, ions, and oxygen is increased in several types of bioreactors, leading to increased cellular proliferation, matrix deposition, and differentiation	(Martin, Wendt, & Heberer, 2004)
Shear Stresses	Bioreactors and Microfluidic Bioreactors	Shear stresses are modulated through changes in design, fluid flow and fluid velocity throughout microfluidics and bioreactors	(Martin, Wendt, and Heberer 2004)

Table 2.1 Strategies to Engineer Various Components of the Stem Cell Niche.

LIST OF REFERENCES

Adams, G.B, Chabner, K.T, Alley, I.R., Olson, D.P., Szczepiorkowski, Z.M., Poznansky, M.C., Kos, C.H., Pollak, M.R., Brown, E.M., & Scadden, D.T. (2005). Stem cell engraftment at the endosteal niche is specified by the calcium-sensing receptor. *Nature,* 439, 7076: 599–603.

Adler, Micha, Mark Polinkovsky, Edgar Gutierrez, & Alex Groisman. (2010). Generation of oxygen gradients with arbitrary shapes in a microfluidic device. *Lab chip,* 10: 388-91.

Akselrod, G M, W Timp, Q Zhao, C Li, U Mirsaidov, R Timp, K Timp, P Matsudaira, & G Timp. (2005). Laser-Guided Assembly of Heterotypic 3D Living Cell Microarrays. *Biophy J,* 91: 3465-73.

Albrecht, D.R, Underhill, G.H., Mendelson, A., & Bhatia, S.N. (2007). Multiphase electropatterning of cells and biomaterials. *Lab chip,* 7: 702-9.

Allen, P.B, Milne, G., Doepker, B.R., & Chiu, D.T. (2010). Pressure-driven laminar flow switching for rapid exchange of solution environment around surface adhered biological particles. *Lab chip,* 10: 727-33.

Ashkin, A, J.M. Dziedzic, & T. Yamane. (1987). Optical Trapping and Manipulation of Single Cells using Infared Laser Beams. *Nature,* 330: 769-71.

Badylak, S.F., Freytes, D.O., & Gilbert, T.W. (2009). Extracellular matrix as a biological scaffold material : Structure and function. *Acta Biomaterialia,* 5: 1-13.

Benoit, D.S.W, & Anseth, K.S., (2005). The effect on osteoblast function of colocalized RGD and PHSRN epitopes on PEG surfaces. *Biomaterials,* 26: 5209-20.

Bernard, A., Delamarche, E., Schmid, H., Michel, B., Bosshard, H.R., & Biebuyck, H. (1998). Printing patterns of proteins. *Langmuir*, 14: 2225–2229.

Berns, M.W. (2007). Optical Tweezers: Tethers, Wavelenths, and Heat. In *Methods in Cell Biology*, 82:457-466.

Birgersdotter, A., Sandberg, R., & Ernberg, I. (2005). Gene expression perturbation in vitro--a growing case for three-dimensional (3D) culture systems. *Sem Cancer biol,* 15: 405-12.

Braccini, A, D Wendt, C Jaquiery, M Jakob, M Heberer, L Kenins, A. Wodnar-Filipowicz, R Quarto, & I Martin. (2005). Three-Dimensional Perfusion Culture of Human Bone Marrow Cells and Generation of Osteoinductive Grafts. *Stem Cells,* 23: 1066–1072.

Brouhard, G.J, Schek, H.T., & Hunt, A.J. (2003). Advanced optical tweezers for the study of cellular and molecular biomechanics. *IEEE transactions on bio-medical engineering,* 50: 121-5.

Cameron, C., Hu, W.S., & Kaufman, D.S. (2006). Improved development of human embryonic stem cell-derived embryoid bodies by stirred vessel cultivation. *Biotech Bioeng,* 94: 938–948.

Chalfie, M., Tu, Y., Euskirchen, G., Ward, W.W. & Prasher, D.C. (1994). Green fluorescent protein as a marker for gene expression. *Science,* 263: 802–805.

Chen, CS. (1997). Geometric Control of Cell Life and Death. *Science,* 276: 1425-1428.

Chiou, P.Y., Ohta, A.T., & Wu, M.C. (2005). Massively parallel manipulation of single cells and microparticles using optical images. *Nature,* 436: 370-2.

Chou, C, Tegenfeldt, J., Bakajin, O., Chan, S., Cox, E., Darnton, N., Duke, T., & Austin, R. (2002). Electrodeless Dielectrophoresis of Single- and Double-Stranded DNA. *Biophys J,l* 83: 2170-2179.

Chowdhury, F., Na, S., Li, D., Poh, Y., Tanaka, T.S., Wang, F., & Wang, N. (2010). Material properties of the cell dictate stress-induced spreading and differentiation in embryonic stem cells. *Nat Materials,* 9: 82-8.

Collins, C.A., Olsen, I., Zammit, P.S., Heslop, L., Petrie, A., Partridge, T.A., & Morgan, J.E. (2005). Stem cell function, self-renewal, and behavioral heterogeneity of cells from the adult muscle satellite cell niche. *Cell,* 122: 289-301.

Conboy, IM, Conboy, M.J., Wagers, A.J., Girma, E.R., Weissman, I.L., & Rando, T.A. (2005). Rejuvenation of aged progenitor cells by exposure to a young systemic environment. *Nature,* 433: 760-4.

Corre, J, K Mahtouk, M Attal, M Gadelorge, a Huynh, S Fleury-Cappellesso, C Danho, et al. (2007). Bone marrow mesenchymal stem cells are abnormal in multiple myeloma. *Leukemia,* 21: 1079-88.

Cosson, S., Kobel, S.A., & Lutolf, M.P. (2009). Capturing Complex Protein Gradients on Biomimetic Hydrogels for Cell-Based Assays. *Adv Funct Mat,* 19: 3411-3419.

Csucs, G., Kunzler, T., Feldman, K., Robin, F., & Spencer, N.D. (2003). Microcontact printing of macromolecules with submicrometer resolution by means of polyolefin stamps. *Langmuir,* 19: 6104–6109.

Dawson, E., Mapili, G., Erickson, K., Taqvi, S., & Roy, K. (2008). Biomaterials for stem cell differentiation. *Adv Drug Delivery Rev,* 60: 215-228.

Doane, K.J., & Birk, D.E. (1991). Fibroblasts retain their tissue phenotype when grown in three-dimensional collagen gels. *Exp Cell Res,* 195: 432-42.

Eriksson, E., Sott, K., Lundqvist, F., Sveningsson, M., Scrimgeour, J., Hanstorp, D., Goksör, M., & Granéli, A. (2010). A microfluidic device for reversible environmental changes around single cells using optical tweezers for cell selection and positioning. *Lab chip,* 10: 617-25.

Evans, N., Minelli, C., Gentleman, E., LaPointe, V., Patankar, S.N., Kallivretaki, M., Chen, X., Roberts, C.J., & Stevens, M.M. (2009). Substrate stiffness affects early differentiation events in embryonic stem cells. *Euro Cells & Mat,* 18: 1-13.

Fan, V.H, Tamama, K., Au, A., Littrell, R., Richardson, L.B., Wright, J.W., Wells, A., & Griffith, L.G. (2007). Tethered epidermal growth factor provides a survival advantage to mesenchymal stem cells. *Stem cells,* 25: 1241-51.

Frisch, S.M., & Francis, H. (1994). Disruption of epithelial cell-matrix interactions induces apoptosis. *J Cell Biol,* 124: 619-26.

Gray, D. (2004). Dielectrophoretic registration of living cells to a microelectrode array. *Biosens Bioelect,* 19: 771-780.

Groves, J.T., & Boxer, S.G. (2002). Micropattern formation in supported lipid membranes. *Accounts of chemical research,* 35: 149-57.

Ha, T., Enderle, T., Ogletree, D.F., Chemla, D.S., Selvin, P.R., & Weiss, S. (1996). Probing the interaction between two single molecules: fluorescence resonance energy transfer between a single donor and a single acceptor. *PNAS,* 93: 6264-8.

Hahn, M.S., Taite, L.J., Moon, J.J., Rowland, M.C., Ruffino, K.A., & West, J.L. (2006). Photolithographic patterning of polyethylene glycol hydrogels. *Biomaterials*, 27: 2519-24.

Huang, L., Maerkl, S.J., & Martin. O.J.F. (2009). Integration of plasmonic trapping in a microfluidic environment. *Optics express,* 17: 6018-24.

James, C.D., Davis, R.C., Kam, L., Craighead, H.G., Isaacson, M., Turner, J.N., & Shain, W. (1998). Patterned protein layers on solid substrates by thin stamp microcontact printing. *Langmuir,* 14: 741–744.

Jordan, P., Leach, J., Padgett, M., Blackburn, P., Isaacs, N., Goksör, M., Hanstorp, D., Wright, A., Girkin, J., & Cooper, J. (2005). Creating permanent 3D arrangements of isolated cells using holographic optical tweezers. *Lab chip,* 5: 1224-8.

Kale, S., Biermann, S., Edwards, C., Tarnowski, C., Morris, M., & Long, M.W. (2000). Three-dimensional cellular development is essential for ex vivo formation of human bone. *Nat Biotechnology,* 18: 954-958.

Kane, R.S., Takayama, S., Ostuni, E., Ingber, D.E., & Whitesides, G.M. (2006). Patterning proteins and cells using soft lithography. *Biomaterials,* 20: 161.

Khademhosseini, A., Ferreira, L., Blumling III, J., J Yeh, J., Karp, J.M., Fukuda, J., & Robert Langer. (2006). Co-culture of human embryonic stem cells with murine embryonic fibroblasts on microwell-patterned substrates. *Biomaterials,* 27: 5968–5977.

Lee, JY, Shah, S.S., Zimmer, C.C., Liu, G., & Revzin, A. (2008). Use of photolithography to encode cell adhesive domains into protein microarrays. *Langmuir,* 24: 2232–2239.

Lee, S., Moon, J.J., & West, J.L. (2008). Biomaterials Three-dimensional micropatterning of bioactive hydrogels via two-photon laser scanning photolithography for guided 3D cell migration. *Nat Materials,* 29: 2962-2968.

Lewis, J. (2004). Direct writing in three dimensions. *Mat Today,* 7: 32–39.

Liang, H., Vu, K.T., Krishnan, P., Trang, T.C., Shin, D., Kimel, S., & Berns, M.S. (1996). Wavelength dependence of cell cloning efficiency after optical trapping. *Biophys J,* 70: 1529–1533.

Lutolf, M.P, & Hubbell, J.A. (2005). Synthetic biomaterials as instructive extracellular microenvironments for morphogenesis in tissue engineering. *Nat Biotechnol,* 1: 47-55.

Marshman, E., Booth, C., & Potten, C.S. (2002). The intestinal epithelial stem cell. *BioEssays,* 24: 91-8.

Martin, I., Obradovic, B., Freed, L.E., & Vunjak-Novakovic, G. (1999). Method for quantitative analysis of glycosaminoglycan distribution in cultured natural and engineered cartilage. *Annals Biomed Eng,* 27: 656-62.

Martin, I., Wendt, D., & Heberer, M. (2004). The role of bioreactors in tissue engineering. *Trend Biotech,* 22: 80–86.

Mazolli, A., Neto, P.M., & Nussenzveig. H. (2003). Theory of trapping forces in optical tweezers. *Proc Royal Soc London. Series A: Mathematical, Physical and Engineering Sciences* , 459: 3021.

McBeath, R., Pirone, D.M., Nelson, C.M., Bhadriraju, K., & Chen, C.S. (2004). Cell shape, cytoskeletal tension, and RhoA regulate stem cell lineage commitment. *Dev Cell,* 6: 483–495.

Mirsaidov, U., Scrimgeour, J., Timp, W., Beck, K., Mir, M., Matsudaira, P., & Timp, G. (2008). Live cell lithography: Using optical tweezers to create synthetic tissue. *Lab Chip,* 8: 2174–2181.

Mirsaidov, U., Timp, W., Timp, K., Mir, M., Matsudaira, P., & Timp, G. (2008). Optimal optical trap for bacterial viability. *Phys Rev E.,* 78: 21910.

Morgan, H, Hughes, M.P., & Green, N.G. (1999). Separation of submicron bioparticles by dielectrophoresis. *Biophys J,* 77: 516–525.

Nahmias, Y,. Schwartz, R.E., Verfaillie, C.M., & Odde, D.J. (2005). Laser-guided direct writing for three-dimensional tissue engineering. *Biotech Bioeng,* 92: 129–136.

Nuttelman, C.R, Tripodi, M.C., & Anseth, K.C. (2005). Synthetic hydrogel niches that promote hMSC viability. *Matrix Biology,* 24: 208 - 218.

Odde, D.J, & Renn, M.J. (2000). Laser-guided direct writing of living cells. *Biotech Bioeng,* 67: 312-8.

Odom, T.W., Love, J.C., Wolfe, D.B., Paul, K.E., & Whitesides, G.M. (2002). Improved pattern transfer in soft lithography using composite stamps. *Langmuir,* 18: 5314–5320.

Offenhausser, A., Bocker-Meffert, S., Decker, T., Helpenstein, R., Gasteier, P., Groll, J.,Moller, M., Reska, A., Schafer, S., & Schulte, P. (2007). Microcontact printing of proteins for neuronal cell guidance. *Soft Matter*, 3: 290-298.

Ohyama, M., Terunuma, A., Tock, C.L., Radonovich, M.F., Pise-masison, C.A., Hopping, S.B., Brady, J.N., Udey, M.C., & Vogel J.E. (2006). Characterization and isolation of stem cell – enriched human hair follicle bulge cells. *J Clin Inv,* 116: 249-260.

Palmer, T.D., Willhoite, A.R. & Gage, F.H. (2000). Vascular niche for adult hippocampal neurogenesis. *J Comp Neuro* 425: 479-94.

Park, T., & Shuler, M.L. (2003). Integration of Cell Culture and Microfabrication Technology. *Cell*, 607: 243-253.

Pethig, R., & Markx, G.H. (1997). Applications of dielectrophoresis in biotechnology. *Trend Biotech,* 15: 426-432.

Phillippi, J., Miller, E., Weiss, L. Huard, J., Waggoner, A., & Campbell, P. (2008). Microenvironments engineered by inkjet bioprinting spatially direct adult stem cells toward muscle- and bone-like subpopulations. *Stem cells,* 26: 127-34.

Pittenger, M. F. (1999). Multilineage Potential of Adult Human Mesenchymal Stem Cells. *Science*, 284: 143-147.

Righini, M, Zelenina, A.S., Girard, C. Quidant., R. (2007). Parallel and selective trapping in a patterned plasmonic landscape. *Nature Physics,* 3: 477–480.

Roessel, P., & Brand, A.H. (2002). Imaging into the future: visualizing gene expression and protein interactions with fluorescent proteins. *Nat Cell Biol,* 4: E15-20.

Roth, E.A., Xu, T., Das, M., Gregory, C. Hickman, J., & Boland, T. (2004). Inkjet printing for high-throughput cell patterning. *Biomaterials* 25: 3707–3715.

Ruiz, A., Buzanska, L., Gilliland, D., Rauscher, H., Sirghi, L., Sobanski, T., & Zychowicz, M. (2008). Micro-stamped surfaces for the patterned growth of neural stem cells. *Biomaterials,* 29: 4766-74.

Sahni, A., Sporn, L.A., & Francis, C.W. (1999). Potentiation of endothelial cell proliferation by fibrin(ogen)-bound fibroblast growth factor-2. *J Biol Chem,* 274: 14936-41.

Schofield, R. (1978). The relationship between the spleen colony-forming cell and the haemopoietic stem cell. A hypothesis. *Blood Cells*, 4: 7-25.

Shi, S., &Gronthos, S. (2003). Perivascular niche of postnatal mesenchymal stem cells in human bone marrow and dental pulp. *J Bone Miner Res,* 18: 696-704.

Shiozawa, Y, Havens, A.M., Pienta, K.J. & Taichman, R.S. (2008). The bone marrow niche : habitat to hematopoietic and mesenchymal stem cells , and unwitting host to molecular parasites. *Leukemia,* 22: 941-950.

Sun, B., Roichman, Y., & Grier, D.G. (2008). Theory of holographic optical trapping. *Optics Express*, 16: 15765–15776.

Suzuki, M., Yasukawa, T., Shiku, H., & Matsue, T. (2008). Biosensors and Bioelectronics Negative dielectrophoretic patterning with different cell types. *Biosens Bioelect,* 24: 1043-1047.

Tada, S., Tarbell, J.M., Shi, Z., Ji, X., Qazi, H., Rizzo, V., & Mccarty, W.J. (2000). Interstitial flow through the internal elastic lamina affects shear stress on arterial smooth muscle cells Interstitial flow through the internal elastic lamina affects shear stress on arterial smooth muscle cells. *Am J Phys. Heart and Circulatory Physiology*, 278: H1589-H1597.

Terskikh, A., Fradkov, A., Ermakova, G., Zaraisky, A., Tan, P., Kajava, A.V., Zhao, X., Lukyanov, S., Matz, M., & Kim, S. (2000). " Fluorescent timer": protein that changes color with time. *Science,* 290: 1585.

Thomas, R.S., Morgan, H., & Green, N.G. (2009). Negative DEP traps for single cell immobilisation. *Lab Chip,* 9: 1534–1540.

Tumbar, T., Guasch, G., Greco, V., Blanpain, C., Lowry, W.E., Rendl, M., & Fuchs, E. (2004). Defining the epithelial stem cell niche in skin. *Science,* 303: 359-63.

Vorobjev, I, Liang, H., Wright, W., & Berns, M. (1993). Optical trapping for chromosome manipulation: a wavelength dependence of induced chromosome bridges. *Biophys J*, 64: 533-538.

Wang, Y, Botvinick, E.L., Zhao, Y., Berns, M.W., Usami, S., Tsien, R.Y., & Chien, S. (2005). Visualizing the mechanical activation of Src. *Nature,* 434: 1040–1045.

Watt, F.M, & Hogan, B.L.M. (2008). Out of Eden : Stem Cells and Their Niches. *Science,* 287*:* 2000.

Wendt, D., Riboldi, S.A., Cioffi, M., & Martin, I. (2009). Potential and bottlenecks of bioreactors in 3D cell culture and tissue manufacturing. *Adv Mat,* 21: 3352–3367.

Whitesides, G.M., Ostuni, E., Takayama, S., Jiang, X., & Ingber, D.E. (2001). Soft lithography in biology and biochemistry. *Ann Rev Biomed Eng,* 3: 335–373.

Winer, J.P, Janmey, P.A., McCormick, M.E., & Funaki, M. (2009). Bone marrow-derived human mesenchymal stem cells become quiescent on soft substrates but remain responsive to chemical or mechanical stimuli. *Tiss Eng Part A,* 15: 147-54.

Xia, Y., & Whiteside, G.M. (1998). Soft lithographography. *Ann Rev Mat Sci,* 28: 153-84.

Xu, Tao, Joyce Jin, Cassie Gregory, JJ Hickman, & Thomas Boland. (2005). Inkjet printing of viable mammalian cells. *Biomaterials,* 26: 93–99.

Yarmush, M.L., & King, K.R. (2009). Living-cell microarrays. *Ann Rev Biomed Eng,* 11: 235-57.

Zandstra, P.W., Eaves, C.J., & Piret, J.M. (1994). Expansion of hematopoietic progenitor cell populations in stirred suspension bioreactors of normal human bone marrow cells. *Nature Biotech,* 12: 909–914.

Zhang, J., Niu, C., Ye, L., Huang, H., He, X., Tong, W.G., Ross, J., Haug, J., Johnson, T., & Feng, J.Q. (2003). Identification of the haematopoietic stem cell niche and control of the niche size. *Nature* 425: 836-841.

Zhao, F., Grayson, W.L., Ma, T., & Irsigler, A. (2009). Perfusion affects the tissue developmental patterns of human mesenchymal stem cells in 3D scaffolds. *J Cell Phys,* 219: 421–429.

CHAPTER THREE

CELL-CELL COMMUNICATION MODEL SYSTEM

3.1 INTRODUCTION

The ability of cells to sense and respond to their environment is integral for tissue function, stem cell homeostasis and differentiation, and activation of immune functions. Cellular communication from nearby cells or invading organisms occurs through three different mechanisms: 1) gap junctions that directly connects the cytoplasm of adjacent cells which allow molecules to diffuse freely between them; 2) direct contact between two cells through adherens and tight junctions; and 3) paracrine and endocrine signaling through diffusible molecules that activate cell surface receptors (Grellier, Bordenave, & Amédée, 2009). Cellular signaling occurs through three distinct events: binding of stimuli secreted from neighboring cells or invading pathogen to cell surface receptors or cell junctions, the release of morphogens in response to stimuli, and the response of recipient cells to the secreted morphogens. The spatial and temporal presentation of such signals presented to the cells affects cellular migration, growth, and fate decisions. The loss of these signaling mechanisms leads to abnormal tissue and organ development as well as contribute to tumorogenesis (Rossello & Kohn, 2010). Understanding how cellular communication networks modulate cellular function and how changes in this these networks affect cellular function is essential for developing new therapies and drugs, understanding cancer and disease states, as well as lead to effective culture and modulation of cell and stem cell maintenance and function.

There have been many efforts to identify cellular signaling networks in normal and diseased tissues and cells. Methods include bolus transfer of conditioned medium from one group of cells to another, transwell assays that allow for separation of cells yet permit media and soluble signals to flow through them, and co culture experiments where multiple types of cells are cultured together in a tissue culture dish. While these methods have proved a useful tool to study cellular communication events and for identification of factors affecting cellular

proliferation and differentiation, the effectiveness of these assays are limited because they are not able to control the position and distance of cells in relation to one another or provide control over the spatial and temporal presentation of molecules to cells. Within physiological tissue, gradients of soluble or immobilized molecules direct migration and differentiation of cells (Kholodenko, 2006). Culture of cells within standard tissue culture flasks create conditions where large air-fluid interfaces create convective flow conditions which rapidly move molecules away from cells and interferes with natural signaling gradient creation and molecule buildup leading to delayed or aberrant responses from target cells (Yu, Alexander, & Beebe, 2007). Direct co culture of cells allow for gap and adherens junction signaling through cell-cell contact and paracrine signaling, but often it is difficult to discern the responses of the cell type of interest (Grellier, Bordenave, & Amédée, 2009). The ratio and positioning of cells in respect to one another may also affect communication evens. Lastly, signaling molecules are also bound and form gradients in ECM that is not present in traditional culture methods.

The overall goal of this thesis was to create a defined cell culture model (1) that provides a platform for the spatial patterning of cells and temporal control over soluble molecule diffusion between these cells; and (2) monitor cellular activity in real-time within the culture system. In order to validate the effectiveness of engineered tissue culture systems, a well-defined cellular communication model system is needed where cells respond to and secrete soluble molecule stimuli. An optimal cellular communication model system should incorporate cells that sense and respond relatively rapidly to stimuli (< 3 days) to avoid issues of long-term viability within engineered environments. Communication between cells should be mediated by soluble molecules to demonstrate the effectiveness of the engineered system to control and modulate fluid and molecule flow. Lastly, the activity of cells within the communication system should be easily monitored, either visibly through phenotypic changes or fluorescent reporter systems or via detection of mediators released from activated cells. Based on these criteria, we hypothesized that the well-defined innate immune signaling networks between bacteria, macrophages, and tumor-necrosis factor α (TNFα) responsive cells would be an appropriate, physiologically relevant communication system to serve as our model system. The interaction of lipopolysaccharides (LPS) released from pathogenic bacteria and

macrophages have been extensively studied and are well characterized. Upon stimulation by LPS, macrophages are rapidly induced to secrete TNFα, which in turn binds to and activates cellular signaling cascades in nearby cells. This chapter describes the creation and validation of a cellular communication system utilizing pathogenic *E. coli* ATCC 25922, the mouse macrophage cell line Raw 264.7, and the human embryonic kidney cell line HEK 293. In this system, each cell plays a pivotal role in the activation and response of another cell type (figure 3.1). Fluorescent reporter systems were created and transfected into cells to monitor gene expression and cellular communication within hours of activation. This system then provides an appropriate communication system to test and validate engineered cell culture systems.

3.1.1 Mechanisms of Signaling

The signaling mechanisms utilized in this cellular communication system are widely studied and well characterized. Lipopolysacharride (LPS) is a major component of Gram negative bacteria membranes and a strong activator of the innate immune system in mammals. LPS secreted by ATCC 25922 E. coli is widely known as a potent activator of macrophages and the macrophage cell line Raw 264.7 LPS is composed of a hydrophobic lipid A domain, a hydrophilic polysaccharide O-antigen, and a oligosaccharide core domain (Fujihara, 2003). LPS is recognized by the TLR4/CD14/MD-2 receptors on monocytes and macrophages that are then mobilized to secrete inflammatory cytokines such as tumor necrosis factor α (TNFα) and interleukins (IL) and mount an immune response to bacterial infection.

During a bacterial infection, LPS is released from bacterial cell walls where it is bound by LPS binding protein (LBP), which is a blood borne protein produced in the liver and lung. LBP accelerates the binding of LPS to the CD14 receptors in blood and on monocytes and macrophages, enhancing their sensitivity to bacterial infection 100-1000 fold (Fujihara, 2003). CD14 itself has no signaling capabilities as it lacks transmembrane and cytoplasmic domains. Instead, CD14 facilitates the interaction of LPS with the LPS receptor, toll-like receptor 4 (TLR4). TLR4 is a member a family of Toll-like receptors (TLRs) that recognize and respond to various microorganisms. There are at least 10 members of the TLR family, which are type I

transmembrane proteins that have and extracellular domain composed of multiple leucine-rich repeats (LRR), a transmembrane domain, and an intracellular Toll/IL-1 receptor/Plant R (TIR) homology domain (H. Fan & Cook, 2004).

LPS signaling through TLR4 requires a soluble co-receptor, MD-2. MD-2 is an 18-25kDa protein that is bound to TLR4 and secreted as a soluble molecule from MD-2 expressing cells fan and cook (H. Fan & Cook, 2004). Once LPS binds to the TLR4/MD-2 complex, intracellular signal transduction is initiated. Upon activation of the receptor complex, IRAK is recruited to the cytoplasmic domain of the TLR4 receptor through the adaptor protein, MyD88. IRAK is subsequently phosphorylated and released from the receptor complex and interacts with the adaptor molecule TRAF6. TRAF6 activates MAPK kinases and inhibitors of κB (IKK) complexes. IKK induces the phosphorylation of IκB, which results in polyubiquinitation and subsequent degradation of IκB. The degredation of IκB allows NFκB to translate to the nucleus which activates expression of many genes, including the proinflammatory cytokine TNFα (Beutler, 2000; Fitzgerald, Rowe, & Golenbock, 2004)

In macrophages, activation of TLR4/CD14/MD-2 receptors by LPS induces TNF protein expression. TNF is first presented as a type II transmembrane protein, which is then released from the cell membrane by the metalloprotease TNF alpha converting enzyme (TACE), producing a soluble form of TNFα. TNFα is a major proinflammitory cytokine, and most cells will show some biological responses to TNF. In our system, HEK 293 cells edogenously express at least one member of the TNF receptor family, TNF R1. Binding of TNF to its receptors recruits TNFR-associated death domain (TRADD) to bind to the cytoplasmic domain of TNF receptors. TRADD recruits at least three other signaling mediators, including TNF receptor associated factor 2 (TRAF-2). Similar to TLR4 signaling discussed above, TRAF-2 plays a key role in activation of IKK complexes. The activation of IKK and subsequent degradation of IκB activates NFkB signaling (Baud & Karin, 2001; Wajant, Pfizenmaier, & Scheurich, 2003).

3.2: MATERIALS AND METHODS

3.2.1 CELL CULTURE

Raw 264.7 (ATCC TIB-71) were cultured in DMEM medium (Sigma) supplemented with 10% fetal bovine serum (Gemini) and 100U/ml penicillin/streptomycin (Gibco) at 37ºC and 5% CO_2. Cells were passaged every 2-3 days by mechanical dissociation with a cell scraper. HEK293 cells were cultured in DMEM media supplemented with 10% fetal bovine serum and 100U/ml Penicillin/streptomycin and incubated at 37ºC and 5% CO_2. Cells were passaged at 80% confluence by trypsinization (0.5% trypsin/EDTA) every 2-3 days. ATCC 25922 *E. coli* were grown in LB broth at 37ºC and shaking culture until mid-logarithmic stage.

3.2.2 DEVELOPMENT OF TNF-PTIMER VECTOR

The ptimer-1 vector (Clonetech) was digested with Xho I and Eco RI restriction enzymes (NEB) at 37°C for one hour and dephosphorylated with thermo sensitive alkaline phospatase (TSAP, Promega) according to manufacturer's instructions to prevent vector ligation. The vector backbone was then purified to remove excised DNA (PCR clean-up kit, Qiagen). The human TNF promoter sequence from -421 to 0 was amplified with the primers TNF-421 5'-TACTCGAGGCCCCTCCCAGTTCTAGTT-3' and TNF-0 5'- CTGAATTCTGGGTGTGCCAACAACTGCCTTT-3'. These primers included the Xho I and Eco RI restriction sites for cloning into the ptimer-1 vector. After PCR amplification, the DNA was run on a 1% agarose gel, excised, and purified using a gel purification kit (Qiagen). The purified DNA was then digested with Xho I and Eco RI restriction enzymes at 37°C for one hour. After digestion, the DNA was again purified (PCR clean-up kit, Qiagen). To anneil the TNF promoter into the ptimer backbone, the purified vector and TNF DNA were ligated overnight at 16°C with T4 DNA ligase (New England Biolabs) and transformed into competent DH5α cells (Invitrogen) and grown on selective plates. Colonies were grown and sequenced with the primer PtimerSeq 5'-GTACTGGAACTGGGGGGACAG-3' to determine if the correct TNF promoter sequence was

inserted within the vector backbone. Figure 3.2 illustrates the vector backbone of the ptimer construct.

3.2.3 TRANSFECTION AND LENTIVIRAL TRANSDUCTION

Raw 264.7 cells were transfected with the TNF-ptimer vector using an Amaxa Nucleofector and nucleofector kit V (Lonza) according to manufacturer's instructions. All plasmid DNA was isolated using an endotoxin-free plasmid isolation kit (Qiagen). Briefly, 2μg plasmid DNA was transfected into $1x10^6$ Raw 264.7 cells. 24-48 hours after transfection, 800 μg/ml g418 (Sigma) was added to culture medium to select for positively transfected cells. The NFκB-GFP lentiviral vector was purchased from SABiosciences. $1x10^4$ HEK cells were seeded into a 96 well plate and incubated with polybrene and lentivirus at a MOI of 20. To generate stable HEK NFκB cell lines, cells were selected by the addition of 800 μg/ml puromycin (Sigma) starting 3-4 days post transduction.

3.2.4 CO-CULTURE AND TITER EXPERIMENTS

To determine the amount of cells required to activate each cell type, titers and co-culture experiments were performed. Sensitivity of Raw 264.7 cells to LPS was determined by plating $5x10^5$ Raw 264.7 cells and stimulating with 1ng to 1 μg LPS for 24 hours. Sensitivity of HEK NFκB to TNF was determined by plating $5x10^5$ HEK cells and stimulating with 10pg-1μg TNFα (Sigma). Relative fluorescence of TNF stimulated HEK cells were acquired by measuring the fluorescent intensity of four images for each stimulation level using Image J software. To determine how many Raw 264.7 cells were needed to visualize TNFα activation in HEK NFκB, $1x10^5$-$1x10^7$ Raw 264.7 cells were stimulated with 1μg LPS for 6 hours. After stimulation, the supernatant was collected and added to $5x10^5$ HEK NFκB cells. Activation was determined through fluorescence microscopy 24 hours after stimulation. Relative fluorescence was calculated using Image J software.

For co-culture experiments, cells were plated in a 24 well plate with a transwell insert that allows for diffusion of soluble molecules between cells without contact between cells. $5x10^5$ Raw 264.7 or HEK NFκB cells were plated on the bottom well or on top of the transwell insert in 2 ml DMEM. 1µg LPS were used to stimulate Raw 264.7 cells. Activation of Raw 264.7 and HEK NFκB was visualized with fluorescent microscopy at 24 hours.

3.2.5 MOUSE TNF ELISA

To detect levels of TNF released from RAW 264.7 cells, a commercial mouse TNF ELISA kit was used (BD OptEIA Mouse TNF ELISA Kid, BD Biosciences). To stimulate TNF production, varying numbers of RAW 264.7 ($1x10^5$-$5x10^6$) cells were stimulated with 1 µg LPS and incubated overnight. Determination of the amount of TNF released from bacterium stimulated Raw 264.7 cells was achieved by co culturing varying amounts of ATCC 25922 bacteria to $5x10^5$ Raw 264.7 cells overnight. Supernatants were collected, centrifuged, diluted, and ELISAs were run in duplicate per manufacturer's instructions. ELISA plates were read at 450 nm using a BioTEK plate reader and Gen5 software (BioTEK).

3.2.6 IMAGE ACQUISITION AND ANALYSIS

Fluorescent images were acquired using a Zeiss Axiovert 200M fluorescent microscope and Axiovision software. Images were processed using Axiovision software or Image J.

3.3: RESULTS AND DISCUSSION

The cell communication model system described in this chapter utilizes the well characterized system of macrophage activation by the innate immune system. We hypothesized that using the proper fluorescent reporters, we would be able to visualize cellular activation by soluble molecules (LPS and TNFα) in real-time without sacrificing cells or ending the experiment. This system could then in turn be used to test and validate engineered cell

culture systems designed to manipulate and control cell communication through soluble molecules. A schematic of this culture system is outlined in figure 3.1. We chose to use the E. coli strain ATCC 25922 due to is known ability to induce TNFα gene and protein in the mouse macrophage cell line, RAW 264.7 (Virca, Kim, Glaser, & Ulevitch, 1989). ATCC 25922 naturally release endotoxin into the growth medium during growth at concentrations of ~4 Endotoxin Units (EU) during logarithmic growth (Eng, Smith, Fan-Havard, & Ogbara, 1993). ATCC 25922 strongly activate RAW 264.7 cells to release TNFα into the surrounding culture medium (Lin et al., 2011). TNFα gene expression in Raw 264.7 cells is up regulated 10-20 fold within 30 minutes hour post stimulation, and protein is detected within 4 hours (Virca, Kim, Glaser, & Ulevitch, 1989). In order to visualize activation of Raw 264.7 cells, we designed a fluorescent reporter system in which the TNFα promoter drives expression of the fluorescent protein DsRedE5, commercially known as ptimer. This fluorescent protein is a mutated version of DsRed that shifts from green to red fluorescence over time. The ratio of green to red fluorescence in cells can be calculated and used to indicate time-dependent gene expression (Terskikh et al., 2000).

To increase complexity of the cellular communication system, we chose to use HEK 293 cells to visualize activation of TNFα. HEK 293 cells are a well-established, easy to transfect cell line that endogenously expresses cell surface receptors for TNFα. Upon activation of TNF receptors, HEK 293 cells rapidly unregulated NFκB gene expression. A commercial lentiviral vector with NFκB driven GFP was used to transduce cells. After stimulation with TNF, GFP expression is seen approximately 360 minutes (6 hours, Figure 3.3). The rapid gene expression in both Raw 264.7 and HEK 293 cells allow full activation of the system in a short time period (24-48 hours).

3.3.1. Determination of TNFA levels to visualize activation in HEK NFκB Cells

Once cells were positively transfected, the levels of TNFα required to visualize fluorescent reporter activity in HEK NFκB cells was determined. HEK NFκB cells were plated at a density of $5x10^5$ cells in 1ml media in a 24 well plate. A titer of 100ng to 1µg commercial TNFα was applied to cells and fluorescence was visualized with a fluorescent microscope after 24

hours of culture. Cells plated with 1ng, 10ng, 100ng, and 1μg/ml of TNFα displayed fluorescent activity that was visibly brighter than controls (no TNFα) cells (Figure 3.4a). Relative fluorescence was calculated by measuring the fluorescent intensity of four replicates of each of the stimulation levels. Average background levels were subtracted from each measurement of the four measurements, and these four background subtracted measurements were averaged (figure 3.4b). Based on visual fluorescence and relative fluorescent intensity measurements, it was concluded that $3x10^5$ HEK NFκB cells require at between 1-10ng/ml TNFα for fluorescence activation.

3.3.2. Determination of Raw 264.7 cell numbers required to visualize activation in HEK NFκB cells

HEK NFκB cells require at least 1ng/ml of commercial TNFα in order to visualize fluorescent reporter activity. However, commercial TNFα is a highly purified product and the biological activity of TNFα secreted from LPS stimulated Raw 264.7 cells may not reflect results seen from TNFα titers. Mouse TNF shares an 80% amino acid homology with human TNF and is able to engage human TNF receptors and initiate TNF signaling within these human cells. However, human cells may not be as sensitive to mouse TNF proteins. To determine the sensitivity of human HEK cells to mouse TNF, Raw 264.7 cells were plated at populations from $1x10^5$ to $1x10^7$ cells in 1ml media per well in a 24 well plate. Raw 264.7 cells were stimulated in 1μg/ml O11:B4 LPS and incubated overnight. Supernatants from incubated Raw 264.7 cells were then added to $3x10^6$ HEK NFκB cells (plated 24 hours previous) and allowed to incubate overnight. After incubation, HEK NFκB fluorescent activation was visualized with a fluorescent microscope. HEK NFκB cells incubated with supernatant from $5x10^5$, $1x10^6$, $2x10^6$, $5x10^6$, and $1x10^7$ Raw 264.7 cells displayed visible fluorescent activity over control cells ($5x10^5$ Raw 264.7 cell supernatant cultured without LPS)(Figure 3.5a). Relative fluorescence was calculated as described above. Fluorescent activity reached a threshold at $5x10^5$ activated Raw cells and above, and therefore we concluded that HEK cells require at least $5x10^5$ activated Raw cells for activation. (Figure 3.5b)

3.3.3. Quantification of TNFα levels secreted from Raw 264.7 cells

To quantify levels of TNFα secreted from Raw 264.7 cells under various conditions, a mouse TNFα ELISA was performed. Raw cells at concentrations of $1x10^5$, $3x10^5$, $5x10^5$, $1x10^6$, and $5x10^6$ were stimulated with LPS and supernatant was collected after 5 hours stimulation and assayed for TNFα levels. Additionally, quantification of TNF levels were conducted with varying amounts of ATCC 25922 E. coli. This experiment is critical as high concentrations of LPS (>1 ng/ml) have been shown to render macrophages unable to induce TNFα RNA (Manthey et al, 1994). Varying levels of ATCC 25922 bacteria ($4x10^9$ to $10x10^{10}$) were incubated with $5x10^5$ Raw 264.7 cells and supernatants were collected after 5 hours stimulation. For both experiments, ELISAs were conducted according to manufacturer's instructions and quantified against a standard curve. Results of the cell titer are shown in figure 3.4. TNFα protein levels present in supernatant increased as cell number increased, with $5x10^6$ cells producing up to 5ng LPS. For bacterial titer experiments, ~$4x10^9$ to $10x10^{10}$ bacterial cells stimulated 5x10^5 Raw 264.7 cells to secrete 0.6-1 ng TNFα (Figure 3.6).

3.3.4. CoCulture Experiments

To assess the ability of Raw 264.7, and HEK NFκB cells to communicate through soluble signaling molecules, all both cell types and controls were cultured in transwells that allow exchange of soluble molecules without direct cell contact. Either Raw 264.7 or HEK cells were plated on the bottom well for imaging and co cultured with or without stimuli. Figure 3.7 illustrates the activation of Raw 264.7 cells in co culture. When LPS was added to cultures of Raw 264.7 cells only or Raw 264.7 cells with HEK NFκB, fluorescent reporter activity was detected within 24 hours. When Raw 264.7 were cultured with HEK with no LPS stimuli, with TNFα or without HEK or stimuli, no fluorescent activation was visible. This data shows that Raw 264.7 cells are only activated by LPS and not by the presence of HEK NFκB cells or TNFα. These experiments were then repeated with HEK NFκB cells. In the presence of Raw 264.7 cells and LPS stimuli, HEK NFκB cells displayed visible fluorescence activation. Co culture of HEK NFκB cells without LPS stimuli did not activate fluorescence over background levels, while the

addition of TNFα to culture medium induced GFP fluorescence. Culture of HEK in the presence of LPS or without stimuli did not produce visible fluorescence (Figure 3.8). These results demonstrate the ability of both Raw 264.7 and HEK NFκB cells to respond and communicate through soluble signaling molecules and not become aberrantly activated unknown factors in the co culture environment.

3.4: CONCLUSIONS

The capabilities of cells to sense, respond, and react to external stimuli is crucial for a variety of cellular process and normal tissue function. This chapter describes the construction of a mammalian cell communication model system that can be used to asses cellular communication events in real – time within *in vitro* cell culture environments. Fluorescent reporters were designed in which activation of Raw 264.7 and HEK 293 cells through LPS secreted by gram-negative *E. coli* and TNFα, respectively, could be visualized within hours of stimulation. Raw 264.7 cells are not activated thorough the addition of TNFα, nor HEK 293 cells able to bind LPS. These signaling capabilities allow one-way communication between the three cell types, which can be easily interrupted by the removal of one or more activators from the cell culture medium. While HEK cells require ~10 higher concentrations (10 ng/ml) of mouse TNF secreted from activated Raw cells, these concentrations reflect physiological levels of TNF. LPS stimulation in mice results in serum TNF levels at 8.5-45 ng/ml, well within the 10 ng threshold for HEK fluorescence activation (Zanetti et al., 1992). The sensitive and rapid signaling and ability to modulate and monitor cellular communication in real time make this system a feasible model of cellular communication and useful for testing engineered cell culture environments discussed later in this thesis.

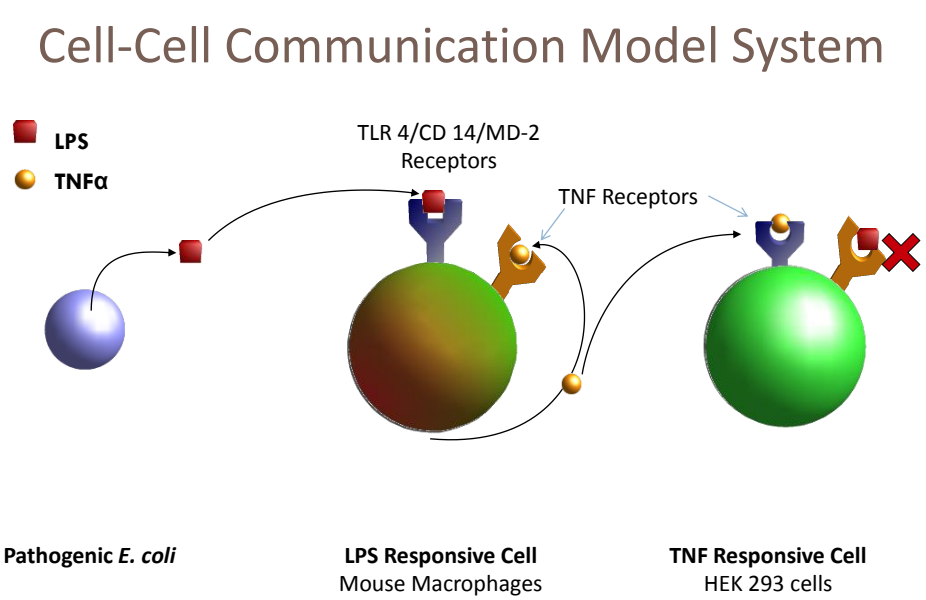

Figure 3.1 Cell Communication Model System. LPS is released from bacterial cell walls into surrounding medium. RAW 264.7 cells transfected with the TNF-ptimer vector bind LPS with the TLR4/CD14/MD-2 receptors and upregulate TNFα gene expression, protein synthesis, and begin fluorescing within hours. HEK 293 cells bind TNF in culture medium, but do not respond to LPS. Once bound to TNF receptors, HEK cells activate NFκB gene expression and GFP fluorescence.

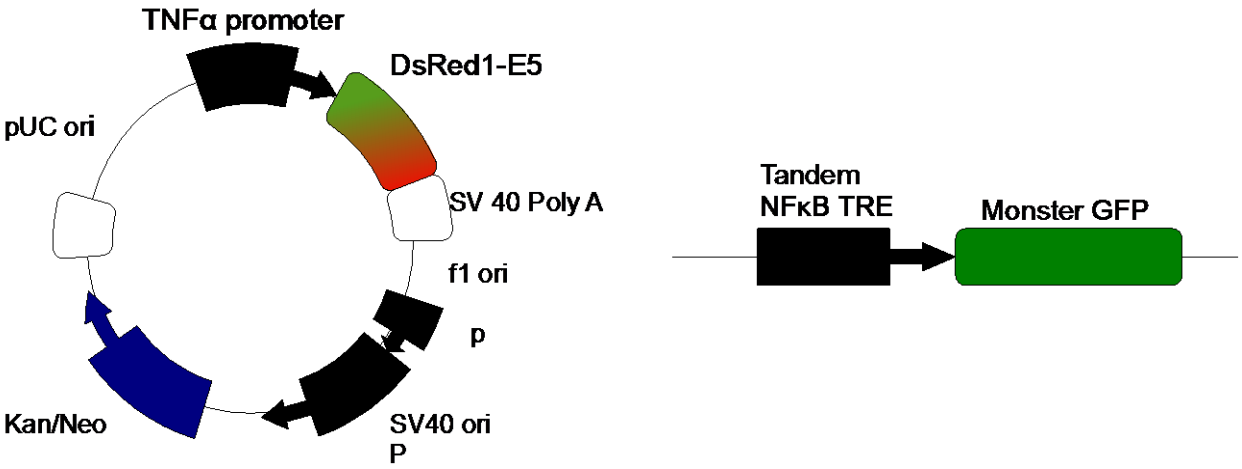

Figure 3.2. Fluorescent Reporter Vectors. (A) Vector backbone of TNF-ptimer vector. The TNFα promoter was cloned into the multiple cloning site to drive DsRed1-E5 fluorescence. Kan/new cassetes infer kanamycin and g418 resistance for plamid propagation in bacteria and generation of stably transfected mammalian cells. (B) SA Biosciences commercial NFκB lentiviral vector backbone. Five NFκB response element repeats drive monster GFP expression.

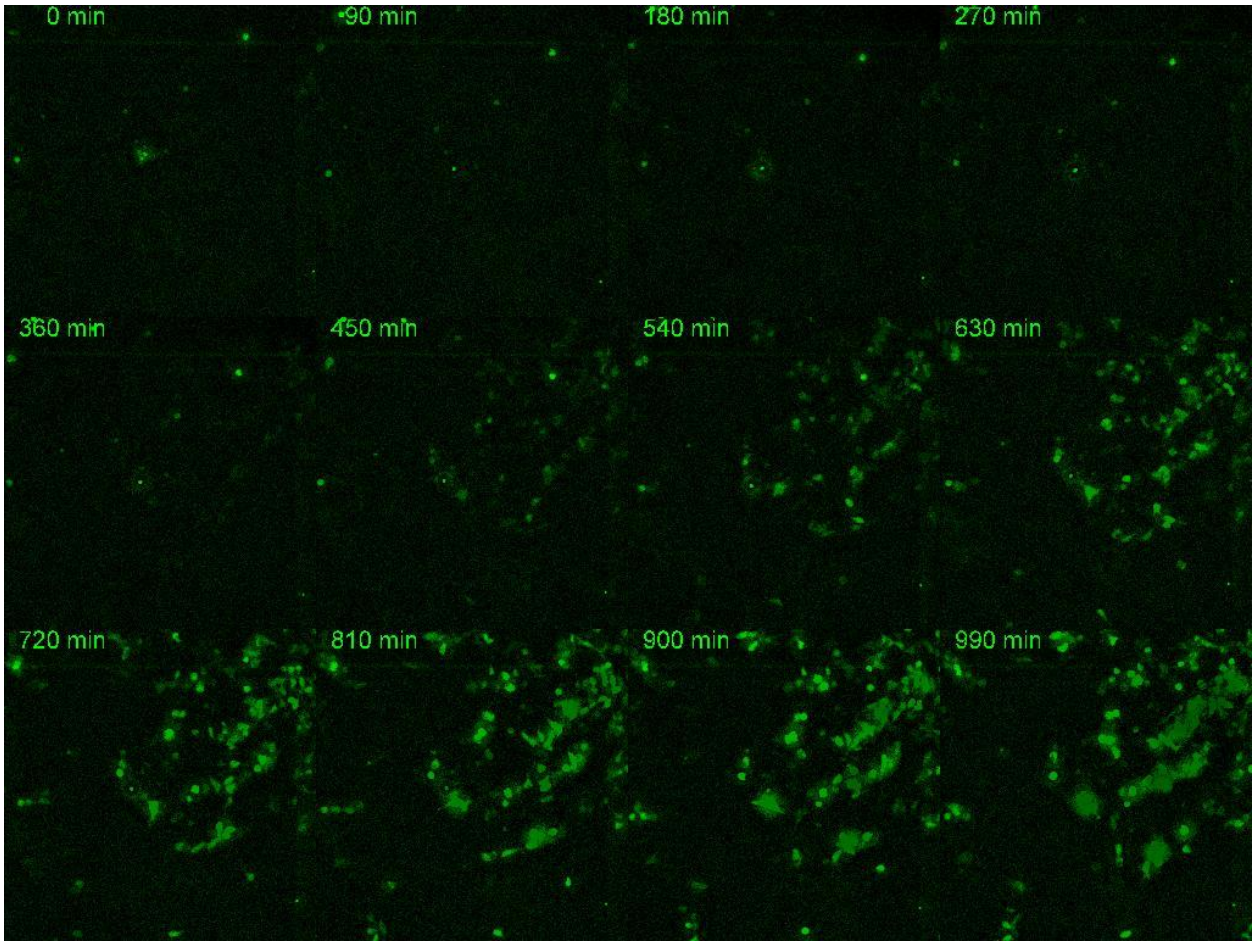

Figure 3.3. Kinetics of HEK NFκB Fluorescence. HEK NFκB cells were plated in a cell culture dish with a coverslip for imaging, and stimulated with 1µg/ml TNF. Images were taken every 15 minutes for 17 hours. Fluorescence becomes visible around 360 minutes (6 hours), with fluorescence levels peaking at 720 minutes (12 hours).

A.

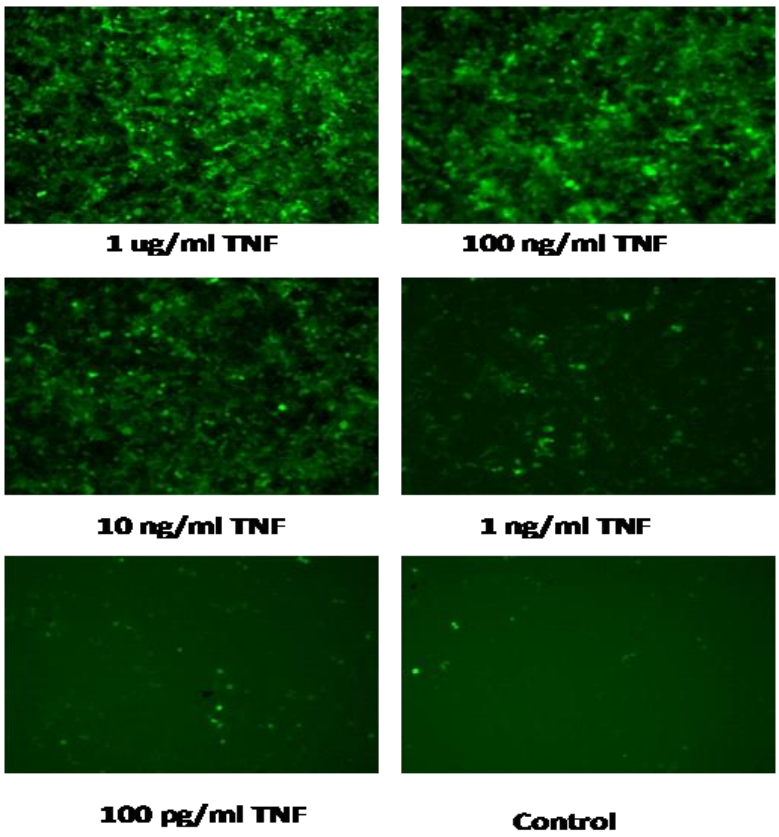

B.

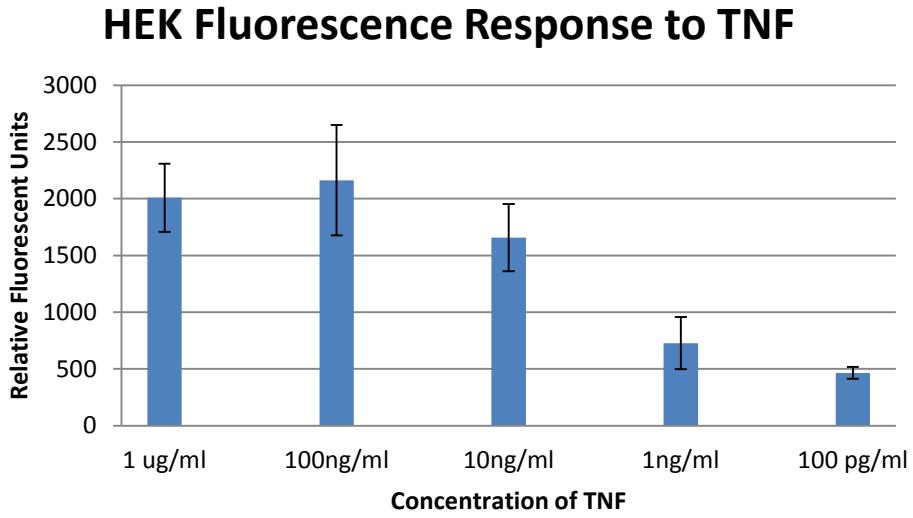

Figure 3.4. Determination of HEK NFκB Fluorescence Sensitivity to TNF proteins. (A) $3x10^5$ HEK-NFκB cells were plated and activated with 1µg, 100ng, 10 ng, 1 ng, and 100pg/ml TNFα and visualized under a fluorescent microscope after 24 hours stimulation. HEK cells displayed levels of fluorescence higher than background with 1 ng/ml TNF. (B) Relative fluorescence of TNF stimulated HEK cells. Fluorescence intensity was measured in four areas of the tissue culture well for each level of TNF stimulation using Image J software. Error Bars= standard deviation.

A.

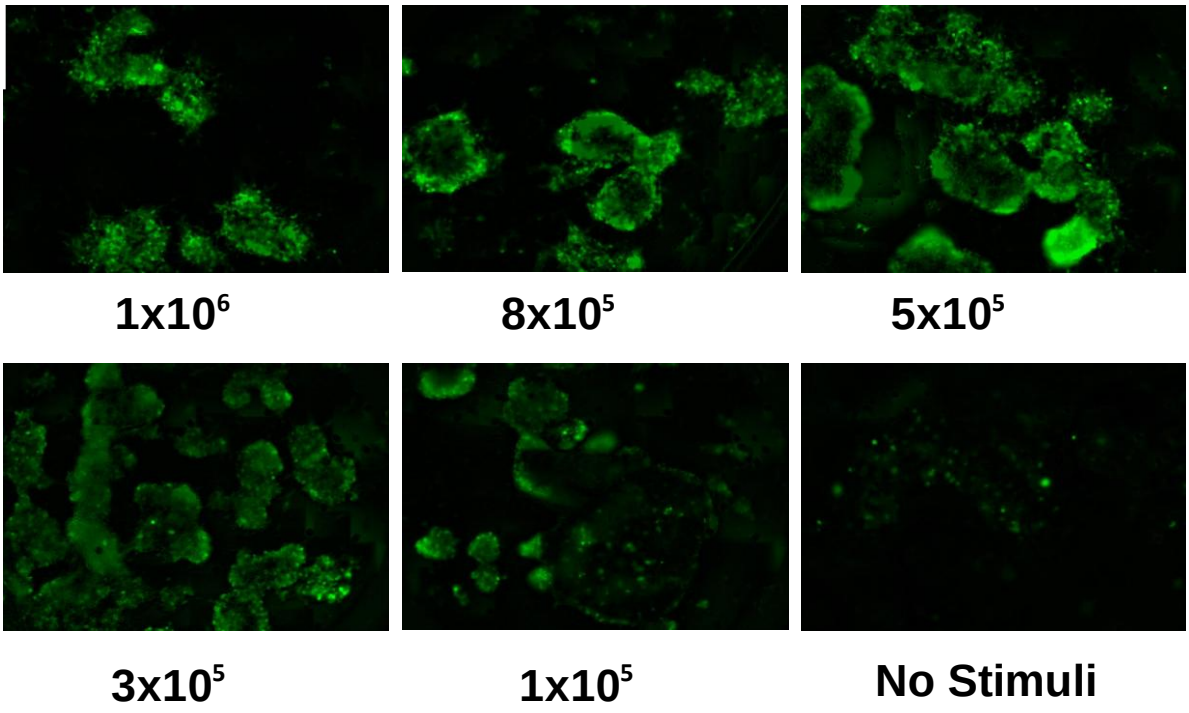

B.

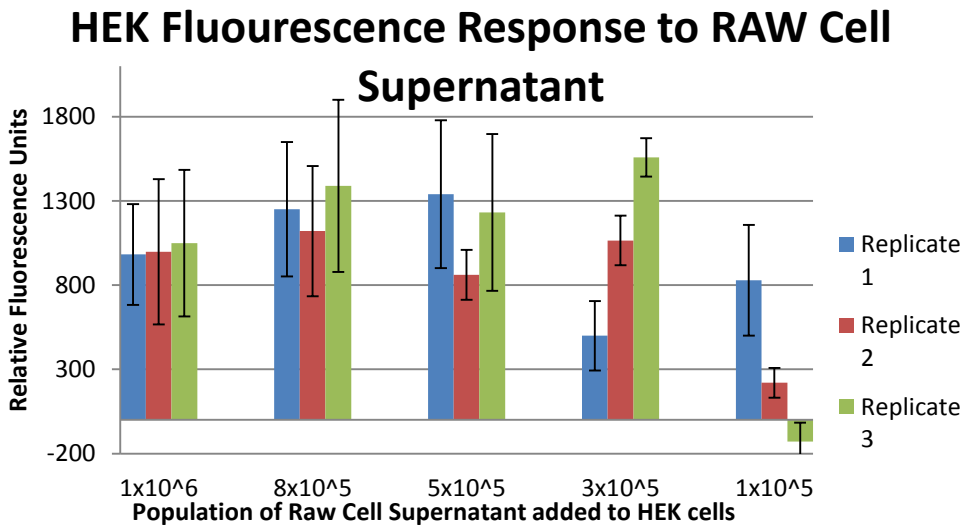

Figure 3.5. Determination of HEK NFκB Sensitivity to TNF from Activated Raw 264.7 Cells. (A) $1x10^5$ HEK NFκB cells were plated and stimulated with the supernatant of varying numbers of Raw 264.7 cells that were activated with 1 µg/ml LPS. Based on these data, the supernatant from approximately 3-$5x10^5$ activated Raw 264.7 cells are required to visualize florescence in HEK NFκB cells. (B) Relative fluorescence of HEK NFκB cells in response to Raw 264.7 cells. Fluorescence intensity was measured in four areas of each of three experimental replicates using Image J software. Fluorescent intensity reached a plateau at populations of $5x10^5$ and above. Error bars=standard deviation.

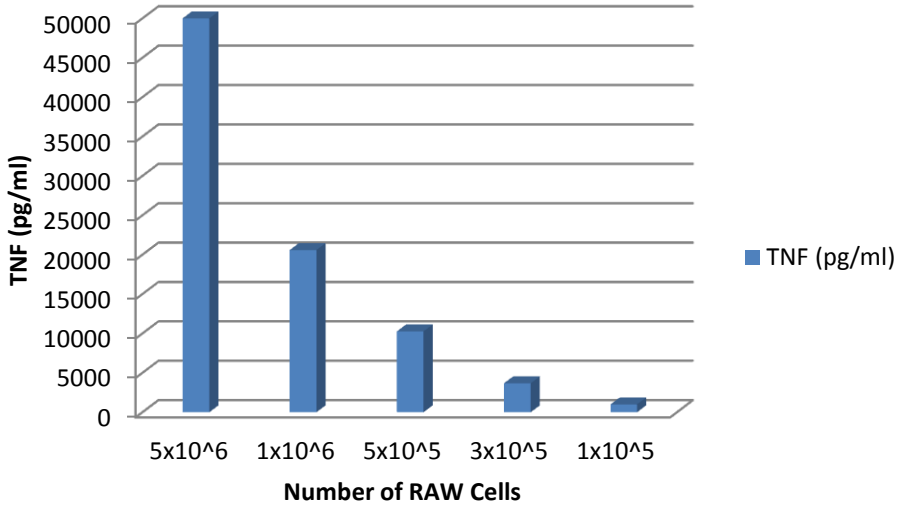

Figure 3.6. Quantification of TNF Secreted from Raw 264.7 Cells. Varying amounts of Raw 264.7 cells were plated and stimulated with 1µg LPS for 6 hours. Supernatants were collected and TNF was quantified using a mouse TNF ELISA kit. Note that $5x10^5$ cells released 10ng TNF.

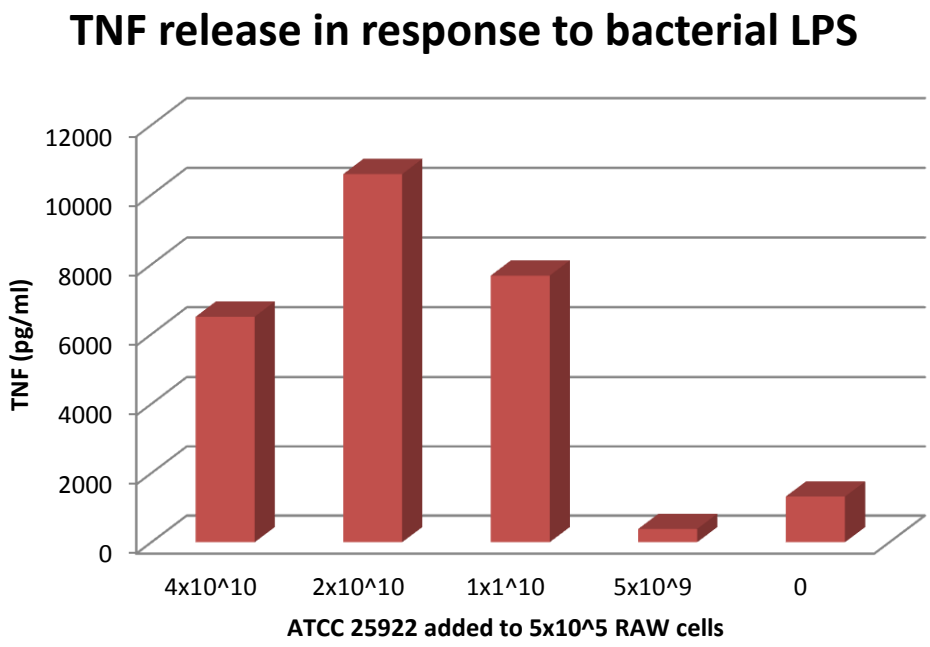

Figure 3.7. Quantification of TNFα Released from Raw 264.7 Cells with Different Levels of ATCC *E. coli.* $5x10^5$ Raw 264.7 cells were plated and stimulated with varying levels of ATCC *E. coli*. Supernatants were collected and assayed for TNFα levels. Approximately $2x10^{10}$ bacteria were required to stimulate Raw 264.7 cells to release 10 ng/ml TNF.

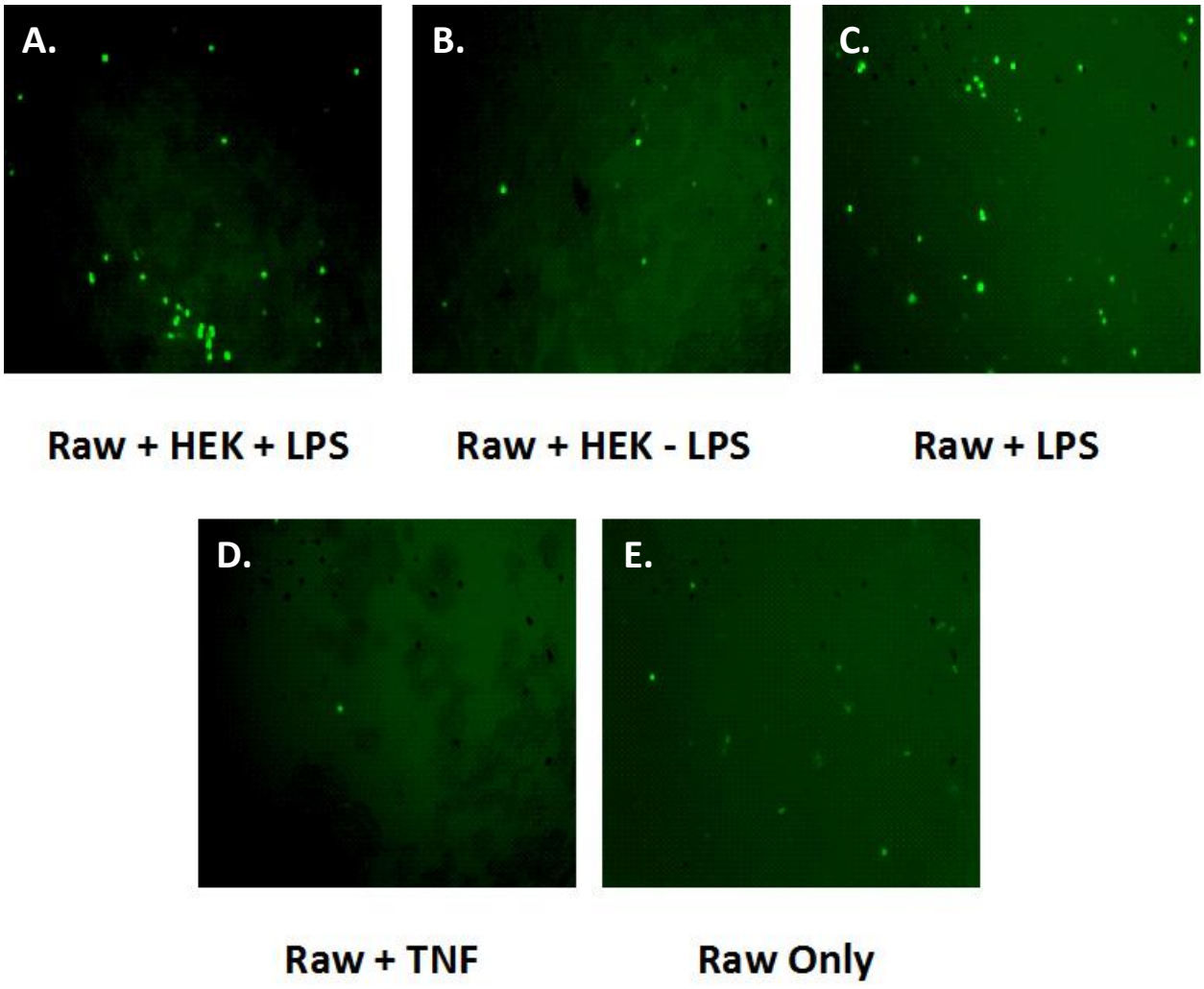

Figure 3.8. Transwell Co Culture assays of Raw 264.7 and HEK 293 Cells. Raw 264.7 cells were plated on the bottom of a 24 well plate, and HEK 293 cells were placed in the transwell. (A) Fluorescent image of Raw 264.7 cells culture with HEK cells and stimulated with 1µg LPS. Raw 264.7 cells display activation of TNF gene expression and ptimer fluorescent reporter activity. (B) Fluorescent image of Raw 264.7 cells and HEK 293 cells co cultured without LPS stimulation. Raw 264.7 cells do not display fluorescence above control levels, indicating that the presence of HEK 293 cells in culture do not activate TNFα gene expression or fluorescent reporter activity. (C) Fluorescent image of Raw 264.7 cells not in co culture with HEK cells and stimulated with 1µg LPS. Raw 264.7 cells display activation of the ptimer fluorescent reporter. (D) Fluorescent image of Raw 264.7 cells stimulated with 1ng/ml TNF. Raw 264.7 cells do not activate TNF gene expression or fluorescent reporter in the presence of TNFα. (E) Fluorescent image of Raw264.7 cells cultured in medium alone, without stimulation.

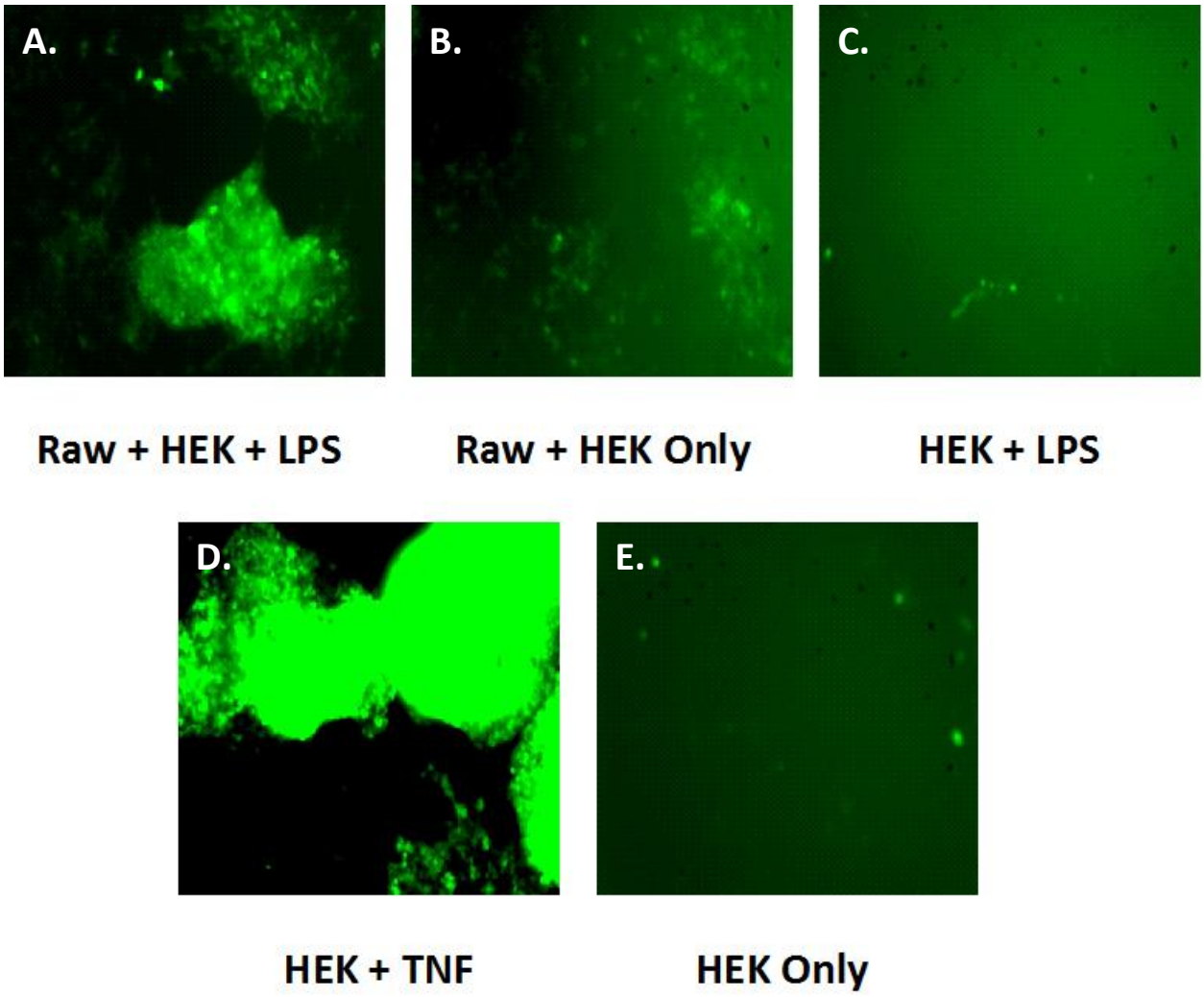

Figure 3.9. Transwell Co Culture Assays of Raw 264.7 and HEK 293 cells. HEK 293 cells were plated on the bottom of a 24 well plate, and Raw 264.7 cells were placed in the transwell. (A) Fluorescent image of HEK 293 cells cultured with Raw 264.7 cells and stimulated with 1µg LPS. HEK 293 cells display fluorescent activation in co culture with activated Raw 264.7 cells. (B) Fluorescent image of HEK 293 cells cultured with Raw 264.7 cells but without LPS activation. HEK 293 cells show some fluorescence over background levels; however this may be due to small amounts of TNFα secreted from Raw 264.7 cells. TNFα gene expression is thought to be constitutively active in macrophages at very low expression levels. (C) Fluorescent image of HEK cells cultured in the presence of LPS. LPS does not induce NFκB expression in HEK 293 cells due to the lack of TLR4/CD14/MD-2 receptors. (D) Fluorescent image of HEK 293 cells stimulated with 1ng TNFα, demonstrating activation of NFκB reporter activity. E. Fluorescent image of HEK 293 cells in culture without stimulation.

LIST OF REFERENCES

Baud, V., & Karin, M. (2001). Signal transduction by tumor necrosis factor and its relatives. *Trends Cell Biology*, *11*(9), 372–377.

Beutler, B. (2000). Tlr4: central component of the sole mammalian LPS sensor. *Current opinion immunology*, *12*(1), 20-6.

Eng, R. H., Smith, S. M., Fan-Havard, P., & Ogbara, T. (1993). Effect of antibiotics on endotoxin release from gram-negative bacteria. *Diag Micro Inf Dis*, *16*(3), 185-9.

Fan, H., & Cook, J. (2004). Molecular mechanisms of endotoxin tolerance. *J Endotoxin Rese*, *10*(2), 71-84.

Fitzgerald, K. a, Rowe, D. C., & Golenbock, D. T. (2004). Endotoxin recognition and signal transduction by the TLR4/MD2-complex. *Microbes infection* , *6*(15), 1361-7.

Fujihara, M. (2003). Molecular mechanisms of macrophage activation and deactivation by lipopolysaccharide: roles of the receptor complex. *Pharmacology & Therapeutics*, *100*(2), 171-194.

Grellier, M., Bordenave, L., & Amédée, J. (2009). Cell-to-cell communication between osteogenic and endothelial lineages: implications for tissue engineering. *Trends in Biotechnology*, *27*(10),

Kholodenko, B. N. (2006). Cell-signalling dynamics in time and space. *Nature reviews. Mol Cell Bio*, *7*(3), 165-76.

Lin, W.-H., Wu, C.-R., Fang, T. J., Lee, M.-S., Lin, K.-L., Chen, H.-C., et al. (2011). Adherent Properties and Macrophage Activation Ability of 3 Strains of Lactic Acid Bacteria. *J Food Science*, *76*(1), M1-M7.

Manthey, C.L. & Vogel, S.N. (1994). Interactions of Lipopolysaccharide with Macrophages. In Zwilling, B.S. & Eisenstein, T.K. (Eds.), *Macrophage-Pathogen Interactions* (pp. 63-81). New York, NY: Marcel Dekker, Inc.

Rossello, R. A., & Kohn, D. H. (2010). Cell communication and tissue engineering on Secondary Signals. *Communicative & Integrative Biology*, *3*, 53-56.

Terskikh, A., Fradkov, A., Ermakova, G., Zaraisky, A., Tan, P., Kajava, A. V., et al., others. (2000). " Fluorescent timer": protein that changes color with time. *Science*, *290*(5496): 1585.

Virca, G. D., Kim, S. Y., Glaser, K. B., & Ulevitch, R. J. (1989). Lipopolysaccharide induces hyporesponsiveness to its own action in RAW 264.7 cells. *J Biological chemistry*, *264*(36): 21951-6.

Wajant, H., Pfizenmaier, K., & Scheurich, P. (2003). Tumor necrosis factor signaling. *Cell death and differentiation*, *10*(1): 45-65.

Yu, H., Alexander, C. M., & Beebe, D. J. (2007). Understanding microchannel culture: parameters involved in soluble factor signaling. *Lab chip*, *7*(6): 726-30.

Zanetti, G., Heumann, D., Gerain, J., Kohler, J., Abbet, P., Barras, C., Lucas, R., Glauser, M. & Baumgartner, J. (1992). Cytokine Production After Intravenous or Peritoneal Gram-Negative Bacterial Challenge in Mice. *J Immunol.* 148 (6): 1890-1897.

CHAPTER 4

PRECISION PLACEMENT OF MAMMALIAN CELLS WITHIN THREE-DIMENSIONAL SCAFFOLDS

4.1 INTRODUCTION

In vivo cell microenvironments regulate cell specific fate and functions through cell-cell interactions, extra cellular matrices, and soluble signaling molecules. The investigation of cellular responses to environmental stimuli is often performed using two dimensional (2D) cell cultures that do not accurately recapitulate the physiology of the native tissue environment. Culture on rigid, 2D surfaces of tissue culture polystyrene (TCP) removes tissue specific architecture, cell-cell interactions, and extracellular matrix (ECM) interactions found in native tissue, often resulting in altered cell phenotype and function (Griffith & Swartz, 2006). For example, Bissell et al. observed gross genotypic and phenotypic changes in normal and malignant breast cancer cells cultured in 2D vs. 3D microenvironments (Bissell et al., 2002). Furthermore, cell-cell interactions and individual cell microenvironments are difficult to define in a precise manner in many culture systems due to the inability to control cellular seeding and placement within the culture dish. As a result such culture methods may not accurately predict *in vivo* behavior of cells and responses to stimuli may vary widely between the culture dish and native tissue.

Physiologically relevant cell culture systems must provide control over cell-cell and cell-environment interactions to accurately predict *in vivo* cell behavior. As a result, more appropriate and predictive *in vitro* cell culture systems are required for understanding cellular behavior, expansion and direct differentiation of stem or precursor cells, testing of small molecules and drugs, as well as aid in elucidating how these environments are altered in disease and cancer states.

Hydrogels have recently emerged as a biological tool to provide 3D support of cultured cells. Made of natural or synthetic materials such as alginate, collagen, poly (ethylene glycol) diacrylate (PEGDA) and polyesters, these materials form highly hydrated biocompatible networks that allow the rapid diffusion of nutrients, metabolites, and small molecules to and away from encapsulated cells, and are resistant to protein absorption (Hubbell, 1995). Many hydrogel materials can be modified to include extracellular matrix molecules, vary mechanical stiffness, and control degradation properties. PEGDA scaffolds are of particular interest because they are rapidly polymerized in the presence of appropriate photoinitiators and UV light. The photopolymerization process allows for control over hydrogel shape, size, and stiffness and can be formed within seconds with minimal damage to encapsulated cells. PEGDA scaffolds have been used to encapsulate hepatic cells (Itle, Koh, & Pishko, 2005), neurons (Mahoney & Anseth, 2006), keratocytes (Garagorri et al., 2008), and encapsulate and differentiate bone marrow and embryonic stem cells (Benoit, Collins, & Anseth, 2007; Bosnakovski et al., 2006; Buxton et al., 2007; Hwang, Varghese, Zhang, & Elisseeff, 2006; Karp et al., 2007). A number of methods exist to control the patterning of one or more cell types within PEGDA scaffolds such as soft lithography, electropatterning, and gradients of ECM molecules (Bhatia et al., 1997; Hui & Bhatia, 2007; Tsang et al., 2007). However, these methods lack the ability to repeatedly define with high (nanometer-scale) precision the position of single cells and cell-cell interactions important for normal cellular function (Albrecht, Tsang, Sah, & Bhatia, 2005; Hahn et al., 2006; Khademhosseini et al., 2006; Revzin, Tompkins, & Toner, 2003; Wang & Ho, 2004). Methods to reproducibly pattern cells within the 3D scaffolds would enable the accurate modeling of physiological tissue environments.

One strategy to manipulate single cells and their environment is the use of laser tweezers and optical traps. Pioneered by Ashkin et al. (Ashkin, Dziedzic, & Chu, 1986) laser tweezers have supported the manipulation of bacteria and viruses (Ashkin & Dziedzic, 1986), study cellular forces (Titushkin & Cho, 2006), and the manipulation of DNA (Wang, Yin, Landick, Gelles, & Block, 1997). Laser tweezers and optical traps are formed by tightly focusing a laser beam onto cells where gradient forces trap the object near the focal point of the laser. This technology allows the manipulation and precise placement of single cells, resulting in stringent

control of a cell's interaction with other cells and other environmental stimuli. Multiple optical traps are formed by time-sharing an optical beam between traps, where the beam scans from one trap to the next. The utilization of laser tweezers for long term cellular studies has not yet been realized due to perturbations in cellular activity by laser traps. When biological specimens are manipulated by laser tweezers, proper selection of laser wavelength and time-average laser power is critical to minimize photodamage and thermal effects generated by the optical traps. Maintenance of the relative position and interaction of cells in optical traps requires cells to be held by laser power for extended periods of time which causes significant damage to living objects presumably through local heating of the microenvironment or disruption of the cytoskeleton matrix (Liu et al., 1995; Neuman, 1999; Zhang & Liu, 2008). The use of time-shared optical traps reduces cellular exposure to laser power as the beam scans between multiple traps and thus the cell is in the dark most of the time. Still, long exposures to any type of laser power can be detrimental to cellular activity. To permanently fix cell position and avoid subsequent laser exposure and cellular damage, we and others (Akselrod et al., 2005; Jordan et al., 2005; Mirsaidov et al., 2008) have encapsulated optically trapped cells into 3D scaffolds.

The aim of this study was to develop cell culture systems that precisely and repeatedly define the position and interaction of cells within their microenvironments. To achieve this goal, optical trapping techniques were used to place cells and fix them into specific positions using photopolymerizable PEGDA scaffolds. This technique permits definition of culture environments for single cells as well as for the co-culture of multiple cell types. As model systems to demonstrate hydrogel and laser tweezer platforms, the human monocytic cell line (U937), human embryonic kidney cells (HEK 293) transfected with toll-like receptor 4 (TLR4) and co receptors to confer response to bacterial lipopolysaccarides (LPS) (HEK293 CD14/TLR4/MD2), and porcine mesenchymal stem cells (pMSC) were used. U937 cells were selected for optical manipulation because they are non-adherent and rapidly responds to small molecule stimuli such as LPS or phorbol 12-myristate 13-acetate (PMA). Small molecule stimuli can readily diffuse through the hydrogel so gene expression or phenotypic changes can be observed within 4-48 hours post stimulation. HEK cells were chosen since they represent a well-established cell line that proliferates rapidly and is easily transfected with fluorescent reporter

systems or surface molecules for studies in cellular signaling. Porcine MSCs cells were selected as a model for the controlling of the stem cell niche, subsequent stem cell maintenance, and directed differentiation into distinct mesenchymal lineages. Here, we demonstrated the manipulation and encapsulation of human HEK and porcine mesenchymal stem cells by laser tweezers. These methods were extended to construct arrays of two or more cell types to recreate cell-cell interactions observed in native tissue environments. Finally, the biological activity of cells encapsulated in hydrogel scaffolds was demonstrated. The approach presented here demonstrates a culture system in which physical and chemical cues of a 3D tissue environment can be precisely and repeatedly controlled. Thus, a platform suitable to study cell behavior and responses to environmental stimuli is achievable.

4.2 Materials and Methods

All materials were purchased from Sigma-Aldrich, St. Louis MO unless otherwise stated.

4.2.1 Cell Isolation and Culture

Human U937 (ATCC 1593.2) cells were cultured in RPMI 1640 medium supplemented with 10% fetal bovine serum (Gemini) and 100U/ml penicillin/streptomycin (Gibco) at 37ºC and 5% CO_2. Cells were passaged every 2-3 days by removing and replacing medium. HEK293/CD14/TLR4/MD2 cells (Invivogen) were cultured in DMEM media supplemented with 10% fetal bovine serum, 100U/ml Penicillin/streptomycin, 50 µg/ml hygromycin and 10 µg/ml blastocidin and incubated at 37ºC and 5% CO_2. Cells were passaged at 80% confluence by trypsinization (0.5% trypsin/EDTA). Porcine bone marrow was harvested by flushing the femur of 1-3 month old pigs. Bone marrow was washed several times in PBS and deposited on Hystopaque 1077 and centrifuged for 30 minutes at 400*xg*. Mononuclear cells were recovered from the hystopaque interface and washed several times in PBS. Cells were plated at 300,000 cells/cm^2 in DMEM-low glucose (DMEM-LG, 1g/L glucose) supplemented with 10% fetal bovine serum, 100 U/ml penicillin/streptomycin and cultured

at 37ºC, 5% CO_2, and 5% O_2. Medium was replaced at 24-48 hours after seeding to remove non-adherent cells. After initial replacement, medium was replaced every 2-3 days. Cells were passaged at 80% confluency by trypsinization (0.05% trypsin/EDTA) and reseeded at a density of 5,000 cells/cm^2. For endothelial cell isolation, porcine aortas were harvested from pigs of various ages and rinsed with PBS. The aortas were dissected and the luminal side was digested by collagenase treatment for 20 minutes. The luminal surface was gently scraped to remove endothelial cells. The cells were washed 3 times in PBS, resuspended in RPMI 1640 medium and plated onto gelatin coated culture dishes. Cells were incubated at 37C, 5% CO_2 and passaged at 80% confluency. ATCC 25922 *E. coli* were grown in LB broth at 37ºC and shaking culture until mid logarithmic stage.

4.2.2 MICROFLUIDIC DEVICE FABRICATION

The microfluidic devices with channel dimensions of 300μm tall x 1mm wide x 1cm long were formed from poly (dimethylsiloxane) (PDMS) using a mold-casting technique. The master mold, generated through off-site stereolithography based on a CAD file (FineLine Prototyping), is made of DSM Somos ProtoTherm 12120, a strong, high temperature tolerantplastic. To detach the PDMS without tearing the device, the mold was coated with a fluoropolymer, Tridecafluor-1,1,2,2,(Tetryhydrooctyl)-1-Trichlorosilane, using vapor deposition in a vacuum oven at 75^{o}C and 20" Hg vacuum for 2 hrs. The PDMS silicone polymer used to create the chips is commercially available as Sylgard 184 (Dow Corning), a two part polymer mix. The two parts were mixed thoroughly at a 1:5 ratio of curing agent to base and degassed under vacuum for 30 min. The PDMS mixture was poured into the master mold and cured at 75^{o}C for ~2 hrs. After cooling the plastic was peeled away from the mold, yielding a piece of silicone with the inverse pattern of the master mold.

The microfluidic channels were connected to external pressure and fluid reservoirs through a hole punched in the silicone chip at the input and output ports using a blunt syringe needle. Though PDMS is transparent, the microfluidic chip is thick (>1,000 μm) and light scattering through it prevents optical access through the top. To provide optical access, the

bottom of the PDMS was sealed to #1 cover glass. The PDMS was then bound to the coverslip using oxygen plasma in a Harrick plasma cleaner (PDS-32G) for 45 seconds. The oxygen plasma generates silanol(Si-OH) groups on the surface of PDMS, which react with silanol groups on the glass surface to form an Si-O-Si bond. Finally, the PDMS chip was gripped by the sides, and placed in contact with the coverslip, and a uniform pressure was applied for 10 seconds to form the bond and then placed in an 85^{o}C overnight. Lastly, to prevent cells from adhering to the coverslip during trapping, the fluid channels were coated with a 10% bovine serum albumin (BSA) solution for 1-2 hours at 4 ^{o}C

4.2.3 Optical Trapping

Optical trapping was setup as described previously by Askelrod et al and Mirisaidov et al (Akselrod et al., 2005; Utkur Mirsaidov et al., 2008). The setup of the optical trapping system is outlined in figure 4.2. Briefly, time-shared optical traps were generated from a CW-Ti sapphire laser tuned to 900nm using acoustal optical deflectors (AA-Optoelectronic). Each cell was held using 9 optical traps with a dwell time of 10μs. A freely definable shepard beam was used to organize cells within the array. After positioning, cells were encapsulated in the 3D matrix as described below.

4.2.4 Preparation of Hydrogels and Cell Encapsulation

The hydrogel solution was prepared by dissolving 3.4 kDa poly (ethylene glycol) diacrylate (PEGDA; Layson Bio) in sterile PBS to a 20% w/v solution. The photoinitiator Iguracure D2959 was added to the PEGDA solution to a final concentration of 0.1% w/v. To form RGD-conjugated PEGDA, equimolar amounts of GRGD and 3.4 kDa Acryl-PEG-SCM (Laysan Bio) were mixed in sodium bicarbonate buffer, pH 8.2 for two hours, dialyzed overnight, and lyophilized. For all experiments, 65 μl cell suspension, 10 μl photoinitiator, and 25 μl 20% w/v PEGDA were mixed to form a final 5% w/v PEGDA solution. PEGDA/cell suspensions were added to a MatTek culture dish or microfluidic device and photopolymerized with an EXFO UV source filtered through a 340±13nm UV filter (Semrock)

and200μW power as measured entering the back aperture of the 1.3 N.A. 100X FLUAR (Zeiss) objective for 4-10 seconds. To encapsulate induvidual cells within hydrogel, a squre mask was placed in a plane conjugate to the ojective focal plane was used to limit the UV illumination to a square region with a 24 μm edge. After UV exposure the cell was trapped in a square hydrogel spot. Once the hydrogel was polymerized, the cells/hydrogels were washed in PBS and cultured in the appropriate culture medium. For alginate encapsulation, a solution of 3% RGD and non-RGD conjugated low molecular weight alginates were provided by Dr. Hyoon-Joon Kong from the University of Illinois. Cells were harvested by trypsinization, centrifuged, and resuspended in 100-200 μl alginate solution. The cell/prepolymer solution was placed into a mattek tissue culture dish (MatTek) and polymerized with 100mM $CaCl_2$ solution. Immediately after gelation, scaffolds were rinsed with PBS and then cultured in appopriate medium. For photopolymerizable alginates, cells and alginates were prepared in the same manner as PEGDA scaffolds, as a 2% alginate solution with 0.05% D2959 photoinitator and 10-15 UV exposure.

4.2.5 Synthesis of Methacrylated Alginates

The protocol to syntesize methacrylated alginates was adapted from Jeon et al. (Jeon, Bouhadir, Mansour, & Alsberg, 2009). Breifly, 2g low viscosity alginic acid was dissolved at a 1% w/v MES solution (50mM MES solution and 0.5M NaCl) over low heat and vigorous stirring. After dissolving, a 1:2 NHS:EDC (0.53 and 1.75 g, respectively) was added to the alginates and incubated at room temperature for 5 minutes. AEMA (0.76g) was added to make a final NHS:EDC:AEMA ratio of 1:2:1, and alginates were allow to react at room temperature for 24 hours. After reacting, alginates were precipitated with acetone, filtered, and dried under reduced pressure for ~24 hours. Dried alginates were resuspended at 1% w/v in diH20 and dialyzed (3500 MW cutoff dialysis tubing, Pierce) for 72 hours. Dialyzed alginates were the filtered and lyophilized. For cellular encapsulation, lyophilized alginates were resuspended at 4% w/v in diH20, then diluted to 2% in PBS/cell mixture and photopolymerized as described above.

4.2.6 Viability of Encapsulated Cells

Cellular viability was assessed with the Molecular Probes live/dead assay kit (Invitrogen). For all viability experiments, 100 μl of cells with an initial viability of >95% were placed in a MatTek culture dish and encapsulated within 5-10% 3.4 kDa scaffolds with a 63 or 100x objective with various levels of UV exposure. Scaffolds were washed 3x in PBS and incubated with the appropriate culture medium. After the allotted culture time (1-24 hours), encapsulated cells were washed in PBS and incubated with 2μm Calcein AM and 2μm Ethidium homodimer-1 fluorescent dyes for 20 minutes. Fluorescent images were taken with a Zeiss Axiovert 200M. Cells were manually counted in a minimum of four replicate gels for each time point, for a minimum of three experiments. Statistical significance was calculated using the Student's t test. Error bars indicate standard deviation of the experiments.

4.2.7 Confocal Microscopy and Image Analysis

Cells were imaged with a Leica SP2 laser confocal microscope. Confocal images were aquired using a 1.4 N.A. 63x oil immersion objective. 3D images were deconvolved using the Autoquant software. After deconvolution, images were processed using Imaris (Bitplane). 2D images were processed using Image J and Axiovision (Zeiss).

4.3 Results and Discussion

4.3.1 Biological Activity of Encapsulated Cells

The viability of U937, HEK and pMSCs encapsulated in PEGDA scaffolds was monitored for 24 hours to determine optimal PEGDA encapsulation conditions and baseline biological

activity levels of encapsulated cells. Encapsulating cells in PEGDA hydrogels can be detrimental to cellular activity as exposure to UV light can damage DNA, and free radicals generated during polymerization of PEGDA precursor solution may also damage cells. Cellular activity in hydrogels was monitored using a fluorimetric live/dead assay (Molecular Probes). First, U937 and HEK cells were encapsulated in 3.4 kDa PEGDA scaffolds with varying amounts of photoinitiator (D2959, 0.05-0.2%) and encapsulated using different lengths of UV exposure (5-20 seconds) and monitored for 24 hours. UV exposures between 5-20 seconds and photoinitiator concentrations of 0.05-0.2% did not have a significant effect (p-values > 0.05) on HEK and U937 cellular activity in hydrogel. After 24 hours of culture, cellular viability in hydrogels was ~70% (Figure 4.1). Based on these experiments, 5% 3.4kDa PEGDA with 0.05% photoinitiator was exposed to 5 seconds UV for all laser trapping experiments with U937 and HEK293 cells.

After optimizing U937 and HEK encapsulation parameters, similar experiments were repeated using pMSCs. In all conditions tested (5-20 seconds UV, 0.05-0.2% photoinitiator), pMSCs demonstrated poor (~10%) cell activity in hydrogel at 24 hours as demonstrated by live/dead staining. Decreased pMSCs viability may be due to increased sensitivity of primary cell lines to gelation conditions or lack of extracellular matrix components in hydrogel scaffolds. Previous studies have shown that the addition of ECM molecules, such as the integrin binding domain RGD, have enhanced cellular attachment, viability, and differentiation of MSCs in PEGDA scaffolds (Yang et al., 2005). To determine if RGD rescued pMSC viability, RGDs were incorporated into the PEGDA scaffold at a concentration of 2.5 mM. Addition of 2.5 mM RGD to hydrogel scaffolds permitted the attachment of pMSCs seeded on the hydrogel surface (data not shown), but did not improve the viability of cells encapsulated within the hydrogel. Several other groups (Buxton et al., 2007; Sharma et al., 2007; Yang et al., 2005) have demonstrated MSC biological activity and differentiation in similar hydrogel microenvironments but have created much larger hydrogels with longer, more diffuse UV exposures. Thus, we hypothesized that the focused UV power and rapid gelation parameters necessary for cellular encapsulation with laser tweezers may account for poor pMSC activity within PEGDA hydrogels. Due to

minimal activity of pMSCs in our hydrogel environments, we did not investigate cellular activity of arrayed pMSCs.

4.3.2 Permanent Trapping of Mammalian Cells

Human U937 and HEK293 cells were first used to develop laser parameters for the manipulation of mammalian cells. Optical trapping conditions required to manipulate U937, HEK and pMSC cell types are detailed in Table 4.1. Briefly, HEK and U937 cells were suspended in a 5% (w/v) PEGDA precursor solution with 0.05% photoinitiator. Cells were flowed into a microfluidic channel and manipulated by optical tweezers under a 100x 1.3 NA objective. Cells were fixed into position with a 5 second exposure to UV light. Figure 4.3 shows a 4x4 array of U937 cells formed by direct manipulation with laser tweezers. A similar 3x3 array of U937 cells was formed and stained for cellular activity one hour after trapping. Figure 4.3b demonstrates approximately 8 of 9 (88%) U937 cells had metabolic activity after one hour and thus laser trapping parameters had minimal effect on cellular activity one hour after trapping.

A second approach to manipulating and encapsulating cells in hydrogel scaffolds involves a step and repeat process. Once placed into position, individual cells must still be held by optical traps while the rest of the array is assembled, increasing the average time a cell is exposed to laser power. Using the step and repeat process, individual cells are encapsulated and fixed into place in PEGDA scaffolds prior to assembling the rest of the array. A square mask was placed to limit UV illumination to a 24 µm square area and individual cells were encapsulated into hydrogel using 1.3 seconds UV light. This process was repeated until the array reached the desired size. Figure 1c and d demonstrate an array and cellular activity of HEK 293 cells formed by the step and repeat method. Nine optical traps with a total of 100 mW (~11 mW per trap) were required to manipulate cells through the 5% PEGDA prepolymer solution. Arrayed and individually encapsulated HEK cells as shown in figure 4.3 c and d have 4 of 5 (80%) cells demonstrating metabolic activity similar to non-optically trapped cells after one hour hydrogel. After using the step and repeat process with HEK cells, individual pMSCs were formed into 3x3 and 2x2 arrays as shown in figure 4.4.

4.3.3 HETEROTYPIC ARRAY FORMATION

Cellular microenvironments contain multiple cell types that interact to preserve tissue specific function as well as maintain and direct differentiation of precursor cells. Cellular function and/or differentiation in these multicellular environments was supported by the degree and type (homotypic or heterotypic) cell-cell contacts, as well as cellular cross talk via signaling molecules secreted by neighboring cells. Often, removal of these cell-cell interactions results in altered cell phenotype or response. Therefore, we investigated the ability of the laser tweezer system to create arrays of multiple cell types. First, the formation of arrays with U937 cells with *E. coli* cells was investigated. Lipopolysaccahrides (LPS) secreted by these bacteria is recognized by the CD14/TLR4 receptors on cells of the innate immune system and induce rapid changes in gene expression and signaling molecule secretion. Figure 4 (a and b) demonstrate a U937 cell surrounded by ATCC 25922 *E. coli*. Since it is possible to visibly differentiate between cells, both U937 and ATCC25922 *E. coli* were combined into the PEGDA prepolymer solution. *E. coli* cells were assembled around a U937 cell using ~5mW laser power per *E. coli* and encapsulated into hydrogel using gelation parameters described above.

A second approach to forming heterotypic arrays was used to form arrays of pMSCs with porcine aortic endothelial cells (PAECs). Endothelial cells are present in specialized compartments described as the stem cell niche. Endothelial cells and other cells present in these niches can influence stem cell maintenance and differentiation through signaling molecules and cellular contacts. Since pMSCs and PAEC cells are not easily identified in the PEGDA prepolymer solution, pMSCs were first loaded into the microfluidic device, manipulated and encapsulated in hydrogel with the step and repeat process. After encapsulation, the microfluidic channel was flushed gently with PBS and a PEGDA prepolymer solution with PAECs were loaded into the microfluidic and encapsulated around the pMSCs (figure 4). This method of encapsulation also decreases cellular exposure to other cell types and signaling molecules prior to encapsulation and observation.

4.4 Alternative Approaches and Future Directions

The research presented in this chapter provides a solid base for optically trapping cells and investigating cellular behavior within engineered environments. However, several experiments must still be performed to optimize optical tweezers systems for mammalian cell trapping. Experiments to minimize temperature increases and photodamage to optically trapped cells are key to optimizing this system. Optical tweezers can produce a local increase in temperature at the focal point of the laser dependent on the laser duration and power that can negatively affect cellular viability. At 100 mW laser power, which is the power needed to manipulate optical traps, a 1064 nm Nd:Yag continuous wave (CW) laser produced ~1.4°C temperature increase at the focal point of the laser, but the system returned to baseline temperatures as soon as the trapping beam was turned off (Liu et al., 1995). The use of acoustic optical deflectors (AODs) constantly turning laser light on and off of the trapped particles in our optical tweezer setup is thought to reduce or prevent large increases in local temperature, but local temperature increases should be taken into consideration when testing or troubleshooting viability issues in optically trapped cells.

Photodamage is a major factor concerning cellular activity after optical trapping. Liang et al. Demonstrated laser power, wavelength, and trapping duration dependent effects on clonability of optically manipulated CHO cells (Liang et al., 1996). CHO cells exhibited maximum clonability at 800 and 1064 nm wavelengths, while all other wavelengths between 700-100nm were deleterious to cellular clonability (Figure 4.5). Thus, to optimize cellular viability of trapped cells, we suggest optically trapping mammalian (HEK and Raw) and stem cells at wavelengths of 700-1064 nm. In addition, different time-shared power levels and trapping durations should be tested for each wavelength to determine optical trapping conditions for mammalian cells. Cells should be tested both in media as well as encapsulated in PEGDA hydrogel scaffolds, and monitored at different time points from immediately after trapping up to 48 hours post trapping for the cell-cell communication model system. Cellular activity should first be measured by live/dead fluorescent staining to determine baseline viability. Then, cellular activity should be tested by activating the various fluorescent reporter systems, as encapsulated cells may survive optical trapping but may decrease or halt non-essential cellular

gene and protein expression while the cell repairs itself. The execution of these experiments should indicate optimal optical trapping conditions for each cell line.

Another drawback to this system is the limited cellular viability in PEGDA scaffolds. PEGDA scaffolds were chosen for this system due to the fast photopolymerization of the scaffolds, thus allowing the laser to be removed from the cell soon after trapping, and minimizing laser photodamage effects. Several factors can influence cellular viability in PEGDA scaffolds, including the type and concentration of photoinitiator, UV power and duration, and scaffold pore size. As discussed and demonstrated above, HEK cells demonstrate adequate cellular viability in PEGDA scaffolds, while porcine MSCs demonstrate poor (<10%) cellular viability. As an alternative, MSCs were encapsulated in alginate scaffolds. Alginate is a natural biomaterial extracted from brown algae and is composed of blocks of (1-4)-linked β-D-mannuronate (M) and α-L-guluronate (G) residues. Alginate scaffolds are rapidly polymerized by the addition of divalent cations such as Ca^{2+} or Mg^{2+}. Porcine MSCs were encapsulated in alginate hydrogels conjugated with or without the RGD peptide. In our experiments, the presence of RGDs affected cellular viability at 24 hours (29.7% without vs 58.7% with RGDs), but viability was similar for cells encapsulated in both types of alginate at 72 hours (Figure 6). Additionally, porcine MSCs were encapsulated in hydrogel and cultured under normal or adipogenic-inductive media. After 15 days of culture, cells demonstrated high (90%) viability in both normal and adipogenic conditions (Figure 4.7). The higher viability after two weeks of culture than initial conditions is likely due to the cell proliferation and breakdown and clearance of dead cellular debris.

Alginate scaffolds provide an alternative to PEGDA scaffolds due to their ease of use and ability to support MSC viability and differentiation. However, the inability to photopolymerize and control the size and shape of alginate hydrogels limits their usage in conjunction with our optical trapping systems. As a result, we attempted to synthesize methacrylated alginates that can be photopolymerized similarly to PEGDA scaffolds. Protocols to synthesize methacrylated alginates were adapted from Jeon et al. (Jeon, Bouhadir, Mansour, & Alsberg, 2009). Using these protocols, alginates were photocrosslinked using 0.05% D2959 photoinitiator and 10-15

seconds UV exposure. The ability to photocrosslink alginates makes these scaffolds an attractive alternative to PEGDA scaffolds, however at this time, we found that the photocrosslinked alginate hydrogels were not structurally sound, easily degraded, as well as had a higher prepolymer viscosity than PEGDA hydrogels, requiring higher laser power to manipulate cells. Due to these limitations we did not explore the use of photopolymerizable alginates further.

4.5 CONCLUSIONS

The goal of this study was to create precisely controlled 3D culture systems to observe single cell activity in response to microenvironmental signals. We demonstrate, for the first time, the manipulation and encapsulation of mammalian cells into specific locations within 3D PEGDA scaffolds by optical tweezers. Cell-cell interactions were tailored by adjusting spacing of cells and through a variety of patterns. We also demonstrated arrays of multiple cell types to further recreate complex tissue environments and to observe cellular responses to molecules secreted by nearby cells. The PEGDA scaffolds provided 3D support to the cells and were easily modified to include ECM components such as RGDs and thus recapitulated cell-ECM interactions that exist in native tissue environments. These scaffolds were cultured over extended period of time and are easily imaged by fluorescence and confocal microscopy to monitor cellular activity over time.

The combination of laser trapping and 3D scaffolds provide an important new tool to recapitulate and tailor cell and tissue environments. These methods may aid biologists in understanding cellular behavior and complex tissue environments such as the stem cell niche or provide physiologically relevant culture platforms for the screening of small molecules and drug discovery.

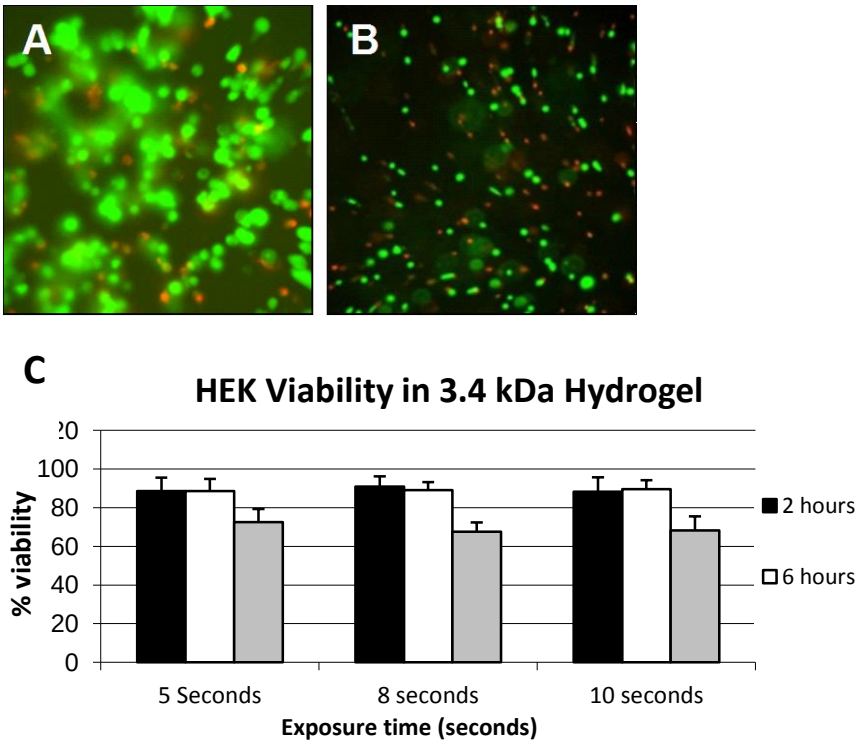

Figure 4.1. **Mammalian Cell Activity in Hydrogel.** (A) Fluorescent image of live/dead test for HEK293 cells in 3.4 kDa PEGDA 24 hours after encapsulation. Green represents live cells while dead cells stain red. (B) Viability of U937 cells in 3.4 kDa PEGDA 24 hours after encapsulation. (C) Viability of HEK cells encapsulated in 3.4 kDa PEGDA with 5, 8, and 10 seconds UV exposure over a 24 hour time period. Cells remained ~70% viable after 24 hours for all exposure times. (Error Bars=SEM)

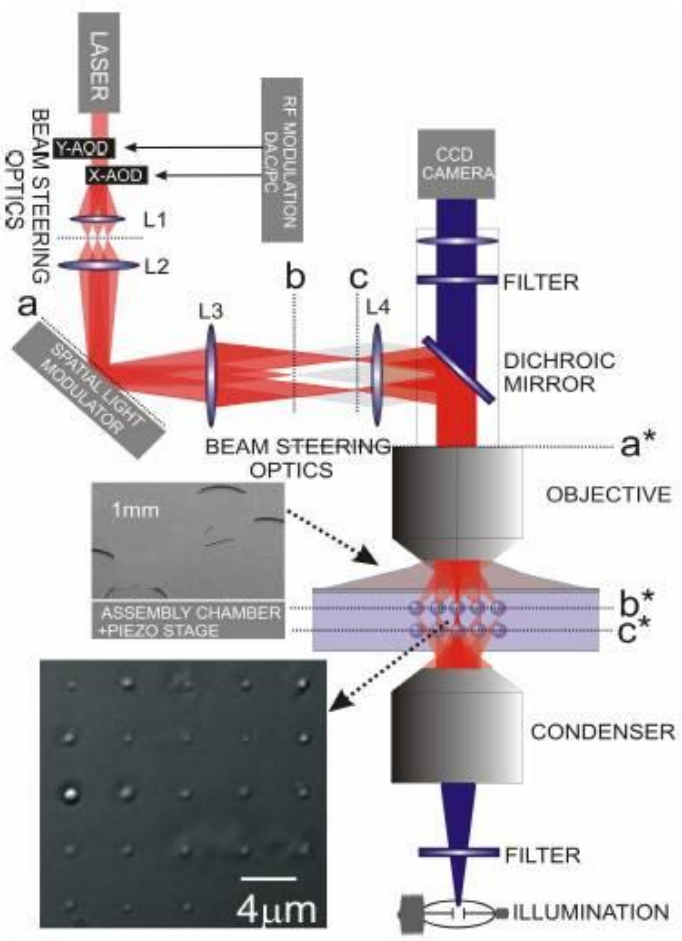

Figure 4.2. Optical Tweezer Setup. Cells are trapped by focusing a laser beam through a high numerical aperature (NA) commercial microscope objective. The spatial light modulator (SLM) and acoustic optical deflectors (AOD). The AODs give control over the x,y position of the trap while the SLM provides the ability to manipulate cells along the z axis. Reprinted from Askelrod et al. With permission from Elsevier.

Laser Trapping Component		UV Gelation Parameters	
Laser Source	Continuous Wave (CW) Ti: Sapphire	UV wavelength	λ=340±13nm
Laser Wavelength	900 nm	UV Power	4-5 mW
Objective	Zeiss FLUAR 1.3 NA oil immersion objective	UV Exposure Time	4-10 seconds
Laser Dwell Time Per Trap	10 μs	PEGDA MW	3.4kDa
Trap Position Precision	±18 nm	Prepolymer Solution	5%
Power per Trap	100mW for cells, 6 mW for bacteria		

Table 4.1. Optical tweezer parameters for manipulation and encapsulation of mammalian cells.

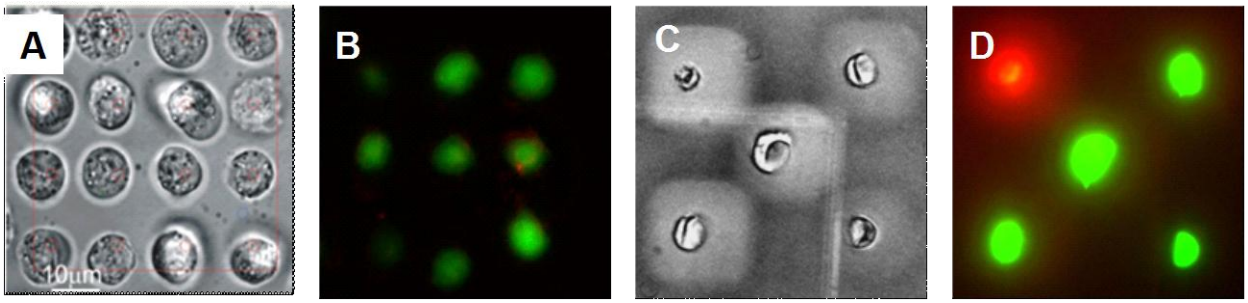

Figure 4.3. **Homotypic Arrays of U937 and HEK 293 cells.** (A) Transmitted image of U937 cells manipulated with optical tweezers into a 4x4 array. (B) Live/Dead image of a separate 3x3 array of optically manipulated U937 cells one-hour post encapsulation. (C) Transmitted image of HEK manipulated into a dice format. (D) Live/Dead image of (C) one hour post encapsulation.

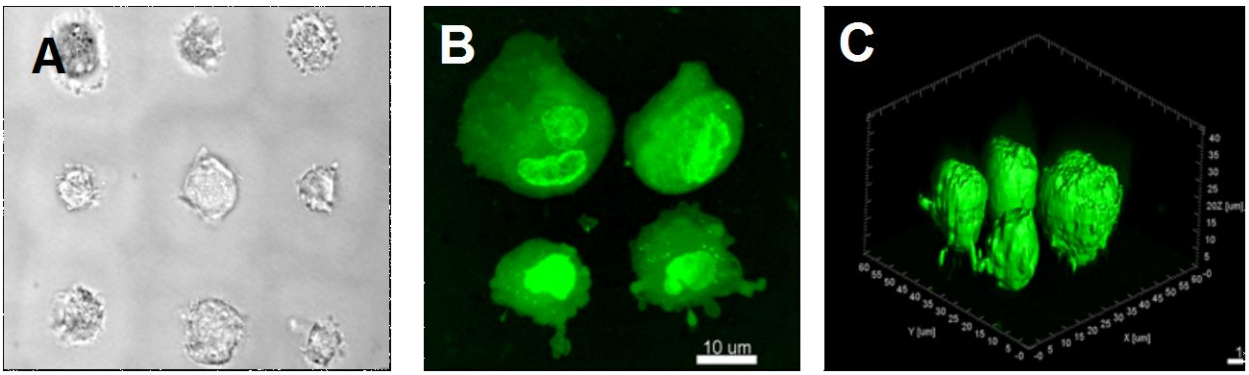

Figure 4.4. Homotypic Array of pMSCs. pMSCs were manipulated by optical tweezers and encapsulated in PEGDA hydrogels. (A) transmitted image of a 3x3 array of pMSCs. Cells were individually encapsulated in hydrogel to reduce laser power exposure needed to maintain cells in place while positioning other cells. (B) SYTO-9 staining of a 2x2 pMSC array (C) 3D rendering of (B). Surfaces were false colored for visualization.

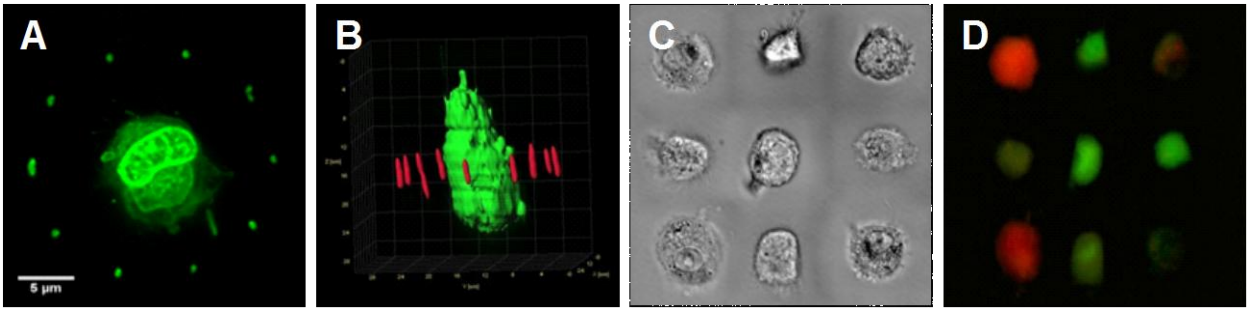

Figure 4.5. **Heterotypic Arrays.** (A). and (B). U937 cell arrayed with ATCC 25922 *E. coli*. (A) 3D max projection and (B) confocal side view of cells and *E. coli.* In (B), the *E. coli* were false colored red for visualization. (C) and (D) transmitted and fluorescent images of pMSCs arrayed with PAECs. In (D), pMSCs are stained green and endothelial cells are stained red.

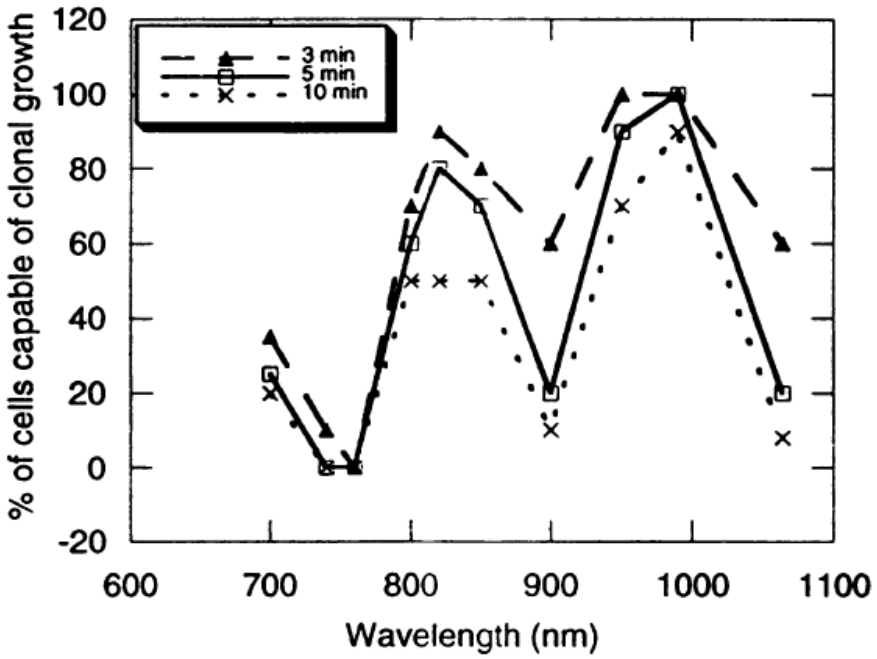

Figure 4.6. **Wavelength and Trapping Duration Dependence on Clonability of CHO Cells.** Cells were exposed to 88mW for 3, 5 and 10 minutes. At all time points, cells showed maximum clonability at 800 and 1064 nm wavelengths. Reprinted from Liang et al. with permission from Elsevier.

A.

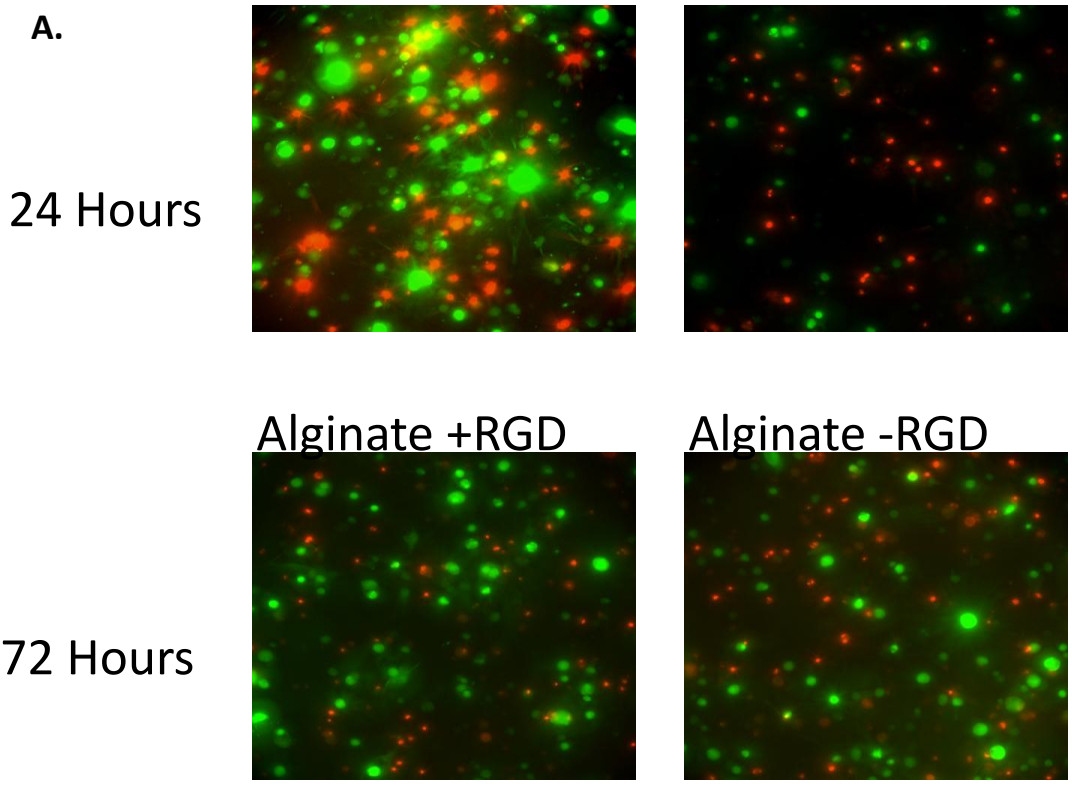

B.

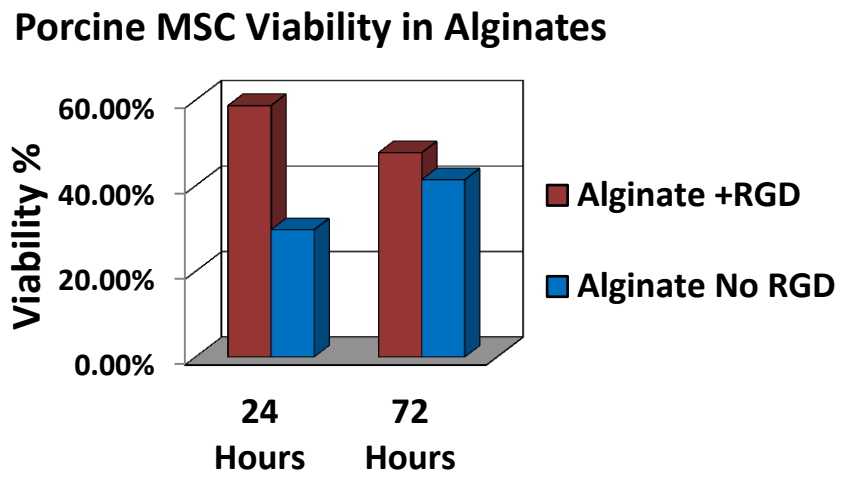

Figure 4.7 Viability of pMSCs Encapsulated in Alginates with or without Conjugated RGD Peptides. (A). live/dead assay of encapsulated pMSCs at 24 and 72 hours post encapsulation. Live cells are stained green while dead cells are stained red. (B). Graphical interpretation of (A). After 72 hours, approximately 50% of cells remained viable in both types of alginates.

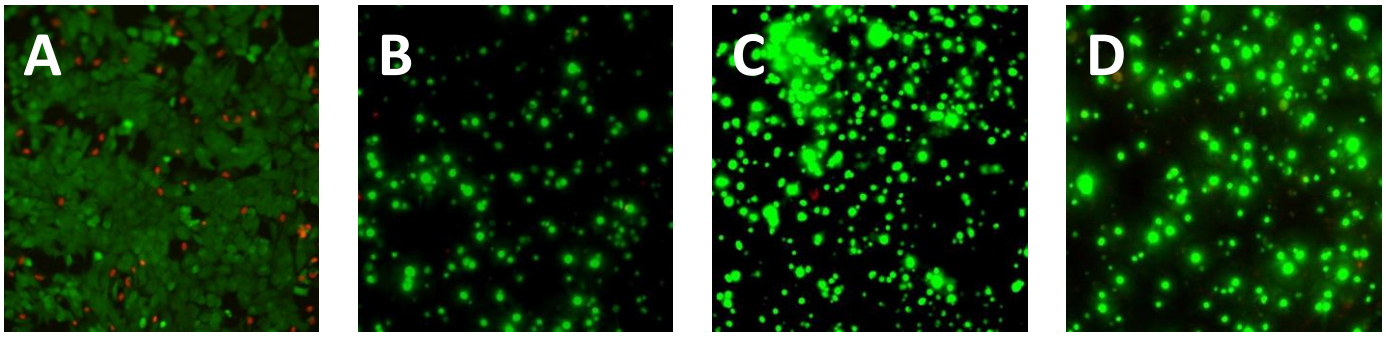

Figure 4.8. Viability of pMSCs in Alginates After 15 Days Culture. Cells were encapsulated in alginate with or without RGD peptide and cultured with adipogenic induction medium or DMEM. (A) Live/ dead control- cells cultured for 15 days in adipogenic induction medium but not in alginate. (B) pMSCs culture in alginate without RGD or adipose induction. (C) pMSCs cultured in alginates without RGD and with adipogenic induction medium. (D) pMSCs cultured in alginates with RGD and adipogenic induction medium. In all cases, cellular viability was high (~90%) demonstrating the ability of alginates to support long term pMSC viability and differentiation.

LIST OF REFERENCES

Akselrod, G. M., Timp, W., Zhao, Q., Li, C., Mirsaidov, U, Timp, R., et al. (2005). Laser-Guided Assembly of Heterotypic 3D Living Cell Microarrays. *Biophys J*, *91*(9): 3465-73.

Albrecht, D. R., Tsang, Valerie Liu, Sah, Robert L, & Bhatia, Sangeeta N. (2005). Photo- and electropatterning of hydrogel-encapsulated living cell arrays. *Lab chip*, *5*(1): 111-8.

Ashkin, A., & Dziedzic, J. M. (1986). Trapping and Manipulation of Viruses and Bacteria. *Science*, *235*: 1517-1520.

Ashkin, A., Dziedzic, J. M., & Chu, S. (1986). Observation of a single-beam gradient-force optical trap for dielectric particles. *Optics letters*, *11*(5): 288-290.

Benoit, D. S. W., Collins, S. D., & Anseth, K. S. (2007). Multifunctional hydrogels that promote osteogenic hMSC differentiation through stimulation and sequestering of BMP2. *Advanced functional materials*, *17*(13): 2085-2093.

Bhatia, S.N., Yarmush, M. L., & Toner, M. (1997). Controlling cell interactions by micropatterning in co-cultures: hepatocytes and 3T3 fibroblasts. *J Biomed Mat Res Part A*, *34*(2): 189–199.

Bissell, M. J., Radisky, D. C., Rizki, A., & W, V. M. W. O. (2002). The organizing principle : microenvironmental influences in the normal. *Cancer*, 537-546.

Bosnakovski, D., Mizuno, M., Kim, G., Takagi, S., Okumura, M., & Fujinaga, T. (2006). Chondrogenic differentiation of bovine bone marrow mesenchymal stem cells (MSCs) in different hydrogels: influence of collagen type II extracellular matrix on MSC chondrogenesis. *Biotech. Bioeng.*, *93*(6): 1152–1163.

Buxton, A. N., Zhu, J., Marchant, R., West, Jennifer L, Yoo, J. U., & Johnstone, B. (2007). Design and characterization of poly(ethylene glycol) photopolymerizable semi-interpenetrating networks for chondrogenesis of human mesenchymal stem cells. *Tiss Eng.*, *13*(10): 2549-60.

Garagorri, N., Fermanian, S., Thibault, R., Ambrose, W. M., Schein, O. D., Chakravarti, S., et al. (2008). Keratocyte behavior in three-dimensional photopolymerizable poly(ethylene glycol) hydrogels. *Acta biomaterialia*, *4*(5): 1139-47.

Griffith, L. G., & Swartz, M. A. (2006). Capturing complex 3D tissue physiology in vitro. *Nat Rev Mol Cell Biol*, *7*: 211-224.

Hahn, M. S., Taite, L. J., Moon, J. J., Rowland, M. C., Ruffino, K. a, & West, Jennifer L. (2006). Photolithographic patterning of polyethylene glycol hydrogels. *Biomaterials*, *27*(12): 2519-24.

Hubbell, J. A. (1995). Biomaterials in tissue engineering. *Nat. Biotech.*, *13*(6): 565–576.

Hui, E. E., & Bhatia, Sangeeta N. (2007). Micromechanical control of cell-cell interactions. *PNAS*, *104*(14): 5722-6.

Hwang, N., Varghese, S., Zhang, Z., & Elisseeff, Jennifer. (2006). Chondrogenic differentiation of human embryonic germ cell derived cells in hydrogels. *Tissue Engineering*, *12*(9): 2643-6.

Itle, L. J., Koh, W.-G., & Pishko, M. V. (2005). Hepatocyte viability and protein expression within hydrogel microstructures. *Biotech progress*, *21*(3): 926-32.

Jeon, O., Bouhadir, K. H., Mansour, J. M., & Alsberg, E. (2009). Photocrosslinked alginate hydrogels with tunable biodegradation rates and mechanical properties. *Biomaterials*, *30*(14): 2724-34.

Jordan, P., Leach, J., Padgett, M., Blackburn, P., Isaacs, N., Goksör, M., et al. (2005). Creating permanent 3D arrangements of isolated cells using holographic optical tweezers. *Lab chip*, *5*(11): 1224-8.

Karp, J. M., Yeh, J., Eng, G., Fukuda, J., Blumling, J., Suh, K.-Y., et al. (2007). Controlling size, shape and homogeneity of embryoid bodies using poly(ethylene glycol) microwells. *Lab chip*, *7*(6): 786-94.

Khademhosseini, A., Eng, G., Yeh, J., Fukuda, J., Blumling III, J., Langer, R., et al. (2006). Micromolding of photocrosslinkable hyaluronic acid for cell encapsulation and entrapment. *J. Biomed Mat Res Part A*, *79*(3): 522–532.

Liang, H., Vu, K. T., Krishnan, P., Trang, T. C., Shin, D., Kimel, S., et al. (1996). Wavelength dependence of cell cloning efficiency after optical trapping. *Biophys J., 70*(3): 1529–1533.

Liu, M. W. B., Y., C., K, D., Sonek, G. J., Berns, M W, Chapman, C. F., et al. (1995). Evidence for localized cell heating induced by infrared optical tweezers. *Biophys J.*, *68*: 2137-2144.

Liu, Y., Cheng, D. K., Sonek, G. J., Berns, M W, Chapman, C. F., & Tromberg, B. J. (1995). Evidence for localized cell heating induced by infrared optical tweezers. *Biophys J., 68*(5): 2137-44.

Mahoney, M. J., & Anseth, K. S. (2006). Three-dimensional growth and function of neural tissue in degradable polyethylene glycol hydrogels. *Biomaterials*, *27*(10): 2265-74.

Mirsaidov, Utkur, Scrimgeour, J., Timp, W., Beck, K., Mir, M., Matsudaira, P., et al. (2008). Live cell lithography: Using optical tweezers to create synthetic tissue. *Lab Chip*, *8*(12): 2174–2181.

Neuman, K. (1999). Characterization of Photodamage to Escherichia coli in Optical Traps. *Biophys J.*, *77*(5): 2856-2863.

Revzin, A., Tompkins, R. G., & Toner, Mehmet. (2003). Surface Engineering with Poly (ethylene glycol) Photolithography to Create High-Density Cell Arrays on Glass Surface Engineering with Poly (ethylene glycol) Photolithography to Create High-Density Cell Arrays on Glass. *Langmuir*, *19*(23): 9855-9862.

Sharma, B., Williams, Christopher G, Khan, M., Manson, P., & Elisseeff, J. H. (2007). In vivo chondrogenesis of mesenchymal stem cells in a photopolymerized hydrogel. *Plastic and reconstructive surgery*, *119*(1): 112-20.

Titushkin, I., & Cho, M. (2006). Distinct membrane mechanical properties of human mesenchymal stem cells determined using laser optical tweezers. *Biophys J., 90*(7): 2582–2591.

Tsang, V.L., Chen, A. A., Cho, L. M., Jadin, K. D., Sah, R.L., DeLong, S., et al. (2007). Fabrication of 3D hepatic tissues by additive photopatterning of cellular hydrogels. *FASEB*, *21*(3): 790.

Wang, M. D., Yin, H., Landick, R., Gelles, J., & Block, S. M. (1997). Stretching DNA with optical tweezers. *Biophys J.*, *72*(3): 1335-1346.

Wang, Y. C., & Ho, C.-C. (2004). Micropatterning of proteins and mammalian cells on biomaterials. *FASEB, 18*(3): 525-7.

Yang, F., Williams, C.G., Wang, D., Lee, H., Manson, P. N., & Elisseeff, J. (2005). The effect of incorporating RGD adhesive peptide in polyethylene glycol diacrylate hydrogel on osteogenesis of bone marrow stromal cells. *Biomaterials*, *26*(30): 5991–5998.

Zhang, H., & Liu, K. K. (2008). Optical tweezers for single cells. *J. R. Soc. Interface*, *5*(24): 671-690.

CHAPTER 5

DEVELOPMENT OF MICROFLUIDIC DEVICES

5.1 INTRODUCTION

A cell in any organism, tissue, or being is not an autonomous entity; it responds to signals from neighboring cells and even from distant tissues. These signals can induce a cell to spring into action, secrete soluble signals, differentiate, or even undergo apoptosis. A good example is the coordinated actions of the innate immune system. Macrophages recruited to the site of injury or invading pathogens are activated to secrete cytokines such as TNFα and IL-8 which in turn recruit and activate leukocytes and the immune system responses. Stem cells are either induced to differentiate; self-renew, or remain quiescent in response to signals secreted from neighboring cells and the composition of the extracellular matrix. These complex signaling networks are in integral in normal function of tissues and organs, wound healing, and immune responses.

While the importance of the cellular environment and cellular communication is clear, the ability to study or manipulate a cells environment *in vitro* is limited in existing 2D and 3D cell culture platforms. Conventional experiments to investigate cellular communication rely on the transfer of conditioned media from one cell type to another or the physical separation of cells in shared medium through a porous membrane. The use of microfabrication technologies has improved methods for spatial patterning of cells. Controlled deposition of ECM, antibodies, or cell resistant surfaces through a variety of methods (i.e. photolithography, inkjet printing) permit cell adhesion to selected areas of the culture system. For example, Stybayeva et al. created a microarray-like culture system by patterning T-cells and mucosal epithelial cells by depositing anti CD-3 antibodies onto silanized glass slides with a robotic microarrayer. T cells selectively adhered to antibody patterned surfaces and mucosal epithelial cells adhered to non-

patterned surfaces (Stybayeva et al., 2009). Similarily, Bhatia et al. used photolithographic techniques to pattern collagen islands for the selective adhesion of hepatocytes to model parenchymal/mesencymal interactions of the liver (Bhatia, Balis, Yarmush, & Toner, 1998). Other investigators have used microfabrication technologies to spatially define cellular co culture in 3D scaffolds while providing ECM and *in vivo* like environments. For example, Hammoudi et al. used photolithographic patterning of PEG based hydrogels to create long term, spatially defined 3D co culture of ligament fibroblasts and marrow stromal cells as a model for stem cell interactions with tendon and ligament tissues (Hammoudi, Lu, & Temenoff, 2010).

Existing co-culture models have proven useful for many biological studies, but lack spatial and/or temporal control over soluble molecule presentation. Bolus delivery of conditioned medium between cell populations represents an aggregate of factors produced by the cells, which do not represent spatial and temporal conditions of physiological tissues. As described above, many techniques exist for the spatial patterning of cells in relation to one another, yet these systems do not offer temporal control over soluble molecule gradients between cell types. Furthermore, the materials and techniques utilized for spatial patterning of cells are often toxic to cells. Most co-culture models are open-air cultures, where large air-fluid interfaces create convective flow conditions which rapidly move molecules away from cells, which interfere with natural signaling gradient creation and molecule buildup leading to delayed or aberrant responses from target cells (Yu, Alexander, & Beebe, 2007). Finally, the observation of cells is generally population-based, endpoint assays that will not detect temporal signaling events or responses of population subgroups.

In order to overcome these limitations, biologists have turned to the use of microfluidic devices, which have been designed to allow precise control over cellular seeding, culture, and the chemical microenvironment. Microfluidic devices can more effectively deliver nutrients than traditional or bioreactor culture through continuous perfusion and use small quantities of cells and reagents (Hu et al., 2008). Microfluidic devices also permit cellular culture in physiologically relevant length scales in the 10 to 100's of microns. Physiological tissues are

supported by networks of capillaries which range in size from 5-10 µm in diameter and 0.5-1 mm in length. Due to diffusion limitations, no cell resides further than ~100 µm away from a capillary. Using various techniques, cells and chemicals can be placed within certain locations within the microdevice with resolution in the micron range. The high surface area to volume ratio in microfluidic devices results in soluble molecule distribution through diffusion instead of convective flow, slowing diffusion for normal cellular function and stable soluble molecule gradients can be formed. Multiple cell types have been deposited in microdevices through several methods to investigate cellular communication events, including cellular chambers with connecting microchannels (Lovchik et al., 2010, Chung et al., 2009 Ma et al., 2010), selective deposition of cells through laminar flow (Kenis et al., 2000), and capillary based patterning (Lee et al., 2010). However, these techniques are largely two dimensional, lack control over soluble molecule flow and gradient formation, or are limited to two cell types.

This chapter describes the development of microfluidic cell culture systems that permit the patterning of cells encapsulated in biologically derived 3D scaffolds. Two microfluidic systems were developed for studying and controlling intracellular communication. The first microfluidic system utilizes laminar flow techniques that pattern collagen or Matrigel scaffolds into distinct architectures. After thermal curing of scaffolds, soluble factors released from cells form gradients between scaffolds. Introduction of fluid flow in the open channels washes away soluble the soluble molecules and thus prevents communication between separate cell types. A second microfluidic co culture system was developed in which Matrigel scaffolds were embedded within polydimethylsiloxane (PDMS) trenches. A second PDMS device with microchannels for fluid flow is placed over the hydrogel trenches, thus allowing soluble molecule diffusion between cell types. In each system, the cell communication model described in chapter 3 was used to validate the utility and functionality of cellular communication within the devices.

5.2 Materials and Methods

5.2.1 Cell Culture

Raw 264.7 (ATCC TIB-71) were cultured in DMEM medium (Sigma) supplemented with 10% fetal bovine serum (Gemini) and 100U/ml penicillin/streptomycin (Gibco) at 37ºC and 5% CO_2. Cells were passaged every 2-3 days by mechanical dissociation with a cell scraper. HEK293 cells were cultured in DMEM media supplemented with 10% fetal bovine serum and 100U/ml Penicillin/streptomycin and incubated at 37ºC and 5% CO_2. Cells were passaged at 80% confluence by trypsinization (0.5% trypsin/EDTA) every 2-3 days. ATCC 25922 *E. coli* were grown in LB broth at 37ºC and shaking culture until mid-logarithmic stage.

5.2.2 Transfection and lentiviral transduction

Raw 264.7 cells were transfected with the TNF-ptimer vector using an Amaxa Nucleofector and Nucleofector kit V (Lonza) according to manufacturer's instructions. All plasmid DNA was isolated using an endotoxin-free plasmid isolation kit (Qiagen). Briefly, 2µg plasmid DNA was transfected into $1x10^6$ Raw 264.7 cells, then 24-48 hours after transfection, 800 µg/ml g418 (Sigma) was added to the culture medium for selection of positively transfected cells. The NFkB-GFP lentiviral vector was purchased from SABiosciences. $1x10^4$ HEK cells were seeded into a 96 well plate and incubated with polybrene and lentivirus at a MOI of 20. To generate stable HEK NFkB cell lines, cells were selected by the addition of 800 µg/ml puromycin (Sigma) starting 3-4 days post transduction.

5.2.3 Fabrication of Microfluidic Masters

To fabricate the SU-8 mold of the features, first, negative images of the microchannels, inlets, and outlets were printed onto a transparency film, using a 5080 dpi printer. Then, the pattern of the microchannels, inlets, and outlets was transferred from the transparency to a 100 µm-thick layer of SU-8 2050 (MicroChem Corporation) spun onto a silicon wafer, via

photolithography. Unexposed SU-8 was dissolved using propylene glycol methyl ether acetate (PGMEA), and the exposed silicon surface was passivated via vapor deposition of (tridecafluoro-1,1,2,2-tetrahydrooctyl) trichlorosilane (Gelest, Inc.) under vacuum.

5.2.4 Fabrication of PDMS devices

PDMS (Sylguard 184) was mixed in a 10:1 ratio with curing agent, mixed, degassed, and poured onto SU8 silanized masters to a thickness of ~10mm. The PDMS was cured for a minimum of 3 hours at 65°C. PDMS was then removed from the masters and holes were punched for inlet and outlet tubing with a blunt 27 gauge needle. To reversibly seal PDMS onto glass slides, 50x50x75mm glass slides were cleaned thoroughly with acetone and isopropyl alcohol. The glass slides and PDMS replicas were placed in an oxygen plasma cleaner (Herrick) and house vacuum was applied until pressures reached 500 millitorr and plasma struck for 1 minute. Immediately after plasma heating, the two surfaces were brought into contact, forming a permanent seal. The devices were then incubated at 65°C overnight. To form trench devices, PDMS was cured for 3 hours, removed from the masters, and holes were punched for inlet and outlet tubing. After formation of Matrigel slabs, the top flow channel portion of the device was placed over the trenches using a stereomicroscope. Since the two PDMS slabs are not permanently sealed, the completed device was placed onto two plexiglass supports. Access ports were drilled on one plexiglass for tubing placement. On each plexiglass support, holes were drilled for placement of screws to secure the device. This setup prevents media and liquid leakage between the two pieces of PDMS.

5.2.5 Formation of Matrigel and Collagen Slabs

All Matrigel experiments and supplies (i.e pipette tips, tubing) were conducted in a cold (4C) room to prevent premature gelation of collagen and Matrigel solutions. Reduced growth factor Matrigel (BD Biosciences) was diluted with PBS at a ratio of 80 Matrigel: 20 PBS. Rat tail type I collagen (Sigma) was diluted in medium and brought to pH 7.4. To construct of Matrigel and collagen slabs in open fluidic channels, the PDMS on glass open channel device was placed

on a microscope to aid in visualization of laminar flow. All devices were sterilized with 70% ethanol and rinsed thoroughly with PBS. Tubing (Cole-Parmer), filled with ice cold PBS, was attached to the outlet channels and to a 100ul gas-tight syringe (Hamilton). Once tubing was attached, 5µl droplets of Matrigel solution or spacing solution (220mg/ml PEG in PBS) were placed onto the device. Vacuum was applied by operating a syringe pump in withdraw mode at 12 µl/min. When the flow was laminar within the device, the device was placed on a 37°C heating pad. Flow inside the device was gradually slowed by decreasing the syringe pump flow rate from 12, 10, 8, 6, 4, 2, 1, 0.5 and 0.1 µl/min over ~1 minute to prevent backflush of Matrigel within the device. After the flow rates were decreased, the tubing was cut and the device transferred to a 37°C incubator for 15 minutes to cure the Matrigel.

To form Matrigel scaffolds within the trench devices, Matrigel prepolymer solution was injected into each slab by pipetting. Pre-cooled 10µl flat gel loading tips (Midwest Scientific) with an outer diameter of 0.17mm were used to pipette 1 µl of Matrigel solution into the open trench. Trenches not being filled were covered with tape or a small PDMS slab. Excess Matrigel was then removed by swiping a sterilized razor blade over the top of the device.

5.2.6 Encapsulation of cells within Matrigel Slabs

To encapsulate cells in Matrigel solution, cells were harvested by scraping or trypsinization and concentrated by centrifugation for 5 minutes at 1000*xg*. Cells were resuspended in serum free culture medium to the desired concentration, and mixed with growth factor reduced Matrigel solution at a ratio of 80:20 Matrigel: cells. Alternatively, high concentration growth factor reduced Matrigel was prepared at a ratio of 50:50 Matrigel: cells. For open channel devices, 5µl of Matrigel: cell suspension was placed on each inlet and formed into slabs as described above. Trench devices were formed in the same matter as described above.

5.2.7 Cell Culture within PDMS devices

Immediately following Matrigel curing, laminar flow devices were gently rinsed with PBS via manual injection into the open channels of the device. Medium was infused into the device and placed into a 37°C 5% CO_2 incubator and attached to a syringe pump. Medium was flowed into the device at a rate of 0.5 µl/min during the culture period to replenish nutrients and counteract evaporation of medium. Similarly, Matrigel trench devices were rinsed with PBS through manual injection into the flow channels. Medium was infused into the device and placed into a 37°C 5% CO_2 incubator and attached to a syringe pump. Medium was flowed into the device at a rate of 0.5 µl/min during the culture period to replenish nutrients and prevent evaporation of medium.

5.2.8 Live/Dead Assay

Cellular viability was assessed with the Molecular Probes live/dead assay kit (Invitrogen). After the allotted culture time (1-24 hours), encapsulated cells were washed in PBS and incubated with 2µm Calcein AM and 2µm Ethidium homodimer-1 fluorescent dyes for 20 minutes. Viability was assesed by counting green or red cells in for different areas of the culture well. Fluorescent images were taken with a Zeiss Axiovert 200M.

5.2.9 Microscopy and Image Analysis

Fluorescent images were acquired using either a Zeiss Axiovert 200M fluorescent microscope or a Zeiss Stereolumar v12 and Axiovision software. Confocal Images were acquired on a Zeiss 710 confocal microscope and Zen 2009 software. Images were processed using Axiovision, Zen 2009 or Image J software.

5.3 Results and Discussion

5.3.1 Cellular compatibility with biomaterial scaffolds and Microfluidic components

Prior to designing microfluidic devices, we ensured that the Raw 264.7 and HEK 293 cells of the cellular communication model system maintained viability and signaling capabilities while encapsulated in hydrogel scaffolds and cultured within microfluidic device components. First, all three cell types of the communication system were encapsulated in Matrigel scaffolds and cultured in 1ml of medium on a 24 well tissue culture plate. At 24 hours, viability was tested with a fluorescent live/dead assay (Figure 5.1). Then, cells were encapsulated in Matrigel as described above but on top of a PDMS slab instead of a tissue culture well and assessed with the fluorescent live/dead assay. Cells cultured on PDMS demonstrated similar viability to cells cultured in tissue culture wells, demonstrating that the presence of PDMS does not affect cellular viability. Lastly, the previous experiment was repeated and activation of HEK NFκB signaling was visualized by fluorescent microscopy. After 24 hours of culture, encapsulated HEK cells displayed fluorescent levels above controls, and thus we concluded that the culture of cells within Matrigel scaffolds and in the presence of PDMS

5.3.2 Formation of Hydrogel Slabs within Open Channel Microdevices

Spatial patterning of liquids within microfluidic devices can be achieved through laminar flow techniques. Laminar flow occurs when fluids flow in parallel within a closed device with minimal mixing or turbulence. We hypothesized that, given the correct conditions, biomaterial scaffolds that are liquid in the prepolymer state (i.e. collagen, Matrigel) could be spatially patterned within microfluidic devices through laminar flow, then the scaffolds polymerized through thermal curing. The patterning of hydrogel slabs would allow for discrete patterning of the three cell types of the cell communication model system while allowing nutrient and soluble molecule diffusion within the spaces between scaffolds. Furthermore, soluble molecule diffusion could be manipulated by flowing medium between the scaffolds and thereby washing

away soluble signals. Other groups have reported the spatial patterning of Puramatrix (Kim, Yeon, & Park, 2007) and Matrigel scaffolds (Wong, Perez-Castillejos, Love, & Whitesides, 2008) through laminar flow techniques and thermal curing of hydrogels, yet they are limited to one or two cell types and do not demonstrate modulation of soluble molecule communication within the microdevices.

The microdevice used for laminar flow patterning of scaffolds is outlined in figure 5.1. The device was fashioned by soft lithography out of polydimethylsiloxane (PDMS), a soft elastomeric material that is optically clear, inert, and generally non-toxic. The device consists of 5 inlet channels - 3 channels for the input of cells/scaffolds materials and 2 'spacer channels' in between the three scaffold channels. Each inlet channel has a width of 300 μm, and the main channel is 2mm in width. The length of the main channel was 10mm and its height was 100μm.

In microfluidic devices, fluid flow is laminar (i.e. the fluid flows in parallel with minimal mixing) when the Reynolds number is less than one. The Reynolds number is a dimensionless number that measures the ratio of inertial forces to viscous forces. The Reynolds number is defined as:

$$Re = \rho v L / \mu$$

Where ρ= density of the fluid (kg/m^3), ν= velocity of the fluid (m/s), L= characteristic dimension of the channel (m), and μ=dynamic viscosity of the fluid (Pa·s). Generally, liquid solutions in microfluidic channels are characterized with a Reynolds number less than 1. This reflects that the viscous forces are stronger than inertial forces, and the resulting streams are linear (Squires & Quake, 2005). Given the dimensions of the microfluidic device described above, and using Matrigel scaffolds, μ = ~0.0152 Pa·s (Albrecht, Underhill, Mendelson, & Bhatia, 2007), ρ= ~12 kg/m^3 (12 mg/ml), L= .005 m, ν = ~ .00025 m/s (15 μl/min flow rate, approximate volume of device = 5 μl and 5mm length gives a velocity of . 015m/min=.00025 m/s). This gives an approximate Reynolds number of 9.87x10$^{-4,}$ demonstrating that the fluid flows will be laminar.

In laminar flow streams operated on horizontal surfaces, the width of each stream is dependent on the flow rate, width of inlet channels, and the viscosity of the fluids within the channel. With equal inlet channels, constant pressure (e.g vacuum in our system), and subsequent equal flow rates, the viscosity of solutions determines stream width. When the liquids have different viscosities, the liquid with the lower viscosity occupies a higher area (i.e a wider stream) of the microchannel (Stiles & Fletcher, 2004) due to higher flow rates. Thus, the width of the hydrogel slabs or media channels can be adjusted by altering the viscosity of the solution that is introduced in the spaces between hydrogels.

Investigation of the spatial patterning of cells and scaffolds requires scaffolds that are 1) liquid in the prepolymer state; 2) gels rapidly after patterning; 3) supports cellular growth and soluble molecule diffusion; and 4) not known to activate components of our cellular communication system. Some natural scaffolds may have residual amounts of growth factors that can possibly activate cells in our system (Lyle, Shallcross, & Durfor, 2009). Other scaffolds are known to activate signaling in Raw 264.7 cells through unknown mechanisms. (Yang & Jones, 2009). Given these criteria, we first chose to use type I collagen scaffolds. Collagen is the most abundant component of the ECM, and is a widely used biomaterial scaffold for the culture of cells. The scaffolds are liquid in the prepolymer state at 4°C, and gel within 45-60 minutes when incubated at 37°C, and are not known to activate Raw 264.7 cells or induce NFκB signaling in HEK cells.

The formation of collagen microslabs requires the device to be first placed on ice to cool the device and prevent premature gelation of collagen. The device was then flushed with PBS, and the outlet connected to a syringe pump with tubing filled with chilled PBS. Collagen solution or 220 mg/ml PEG solution (5 µl) was placed onto inlets. Flow was initiated by operating a syringe pump housing a 1ml syringe in withdraw mode at a rate of 15 µl/min. Once optimal laminar flow conditions were present within the device, observed by the naked eye or under 4x magnification, the tubing to the syringe pump was cut and the device placed at 37°C for 60 minutes for thermal curing of the collagen scaffolds. Figure 1b demonstrates laminar flow of collagen scaffolds and PEG solutions. In order to visualize laminar flow within the

device, PEG solutions were dyed green. In this case, collagen was placed on the outer and middle inlet, and PEG placed on the remaining inlets. Clearly defined areas of collagen (clear) or PEG solution (green) can be seen.

After thermal curing of the collagen scaffolds, gentle (<5µl/min) fluid flow was introduced by attaching tubing into the open inlet channels connected to a syringe filled with medium. However, the collagen scaffolds were not structurally sound to withstand shear forces from infusing medium. The centermost scaffold was usually flushed out of the device, while scaffolds on the edge of the device with a PDMS wall for support remained. In order to provide structural support to the collagen scaffolds, we attempted to place 100 µm microposts inside of the device, based off of the experiments by Huang et al. who demonstrated the patterning of collagen and Matrigel patterning inside microdevices with posts (Huang et al., 2009). The microposts instead prematurely initiated collagen fibril nucleation and formation, presumably because of the added shear stress from flowing past the microposts and differences in fluidic design between Huang et al. (Saeidi, Sander, & Ruberti, 2009). Thus we concluded that collagen is not a viable scaffold material for laminar flow patterning due to the low integrity of the gels and their ability to withstand shear forces.

As an alternative to collagen scaffolds, we choose to form Matrigel scaffolds within our microfluidic devices. Matrigel is a commercially available basement membrane matrix consisting of collagen IV, laminin, and proteoglycans that has been extensively used to culture cells both seeded in and on top of the scaffold. Matrigel is liquid at 4°C and rapidly polymerizes into stiff scaffolds at 37°C. Derived from extracts of Murine tumor epithelium, Matrigel has many unknown and uncharacterized factors present that may affect cellular signaling. To minimize unknown variables produced in Matrigel, we used growth factor reduced Matrigel solutions. Finally, laminar flow patterning of Matrigel scaffolds has been described previously by Wong et al. which provided basis for our methods of laminar flow patterning and indication that Matrigel scaffolds should be sufficiently stiff to withstand forces incurred while infusing devices with medium (Wong, Perez-Castillejos, Christopher Love, & Whitesides, 2008).

Fabrication of Matrigel slabs proceeded similarly to collagen slab formation. Since Matrigel cures rapidly at room temperature, all experiments were conducted in a cold (4°C) room. Pre-chilling devices and conducting experiments on ice did not cool the system enough to prevent premature polymerization during patterning. At 4°C and 220 mg/ml, PEG-8000 has an equal viscosity to Matrigel solution and stream widths are equal within the microchannel (Gonzllez-tello, Camacho, & Bllzquez, 1994), and thus used as our spacing solution. Devices were rinsed with ice cold PBS and the outlet connected to a 100µl gas-tight syringe filled with PBS. 5µl of Matrigel or spacing solution was added to the corresponding inlets and vacuum was applied at a rate of 12 µl/min. When fluid flows within the device were laminar, as observed through a microscope, the device was placed on a warm, 37°C heating pad to initiate thermal polymerization of the Matrigel. After placement on the heating pad, flow rate were reduced from 12 to 0.1 µl/min over a period of 1-2 minutes. This gradual reduction in flow rates coupled with the initiation of thermal curing prevents backflow and deformation of Matrigel from the sudden pressure changes and slight deformation of PDMS from stopping fluid flows immediately. Once fluid rates were at 0.1 µl/min, the outlet tubing was removed and Matrigel was cured in a humidified incubator at 37°C for 15-20 minutes. Once the Matrigel was cured, the PEG solutions were rinsed and replaced with culture medium, with the cured Matrigel slabs able to withstand rinsing without deforming or detaching from the device (Figure 5.2).

5.3.3 Encapsulation of cells within Matrigel Scaffolds

Encapsulation of cells within Matrigel scaffolds was achieved using the laminar flow patterning methods described above. Cells were harvested and resuspended in serum-free culture medium and mixed with Matrigel at a ratio of 80 Matrigel: 20 cells. The Matrigel:cell mixture was placed on inlets as described in figure 5.3 and the outlet tubing attached to a syringe pump. The syringe pump was operated in withdraw mode at a rate of 12 µl/min. Laminar flow patterning of the tree cell types of our communication system is outlined in figure 5.3b. After thermal curing the devices were rinsed with PBS by manual injection into the inlet tubing. Medium was the injected into the system and the device transferred to a tissue culture

incubator, and medium filled syringes and tubing were attached to the inlets. Medium was perfused into the device at a rate of 0.8 µl/min for the culture period. After 24 hours of culture, viability of encapsulated cells was assessed by live/dead assay, which is shown in figure 5.3c.

5.3.4 Characterization of Buried Matrigel Microfluidics

While laminar flow patterning of Matrigel scaffolds is feasible, the techniques described above are very labor intensive, have a long learning curve, and do not produce reliable, consistent results. Approximately 1 out of every 10 microfluidic devices were able to produce well formed Matrigel scaffolds. As an alternative, we designed a microfluidics device where individual Matrigel slabs are formed in open channels in PDMS (Figure 5.4). The device consists of three parallel channels that are 10 mm long, 100 µm deep, 400 µm wide and 300 µm apart. Matrigel is introduced by pipetting into the parallel channels using a flat tip gel loading tip. Laboratory tape or scrap PDMS pieces are used to cover open channels not being loaded to prevent mixing and cross contamination of cells/Matrigel. The Matrigel is then thermally cured for 10-15 minutes in a humidified incubator, and a second 'lid' portion for media introduction is placed on top of the open channels. The lid portion consists of two channels that are 8mm long, 500 µm wide, 100 µm deep, and 200 µm apart. The placement of the lid is such that the fluid channels of the lid overlap 100µm of each scaffold for media perfusion (see figure 5.4 for a schematic drawing of the assembled microfluidics device). Similar to scaffolds patterned by laminar flow, soluble molecules released from a cell type in a Matrigel scaffold are allowed to diffuse into the next scaffold or can be flushed away by rapid media perfusion into the channel. Since the bottom and lid portion are not sealed together, we designed a plexiglass support system that applies even pressure to the two pieces of PDMS without causing structural deformities, but prevented liquid leakage between devices. Holes were drilled in the top area for access to flow channels and insertion of tubing (Figure 5.4).

After designing buried Matrigel devices, the efficiency and ability to load individual Matrigel slabs into each channel was investigated. First, Matrigel was mixed with FITC-LPS and

loaded into one channel of the device. The Matrigel scaffold is then fluorescent, and any overloading or leakage of Matrigel into adjacent channels can be visualized. FITC-Matrigel (3 µl) was loaded into a channel using flat-tipped gel loading tips that have an outer diameter of 0.17mm. The thin, flat edge of the pipette tip can easily fit into a single channel for control of loading. Loading 3 µl of Matrigel into the trenches overfills the trenches, and excess Matrigel is removed by lightly swiping a sterilized razor blade over the channels. Figure 5.5c demonstrates the loading efficiency of Matrigel into the channels. The far left channel contains the FITC-Matrigel which is brightly fluorescent, and the remaining channels show minimal fluorescence. Remaining Matrigel that was not removed by swiping the razor blade over the surface can be removed with careful application of a razor blade or scalpel.

Next, the Matrigel scaffolds within the channels were characterized. PDMS is a hydrophobic material, which can result in bubble formation or partial filling of scaffolds. Oxygen plasma treatment of PDMS increases the wetablility of PDMS surfaces and reduces bubble formation and partial filling of channels (Sodunke et al., 2007). In our case, some bubbles are present within the Matrigel after loading, which can generally be removed with a pipette tip. Partial filling of well and bubbles formed inside of the channels with or without plasma treatment, mainly due to pipetting errors and not necessarily from hydrophobic PDMS surfaces.

To investigate the efficiency of filling the channels with Matrigel, confocal images were taken of channels loaded with fluorescent FITC Matrigel. Growth factor reduced Matrigel demonstrated a concave- like structure within the channel (figure 5.5), and did not fill the channel completely. The formation of concave structures could be due to several factors- Matrigel is highly sensitive to heat and humidity conditions and evaporates over time at room temperature and low humidity. In order to image the scaffolds, the Matrigel was exposed to room temperature and ambient humidity conditions and not bathed in medium, which could result in the Matrigel curing into concave structures. The removal of excess Matrigel may also contribute to scaffold loss. Finally, the scaffold may not polymerize evenly or with the integrity needed to maintain its shape. As an alternative, we investigated the filling efficiency of high

concentration, growth factor reduced Matrigel scaffolds. These scaffolds demonstrated higher structural integrity, and completely filled the device (Figure 5.5 b). High concentration Matrigel may be a sound alternative to its lower concentration counterpart, but levels of contaminating proteins and endotoxins are higher, and the solution is very viscous and difficult to load within the microdevices without cross contamination.

5.3.5 Encapsuation of Cells in Buried Channel Microdevices

Buried channel mircofluidic devices enable the encapsulation of individual cells within hydrogel scaffolds. To investigate the effects of Matrigel encapsulation on the biological activity of the two mammalian cell types of the cell communication system, Raw 264.7 and HEK 293, we encapsulated each cell type into all three channels of the microdevice. Matrigel was allowed to polymerize at 37°C for 10-15 minutes, then the lid portion placed onto the device with the aid of a stereomicroscope, and the entire device placed into the plexiglass support system. Tubing was attached to each of the inlet and outlet ports, and culture medium introduced through gentle injection with a 1 ml syringe. After media injection, devices were placed in a cell culture incubator and syringes attached to a syringe pump located inside the incubator. Medium was perfused at a rate of 0.8 µl/min to counteract media evaporation and dehydration of scaffolds. After 18 hours of culture, devices were gently flushed with PBS and cellular viability assessed with a fluorometric live/dead assay. At 18 hours, both HEK 293 and Raw 264.7 cells demonstrated complete cellular death within buried channel microdevices, while control (same Matrigel:cell preparation cultured in an 96 well plate) Raw 264.7 cells showed 80% and HEK 293 95% viability (Based on counting four separate areas of Matrigel encapsulated cells, figure 5.1 A and B). Several factors were investigated for their contribution to complete cellular death within the buried channel devices. PDMS itself is non-toxic to cells, but the crosslinker used to harden liquid prepolymer is known to be toxic to cells. First, all devices were autoclaved before use and cells introduced with and without 70% ethanol sterilization. However, the sterilization technique had no effect of on cellular viability. A second hypothesis is that since the fluid flow channels do not completely overlap the scaffold channels, medium is not diffusing into the scaffolds and thus affecting cellular viability. To test

this hypothesis, two methods were used. First, cells in Matrigel were loaded into the channels, and instead of placing the lid with perfusion channels, the PDMS devices were simply placed in a petri dish and covered with culture medium. A second approach involved purposely misaligning the perfusion channels so that the channels completely covered two of the three Matrigel channels. In both cases, Raw 264.7 cells showed similar viability to controls (figure 5.1 and figure 5.6), as well as maintained a rounded morphology indicating that endotoxin levels within Matrigel or from possible contaminants were not at levels to activate macrophages. However, HEK 293 cells did not show improvement in viability with these techniques. This could be due to low population levels inside the channels; HEK cells tend to clump together and are much larger than Raw 264.7 cells. Lack of cellular contact or stresses from loading through the small diameter pipette tips may affect cellular viability. Also, only the smaller cell clumps are passing through the pipette tip and thus inadvertently selecting for unhealthy or dead cells. Alternative loading techniques are now being investigated for HEK 293 cells. Since Raw 264.7 cells demonstrate viability on PDMS devices in the petri dish and in misaligned devices, we concluded that viability issues are due to decreased perfusion in the Matrigel scaffolds and not from PDMS itself. Thus, new PDMS lids are currently in fabrication in which are wider and thus will cover more of the channels for increased media perfusion.

5.3.6 Kinetics of Soluble Molecule Perfusion within Buried Channel Microfluidic Devices

In order to determine the signaling kinetics and molecule diffusion within the buried Matrigel microdevices, we calculated the approximate length scale of molecule diffusion within the device. First we examined diffusion kinetics of TNF within device. The rate of flow within the microfluic can affect the concentration of molecules throughout the device. Under static conditions where no fluid flow is present, the time course for a given molecule to diffuse a given distance can be calculated by the equation:

$$t = {x^2}/{2D}$$

Where t= time in seconds, x= distance traveled (cm) and D= the diffusion coefficient of the molecule of interest. In water at 25°C, the 51 kDa TNFα protein has a diffusion constant of ~8.2x10^$^{-7}$ cm2/sec. The shortest distance that a TNFα molecule would have to diffuse within the device is 300 um- the distance between microchannels. Given the equation, it would take a molecule of TNF ~ 548 seconds (9.14 minutes) to travel 300 µm at 25°C. However, diffusion coefficients of TNFα while still in Matrigel will be slightly slower. To approximate the diffusion coefficient of TNFα in Matrigel scaffolds, an equation from Ciocan et al. was utilized (Ciocan et al., 2009). Ciocan et al. measured the diffusion of various molecular weights of PEG in Matrigel scaffolds at 37°C and fitted the data using a power law that resulted in the equation:

$$D = 2.58\, x\, 10^{-7}\, (MW)^{-0.529}$$

Where D= the diffusion coefficient of the molecule, and MW=the molecular weight of the molecule in question. Substituting 51 kDa for MW in the equation, the approximate diffusion coefficient of TNFα in Matrigel at 37°C is approximately 3.22x10^{-7} cm^2/sec. If a cell along the far edge of the wall secreted a molecule of TNFα, it would take approximately 2484 seconds (41 minutes) for the molecule to reach the other end of the scaffold. Adding to the previous calculations, it would take ~50 minutes for a TNFα molecule to flow 400 µm through the gel and then 300 µm through the open channel, and ~91 minutes for that same molecule to flow from the far side of one scaffold to the far side of the next (400 µm in Matrigel + 300 µm in medium + 400 µm in Matrigel). For LPS, D=1.4x10^{-11} m^2/sec. In medium, it takes ~321s or 5.35 minutes for a LPS molecule to diffuse 300 µm.

5.3.7 Mathematical Modeling of TNF Diffusion Within Buried Channel Microdevices

Diffusion kinetics give an idea of the time scales required for a TNF molecule to diffuse through the microfluidic device. Activation of target HEK cells, however, requires the

accumulation of TNF to threshold levels to induce NFκB activation and fluorescent signaling. Fick's law of mass transport predicts how molecule diffusion causes concentration levels to change with time, and thus enables the calculation of the time periods required for TNF to accumulate to threshold levels. Fick's law is defined as:

$$\frac{\partial \phi}{\partial t} = D \frac{\phi \partial^2}{\partial x^2}$$

Where ϕ = concentration in dimensions (pg), t=time, D= diffusion coefficient, and x= length (um). In order to calculate diffusion kinetics within the microfluidic device, several assumptions were made about the protein production kinetics in Raw 264.7 cells and the sensitivity of HEK cells to TNF. These assumptions were based on the titer, co culture, and ELISA data presented in chapter 3. From the ELISA data, we know that $1x10^5$ activated Raw 264.7 cells have produced ~1,000 pg/ml of TNF five hours after stimulation. We first assumed, for calculation purposes, that $1x10^5$ Raw 264.7 cells are producing TNF protein at a rate of ~200 pg/ml per hour. In reality, Raw 264.7 cells do not produce TNF proteins until ~30 minutes after stimulation, and are producing proteins at threshold levels by 4 hours (REF). Given that there are ~50,000 Raw 264.7 cells encapsulated in each trench, we assumed protein production rates at 100 pg/ml per hour. In order to calculate threshold levels of TNF for HEK activation, we assumed that there were approximately 2,000 HEK cells encapsulated in each trench. From co culture data, we know that 3x105 HEK cells require 10,000 pg/ml TNF. For calculation purposes, we assumed that 2,000 cells is a 150 fold dilution of $3x10^5$ cells, and therefore encapsulated HEK cells would require concentrations of ~65 pg/ml for activation. As our diffusion coefficient, we chose to use $3.22x10^{-7}$ cm^2/s, which is the diffusion constant for TNF in Matrigel, and our length was defined as 700 µm.

Using these parameters, we calculated mass transport time scales using Matlab software, and graphical interpretation of these results is outlined in figure 5.7. Within our device, it takes approximately 2-2.5 hours for TNF protein levels to build up to 65 pg/ml 700 µm away from where it was released. Figure 5.7b demonstrates the concentration profile across the device at 2 hours. From chapter 3, we know that HEK cells require ~6 hours post activation

to visualize fluorescence, and thus our communication system requires ~8.5 hours to reach completion after activation of Raw 264.7 cells.

The calculations described above required many assumptions on the protein production rate and sensitivity of HEK cells to TNF proteins. Once adequate medium perfusion and cellular viability is attained within the devices, several experiments can be conducted to more accurately predict protein production rates and HEK sensitivities. The presence of outlet tubing in our microfluidic system enables effluent to be collected, and TNF ELISAs can be conducted at for several time points throughout culture and with varying populations of HEK cells. Co culture of HEK and Raw cells will determine sensitivity of encapsulated HEKs within the device. Finally, signaling kinetics can be visualized through time lapse fluorescent microscopy.

5.4 CONCLUSIONS

This chapter describes the fabrication of two separate microfluidic devices for the spatial patterning of cells. The first method patterns cells within biologically derived collagen and Matrigel scaffolds by laminar flow in an open channel microfluidic device. The use of thermally curable hydrogel scaffolds permits encapsulation of cells without toxic crosslinkers such as UV light. The five inlet design of the device permits formation of several configurations of hydrogel slabs, and the encapsulation of three cell types into spatially defined collagen and Matrigel slabs was demonstrated. Alternatively, we investigated the feasibility of encapsulating cell laden Matrigel scaffolds within micron sized trenches fabricated by soft lithography in PDMS. Currently, cellular viability is not supported in the buried Matrigel devices, presumably due to inadequate medium perfusion. Redesign of the microfluidic system is ongoing to improve perfusion and cellular viability issues within the device. Modeling of TNF diffusion kinetics revealed that the system requires ~8.5 to visualize HEK fluorescence after LPS stimulation within the buried Matrigel devices. We propose that these microfluidic culture systems will provide a platform for the rapid and repeatable patterning of Matrigel scaffolds and cells, and the perfusion of medium between scaffolds permits the temporal control over soluble molecule signaling for investigations into cellular communication events.

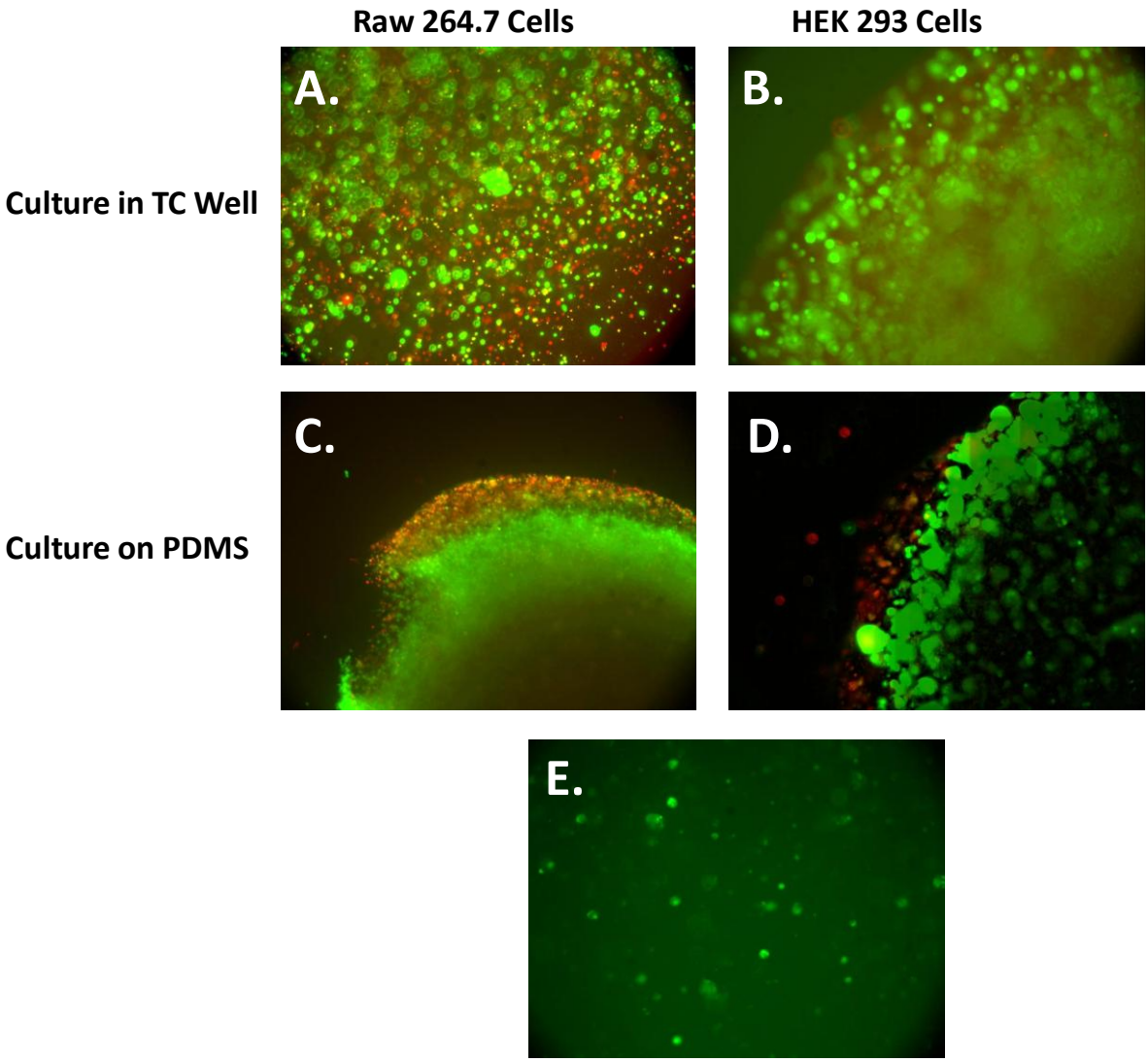

Figure 5.1 Compatibility of Cells with Microfluidic Components. (A). and (B). Live/Dead assay of cells encapsulated in Matrigel and cultured in a tissue culture well. (C) and (D). Live/Dead assay of cells encapsulated in Matrigel and cultured on top of a PDMS slab. (E). Activation of HEK 293 cells in co culture on top of a PDMS slab with Raw 264.7 and E. coli bacterium. These results demonstrate that neither Matrigel nor PDMS interferes with cellular viability or signaling ability.

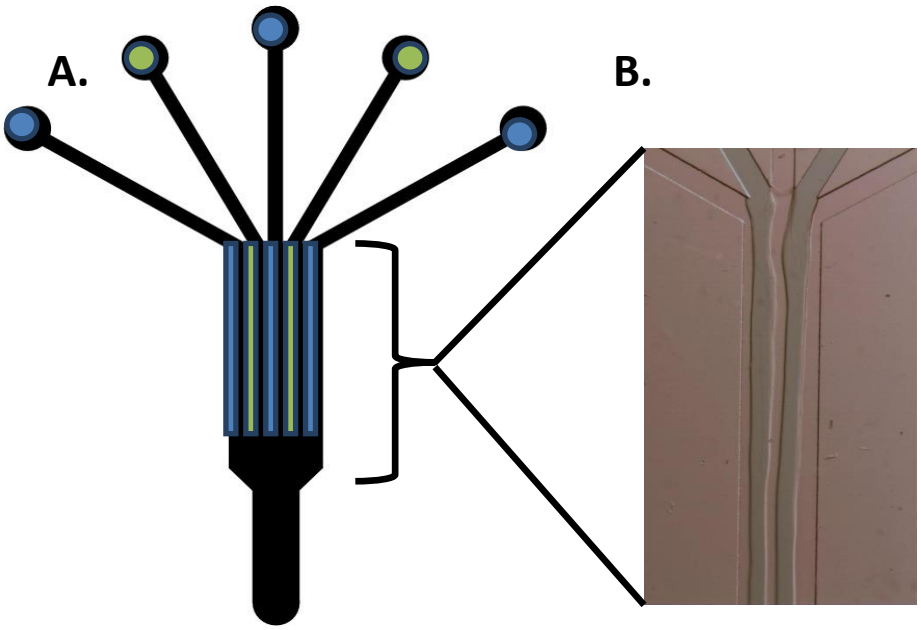

Figure 5.2. Open Channel Microfluidic Device. (A). Schematic of laminar flow patterning microfluidic devices. Five 300 µm inlet channels introduce prepolymer Matrigel solution or PEG-800 into a 1.5 mm wide main channel. Within the main channel, fluid flow is laminar (B). where two liquid streams flow in parallel with minimal mixing. Matrigel scaffolds are patterned via laminar flow and thermally cured to form individual hydrogel slabs for the encapsulation of cells.

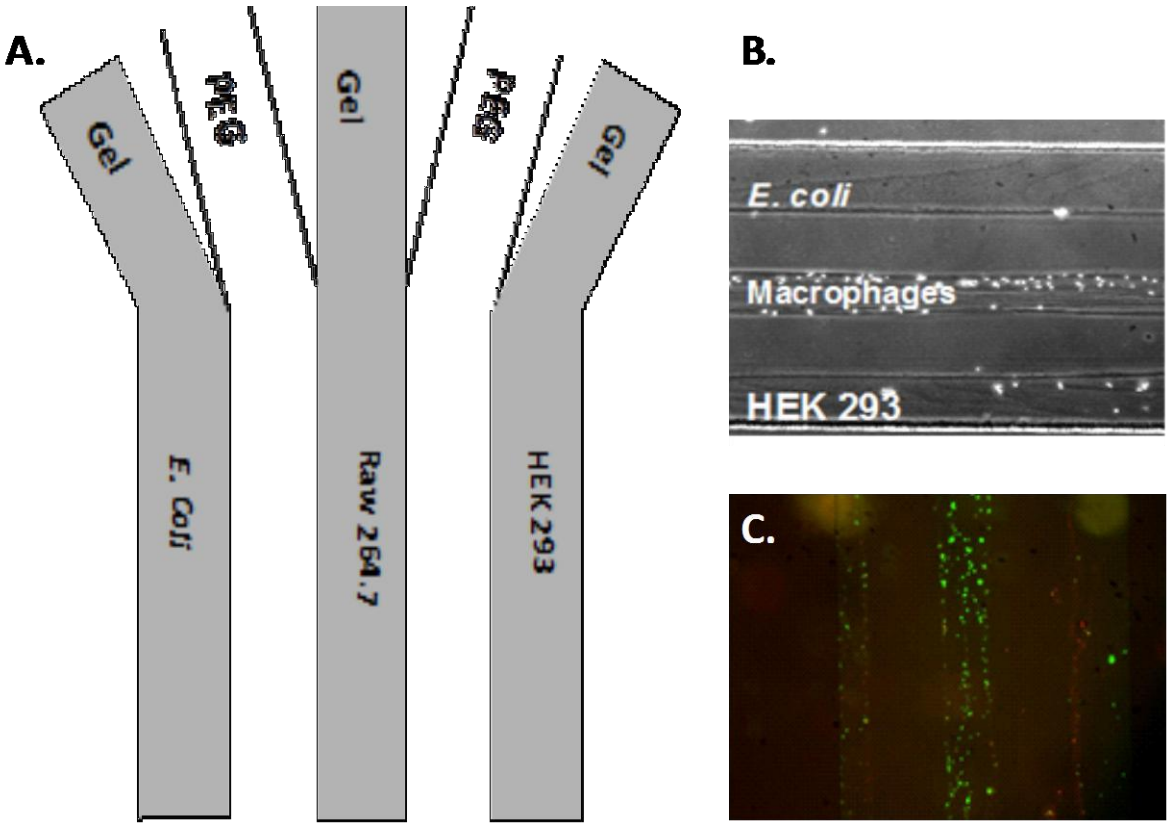

Figure 5.3 Laminar Flow Patterning of Hydrogel Scaffolds. (A). Schematic of cell/Matrigel placement within laminar flow devices. Matrigel/cell suspensions were placed on inlets 1, 3, and 5 and PEG 8000 solution onto inlets 2 and 4. (B). Matrigel was then patterned by applying vacuum and formation of laminar flow streams and thermally cured. (C). Fluorescent Live/Dead assay of laminar flow patterned cells after 24 hours of culture.

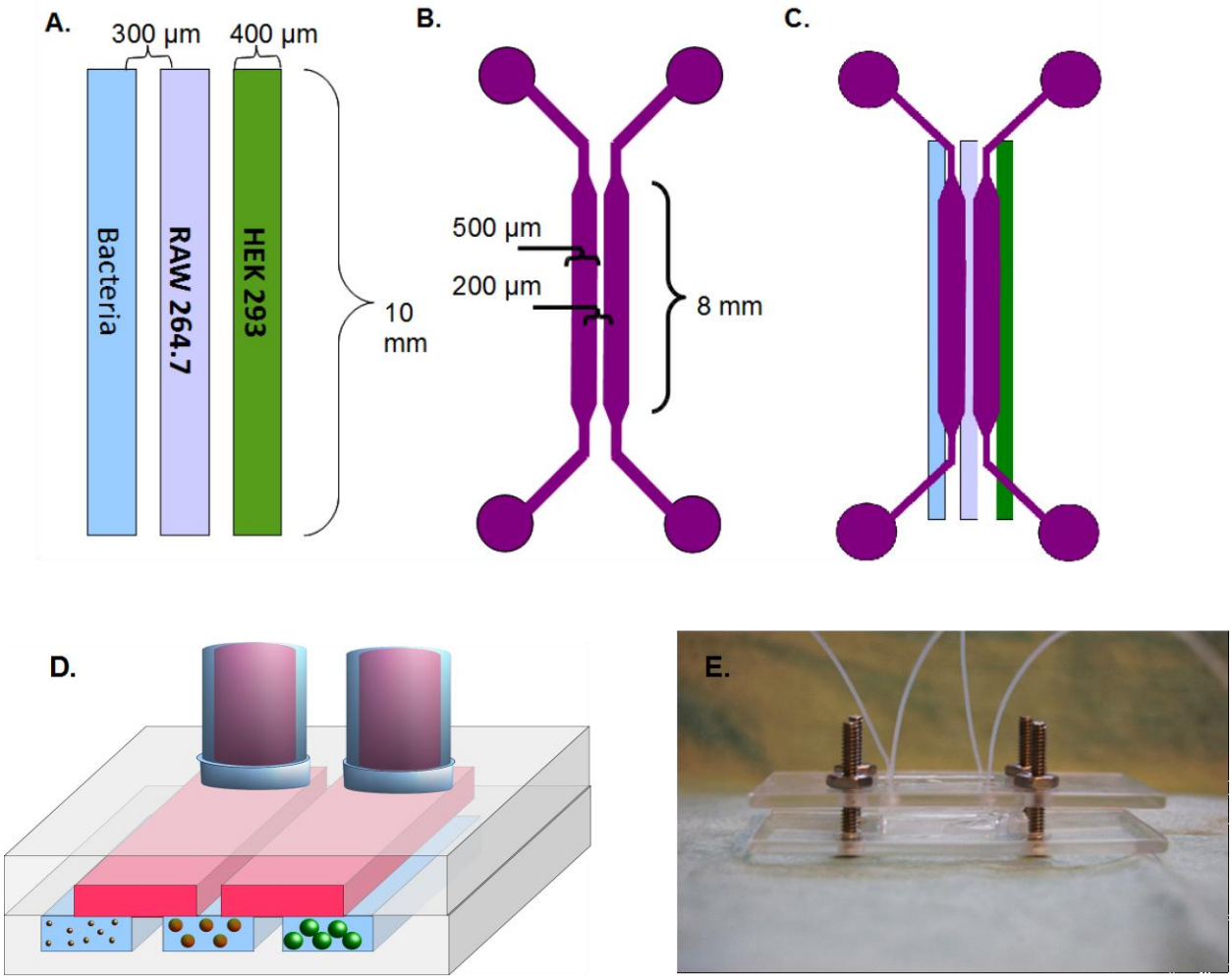

Figure 5.4 Buried Matrigel Microfluidic Devices. (A). Schematic of the buried Matrigel trench device. 400 µm wide by 10 mm long and 100 µm trenches were formed in PDMS by soft lithography techniques. (B). Schematic of the 'lid' portion of the microdevice which permits media perfusion to Matrigel scaffolds. (C). and (D). Top (C) and cut-away side (D) views of assembled devices. (E). An assembled microdevice with plexiglass support system and attached tubing.

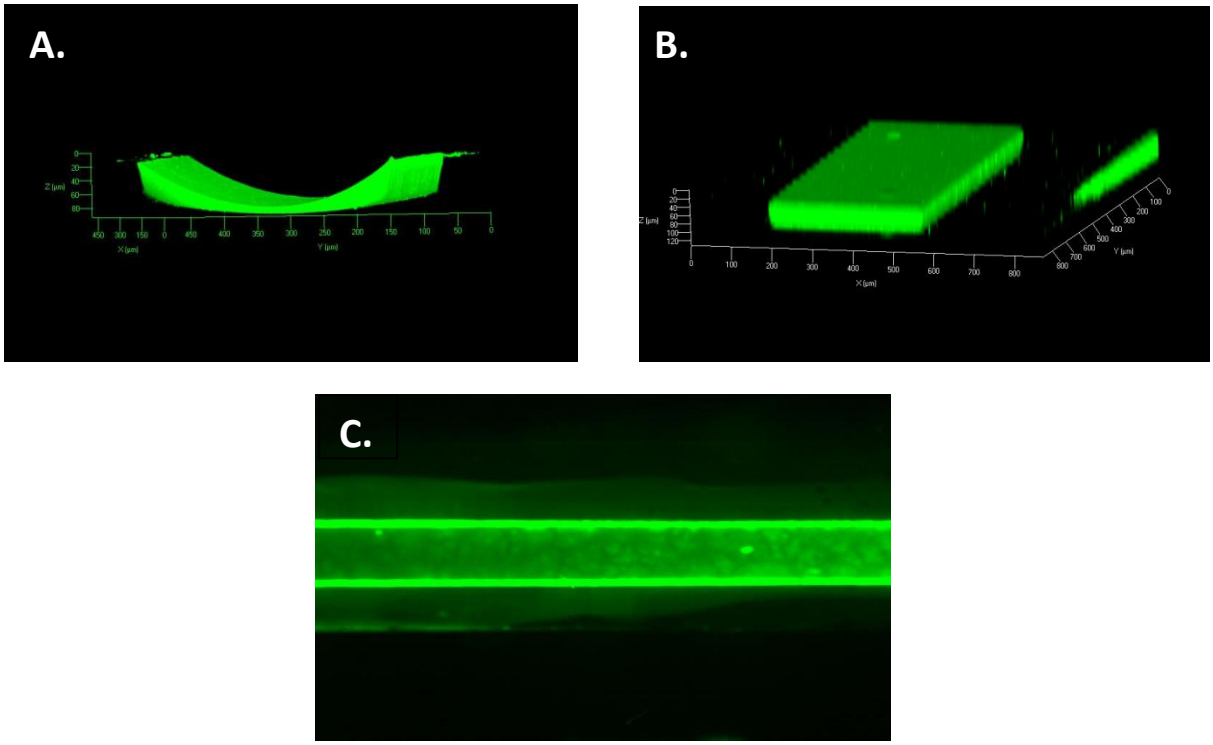

Figure 5.5. Matrigel Loading into Trench Devices. Matrigel (A) or high concentration Matrigel (B) with FITC-LPS was loaded into trench devices and allowed to polymerize for 10 min at 37°C. Devices were placed on a coverslip and imaged using a confocal microscope. Normal concentration Matrigel did not completely fill the trench device, due to loss of Matrigel when removing excess material or evaporation during polymerization. This may require a second loading of Matrigel to fill in gaps. On the other hand, high concentration Matrigel filled the devices, even after removal of excess Matrigel and polymerization. (C). Fluorescent image of FITC-Matrigel scaffolds within buried microchannel devices. Matrigel only fills one trench of the device, demonstrating efficiency of pattern formation and the ability to load trenches without contaminating adjacent trenches.

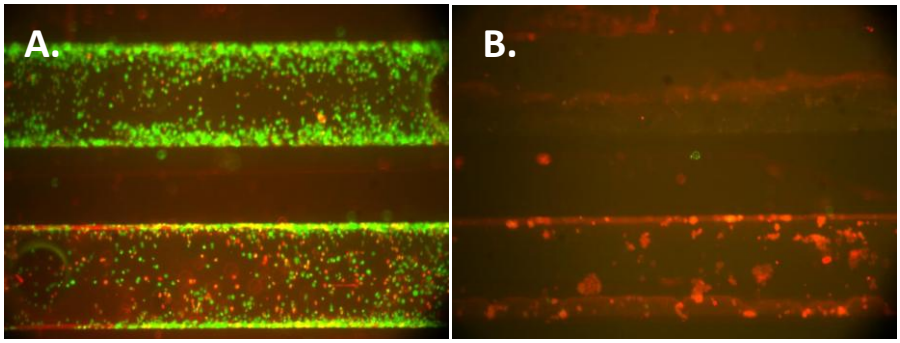

Figure 5.6 Viability of Cells in Misaligned Buried Matrigel Devices. Cellular viability was compromised within the current microfluidic device design. We hypothesized that the cellular viability was compromised due to poor medium perfusion throughout the Matrigel scaffolds. Lid portions of the device were purposely misaligned to completely cover the trenches and increase medium perfusion. Misalignment of the lid rescued Raw 264.7 cell viability (A) but did not improve HEK cell viability (B).

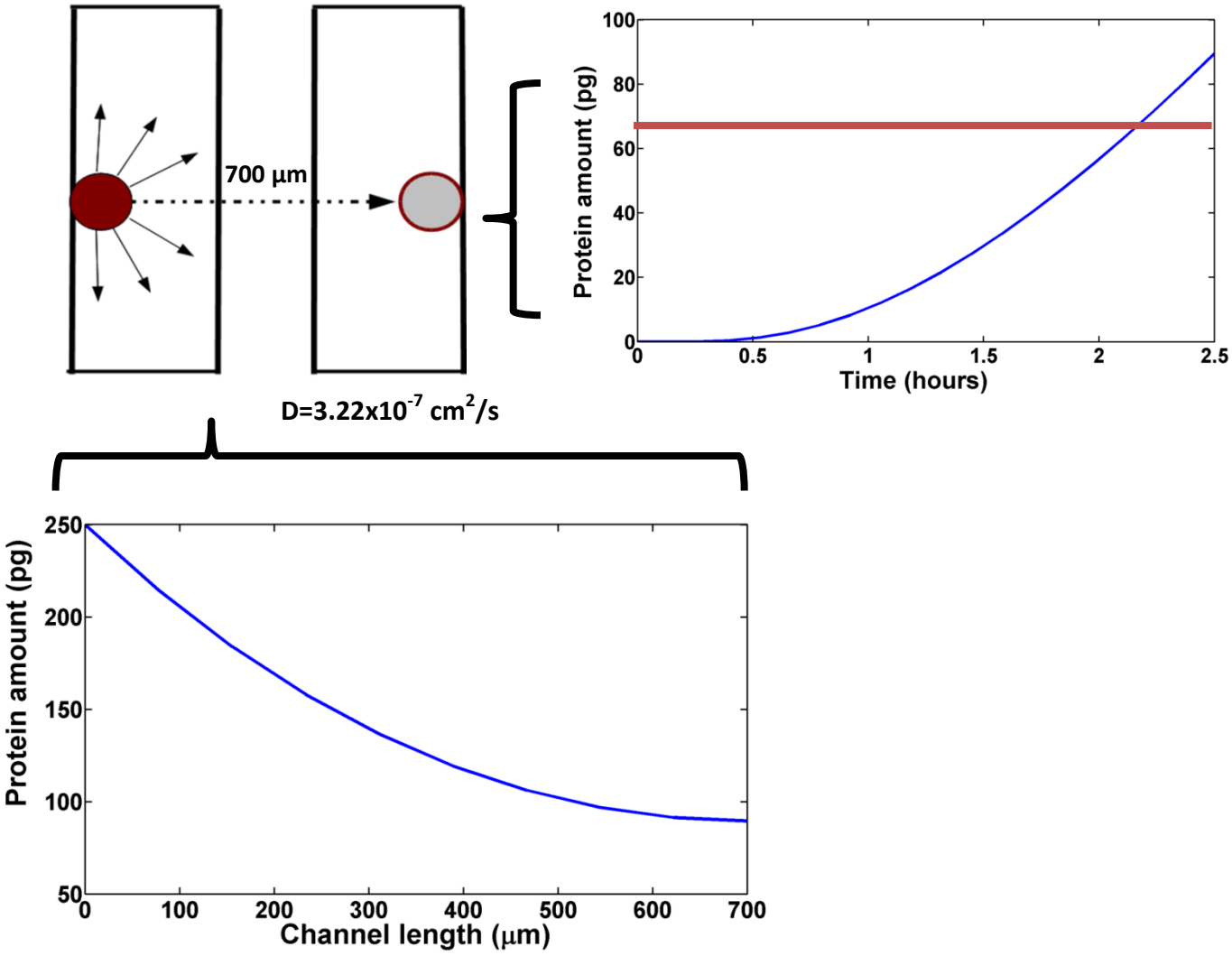

Figure 5.7 Diffusion Profiles of TNF in Buried Channel Microdevices. (A). Schematic of diffusion throughout the microfluidic device. (B). Graphical interpretation of TNF concentration profiles over time 700 µm away from TNF source. (C). Concentration profile of TNF across the 700 µm device at 2 hours post stimulation.

LIST OF REFERENCES

Albrecht, D. R., Underhill, G. H., Mendelson, A., & Bhatia, S.N. (2007). Multiphase electropatterning of cells and biomaterials. *Lab chip*, *7*(6):702-9.

Bhatia, S N, Balis, U. J., Yarmush, M. L., & Toner, M. (1998). Microfabrication of hepatocyte/fibroblast co-cultures: role of homotypic cell interactions. *Biotech progress*, *14*(3): 378-87.

Chung, S., Sudo, R., Mack, P.J., Wan, C., Vickerman, V., & Kamm, R. (2009). Cell migration into scaffolds under co-culture conditions in a microfluidic platform. *Lab Chip,* 9(2): 269-75.

Ciocan, E., & Ciocan, R. (2009). Optimized numerical pharmacokinetics model for optical molecular probes based on diffusion coefficients in matrigel measured using fluorescence imaging. *IEEE Conf. Proc.* 5:4925-4928.

Hammoudi, T. M., Lu, H., & Temenoff, J. S. (2010). Long-term spatially defined coculture within three-dimensional photopatterned hydrogels. *Tiss. Eng. Part C: Methods*, *00:* 381.

Hu, G., & Li, D. (2008) Microfluidic Effects of Transporting Signaling Components in Cell Coculture Chips. *Micro Nano* 6: 99-107.

Huang, C. P., Lu, J., Seon, H., Lee, A. P., Flanagan, L. a, Kim, H.-Y., et al. (2009). Engineering microscale cellular niches for three-dimensional multicellular co-cultures. *Lab chip*, *9*(12): 1740-8.

Kenis, P. J., Ismagilov, R. F., Takayama, S., Whitesides, G M, Li, S., & White, H. S. (2000). Fabrication inside microchannels using fluid flow. *Accounts of chemical research*, *33*(12): 841-7.

Kim, M. S., Yeon, J. H., & Park, J.-K. (2007). A microfluidic platform for 3-dimensional cell culture and cell-based assays. *Biomed microdev*, *9*(1): 25-34.

Lee, S. H., Heinz, A. J., Shin, S., Jung, Y.-G., Choi, S.-E., Park, W., et al. (2010). Capillary based patterning of cellular communities in laterally open channels. *Analytical chemistry*, *82*(7): 2900-6.

Lovchik, R.D., Tonna, N., Bianco, F., Matteoli, M., & Delamarche, E. (2010). A micrfluidic device for depositing and addressing two cell populations with intercellular population communication capability. *Biomed microdev,* 12(2): 275-82.

Lyle, D., Shallcross, J., & Durfor, C. (2009). Screening biomaterials for stimulation of nitric oxide-mediated inflammation. *J. Biomed. Res Part A*, 82-93.

Ma, H., Liu, T., Qin, J., & Lin, B. (2010). Characterization of the interaction between fibroblasts and tumor cells on a microfluidic co-culture device. *Electrophoresis,* 31(10):1599-1605.

Saeidi, N., Sander, E. a, & Ruberti, J. W. (2009). Dynamic shear-influenced collagen self-assembly. *Biomaterials*, *30*(34): 6581-92.

Sodunke, T. R., Turner, K. K., Caldwell, S. a, McBride, K. W., Reginato, M. J., & Noh, H. M. (2007). Micropatterns of Matrigel for three-dimensional epithelial cultures. *Biomaterials*, *28*(27): 4006-16.

Squires, T., & Quake, S. (2005). Microfluidics: Fluid physics at the nanoliter scale. *Rev Modern Physics*, *77*(3): 977-1026.

Stiles, P. J., & Fletcher, D. F. (2004). Hydrodynamic control of the interface between two liquids flowing through a horizontal or vertical microchannel. *Lab chip*, *4*(2): 121-4.

Stybayeva, G., Zhu, H., Ramanculov, E., Dandekar, S., George, M., & Revzin, A. (2009). Micropatterned co-cultures of T-lymphocytes and epithelial cells as a model of mucosal immune system. *Biochem biophys Res Comm*, *380*(3): 575-80.

Wong, A. P., Perez-Castillejos, R., Christopher Love, J., & Whitesides, George M. (2008). Partitioning microfluidic channels with hydrogel to construct tunable 3-D cellular microenvironments. *Biomaterials, 29*: 1853-61.

Yang, D., & Jones, K. S. (2009). Effect of alginate on innate immune activation of macrophages. *J.Biomed Mat Research. Part A*, *90*(2): 411-8.

Yu, H., Alexander, C. M., & Beebe, D. J. (2007). Understanding microchannel culture: parameters involved in soluble factor signaling. *Lab chip*, *7*(6): 726-30.